รายงานวิจัยฉบับสมบูรณ์

โครงการ การพัฒนาลิโพโซมแกนไซโคลเวียร์มุ่งเป้าสู่ดวงตาส่วนหลังด้วยการหยอดตา

โดย รองศาสตราจารย์ ดร. รัฐพล อาษาสุจริต
และคณะ

พฤษภาคม 2563

สัญญาเลขที่ RSA6080034

รายงานวิจัยฉบับสมบูรณ์

โครงการ การพัฒนาลิโพโซมแกนไซโคลเวียร์มุ่งเป้าสู่ดวงตาส่วนหลังด้วยการหยอดตา

รองศาสตราจารย์ ดร. รัฐพล อาษาสุจริต
คณะเภสัชศาสตร์ มหาวิทยาลัยธรรมศาสตร์

สนับสนุนโดยสำนักงานกองทุนสนับสนุนการวิจัย และ
มหาวิทยาลัยธรรมศาสตร์

กิตติกรรมประกาศ

ผู้วิจัยขอขอบพระคุณ ผู้ช่วยศาสตราจารย์ ดร. จิตติมา มานะกิจ อาจารย์ประจำคณะเภสัชศาสตร์ มหาวิทยาลัยศรีนครินทรวิโรฒ อ. ดร.เทวา พนักศรี อาจารย์ประจำวิทยาลัยแพทยศาสตร์นานาชาติจุฬาภรณ์ มหาวิทยาลัยธรรมศาสตร์ ดร. วรปภา ตรีสุภรัชต์ นักวิจัยประจำศูนย์วิจัยค้นคว้าและพัฒนายา สำนักงานวิทยาศาสตร์และเทคโนโลยีขั้นสูง มหาวิทยาลัยธรรมศาสตร์ และดร.อศิรา เฟื่องฟูชาติ ศูนย์เทคโนโลยีโลหะและวัสดุแห่งชาติ สำนักงานพัฒนาวิทยาศาสตร์และเทคโนโลยีแห่งชาติ ที่ให้ความช่วยเหลือด้านเทคนิค เครื่องมือวิจัย ตลอดจนความคิดเห็นที่เป็นประโยชน์ต่อการทำงานวิจัยครั้งนี้

ขอขอบพระคุณ สัตวแพทย์หญิงธัญญธร ยิ้มสู้ รักษาการผู้อำนวยการศูนย์สัตว์ทดลอง มหาวิทยาลัยธรรมศาสตร์ ที่ให้ความช่วยในการดูแล และการปฏิบัติงานเกี่ยวกับสัตว์ทดลอง

ขอขอบพระคุณสำนักงานกองทุนสนับสนุน (สกว.) และมหาวิทยาลัยธรรมศาสตร์ ที่ให้ทุนสนับสนุนการทำวิจัย ภายใต้ทุนพัฒนานักวิจัย (เมธีวิจัยสกว.) ประจำปี 2560 เรื่องการพัฒนาลิโพโซมแกนไซโคลเวียร์มุ่งเป้าสู่ดวงตาส่วนหลังด้วยการหยอดตา รหัสโครงการ RSA6080034

Abstract

Project Code : RSA6080034

Project Title : Development of liposomal ganciclovir targeting the posterior eye segment via topical administration

Investigator : Associate Professor Rathapon Asasutjarit, Ph.D.
Faculty of Pharmacy, Thammasat University

E-mail Address : rathapona@hotmail.com, rathapon@tu.ac.th

Project Period : 3 years

Abstract:

Ganciclovir (GCV) is an antiviral drug that is approved for treatment of cytomegalovirus (CMV) retinitis. Systemic administrations of GCV usually cause severe side effects; thus, formulations of GCV-loaded liposomes targeting the retina for local administrations were developed. The objectives of this study were to develop formulations of transferrin (Tf)-conjugated liposomes containing ganciclovir (Tf-GCV-LPs) that targeted the retina for intravitreal injection and topical instillation, to investigate their cytotoxicity and cellular uptake in the human retinal pigment epithelial cells, the ARPE-19 cells. Formulations of Tf-GCV-LPs were developed by varying the formulation compositions. They were prepared and evaluated their physicochemical properties. The optimized Tf-GCV-LPs were selected and subjected to the cytotoxicity test, cellular uptake evaluation in the ARPE-19 cells and antiviral activity test. The results showed that physicochemical properties of Tf-GCV-LPs were affected by the formulation compositions. The optimized Tf-GCV-LPs had a particle size lower than 100 nm with a negative value of zeta potential. They were safe for the ARPE-19 cells. Tf-GCV-LPs were taken up by these cells via Tf receptors-mediated endocytosis and showed inhibitory activity on CMV in the infected cells. The optimized Tf-GCV-LPs thus were a potential drug delivery system of GCV for treatment of CMV retinitis.

Keywords: Ganciclovir; Liposomes; Transferrin; Ophthalmic drug delivery; Targeted Drug delivery; Retina; Cytomegalovirus

บทคัดย่อ

รหัสโครงการ : RSA6080034

ชื่อโครงการ : การพัฒนาลิโพโซมแกนไซโคลเวียร์มุ่งเป้าสู่ดวงตาส่วนหลังด้วยการหยอดตา

ผู้วิจัย : รองศาสตราจารย์ ดร. รัฐพล อาษาสุจริต
คณะเภสัชศาสตร์ มหาวิทยาลัยธรรมศาสตร์

ที่อยู่อิเล็กทรอนิกส์ : rathapona@hotmail.com, rathapon@tu.ac.th

ระยะเวลาดำเนินงาน : 3 ปี

บทคัดย่อ:

แกนไซโคลเวียร์เป็นยาต้านไวรัสที่ได้รับการรับรองให้ใช้รักษาภาวะจอประสาทตาอักเสบจากการติดเชื้อไซโตเมกาโลไวรัส ซึ่งการนำส่งแกนไซโคลเวียร์แบบทั่วร่างกายมักทำให้เกิดอาการข้างเคียงที่รุนแรง ดังนั้นลิโพโซมที่บรรจุแกนไซโคลเวียร์มุ่งเป้าสู่จอประสาทตาที่บริหารเข้าสู่ดวงตาแบบใช้เฉพาะที่จึงถูกพัฒนาขึ้น วัตถุประสงค์ของงานวิจัยนี้ คือ เพื่อพัฒนาสูตรตำรับลิโพโซมที่บรรจุแกนไซโคลเวียร์ซึ่งมีการติดทรานส์เฟอร์ริน โดยมุ่งเป้าที่จอประสาทตาและสามารถนำส่งเข้าสู่ดวงตาโดยการฉีดเข้าสู่วุ้นดวงตา หรือ การหยอดตา เพื่อศึกษาความเป็นพิษและการนำเข้าสู่เซลล์ของเซลล์บุผิวจอประสาทตามนุษย์ สูตรตำรับของลิโพโซมที่บรรจุแกนไซโคลเวียร์ซึ่งมีการติดทรานส์เฟอร์รินได้ถูกพัฒนาขึ้น โดยการปรับเปลี่ยนส่วนประกอบตำรับ จากนั้นจึงถูกเตรียมและศึกษาสมบัติทางเคมีภายภาพ สูตรตำรับลิโพโซมที่บรรจุแกนไซโคลเวียร์ซึ่งมีการติดทรานส์เฟอร์รินที่เหมาะสมได้ถูกเลือก เพื่อนำมาศึกษาความเป็นพิษ การนำเข้าสู่เซลล์ของเซลล์บุผิวจอประสาทตามนุษย์ และฤทธิ์ต้านไวรัส จากผลการศึกษาพบว่าสมบัติทางเคมีกายภาพของลิโพโซมที่บรรจุแกนไซโคลเวียร์ซึ่งมีการติดทรานส์เฟอร์ริน ได้รับผลกระทบจากส่วนประกอบในสูตรตำรับ ลิโพโซมที่บรรจุแกนไซโคลเวียร์ซึ่งมีการติดทรานส์เฟอร์รินที่เหมาะสมนั้น มีขนาดอนุภาคต่ำกว่า 100 นาโนเมตร มีค่าศักย์ซีต้าที่เป็นลบ มีความปลอดภัยต่อเซลล์บุผิวจอประสาทตามนุษย์ ลิโพโซมที่บรรจุแกนไซโคลเวียร์ซึ่งมีการติดทรานส์เฟอร์รินถูกนำเข้าสู่เซลล์ด้วยกระบวนการเอ็นโดไซโตซิส ผ่านทางตัวรับของทรานส์เฟอร์ริน นอกจากนี้ยังมีฤทธิ์ยับยั้งไวรัสในเซลล์ที่มีการติดเชื้อด้วย ดังนั้นลิโพโซมซึ่งมีการติดทรานส์เฟอร์ริน จึงเป็นระบบนำส่งยาที่เหมาะสม สำหรับการนำส่งแกนไซโคลเวียร์ เพื่อการรักษาโรคจอประสาทตาอักเสบจากการติดเชื้อไซโตเมกาโลไวรัส

คำสำคัญ: ยาแกนไซโคลเวียร์, ลิโพโซม, ทรานส์เฟอร์ริน, การนำส่งยาเข้าสู่ดวงตา, การนำส่งยาแบบมุ่งเป้า, เรตินา, ไซโตเมกาโลไวรัส

โครงการ

การพัฒนาลิโพโซมแกนไซโคลเวียร์มุ่งเป้าสู่ดวงตาส่วนหลังด้วยการหยอดตา

1. Introduction

Ganciclovir (GCV) is an antiviral drug that is currently approved for treatment of cytomegalovirus (CMV) retinitis in immunocompromised patients (Kapanigowda et al., 2015; Moussa et al., 2018). It shows excellent activity against CMV with an IC_{50} of 900 ng/ml (Shen and Tu, 2007). Nowadays, administration of GCV via oral, intravenous, intravitreal route and scleral implant have been accepted for clinical treatment of CMV retinitis (Patel et al., 2013). Unfortunately, they sometimes cause some drawbacks resulting in complications, poor patient compliance, and eventually, unsuccessful treatment. Because of its poor ocular bioavailability, the physicians have to prescribe high doses of either oral GCV or GCV intravenous injections for their patients. Consequently, severe systemic adverse reactions, such as bone marrow suppression, are usually found in these patients (Shen and Tu, 2007). Meanwhile, intravitreal injections can reduce such systemic side effects because they can deliver the drug locally to the retina. However, they cause pain, hemorrhage in the eye, retinal detachment and endophthalmitis (Veloso et al., 1997). To minimize the risk of such adverse effects, the frequency and the volume of intravitreal injection should be lessened (Teoh et al., 2012). For GCV implants, they can prolong the duration of the action of GCV against CMV in the retina for 5-8 months. Nevertheless, they require surgical procedures to implant and to remove them after the drug has been exhausted. The implants also cause hemorrhage and retinal detachment as well as endophthalmitis (Veloso et al., 1997; Patel et al., 2013). Presently, the demand of GCV implants has been decreased; thus, they will no longer be available in the drug market (Lee et al., 2017).

To date, around 90% of marketed ophthalmic products are formulated in a form of a topical eye drop because they are easy to use by the patients themselves via simply instilling into the eye with accurate doses (Patel et al., 2013). However, this conventional dosage form is not effective for relieving disease symptoms in the posterior eye segment, particularly in the retina, because of rapid elimination from the eye surface and anatomical barriers of the eye (Chen, 2015). It was reported that the eye drop was dissipated within the first 15-30 seconds after instillation into the eyes and less than 5% of the applied drug reached intraocular tissues (Diebold and Calonge, 2010). Consequently, the GCV eye drop solution (0.15% w/w), which has been approved for

clinical application, is suitable for only treatment of viral infection in the anterior eye segment (Sahin and Hamrah, 2012).

Liposomes are one of the promising drug delivery systems, which are being widely investigated for targeted drug delivery (Sasaki et al., 2013; Lajunen et al., 2014). They are lipid bilayer vesicles composed mainly of phospholipids and cholesterol (Patel et al., 2013). The surface-modified liposomes can improve physicochemical properties of the drug and facilitate the drug absorption through the ocular tissue resulting in higher drug bioavailability in the posterior eye segment (Sasaki et al., 2013; Lajunen et al., 2014; Al-Halafi, 2014). They can control and sustain drug release at the targeted ocular tissue leading to decrease in frequency of drug administration (Kompella et al., 2013). More importantly, these liposomes can selectively deliver the drug to the retina by intravitreal injection (Bochot and Fattal, 2012) and instillation into the eye (Sasaki et al., 2013; Lajunen et al., 2014). For the intravitreal injection, the particle size of the surface-modified liposomes should be large enough to avoid rapid leakage into the blood vessel. At the same time, it should be small enough for injection and penetration through the ocular barrier (Jiang et al., 2018). Sakurai et al. (2001) reported that the nanoparticles possessing a size smaller than 200 nm could move toward the retina and retain in the retina for 2 months after intravitreal injection. Meanwhile, the larger particles (200 nm-2 μm) mostly distributed in the vitreous cavity. For topical instillation targeting the posterior eye segment, the surface-modified liposomes having particle sizes no greater than 100 nm were potential drug carriers (Sasaki et al., 2013). They could permeate across the arteries in conjunctiva and ciliary body, and then, distributed to the sclera, choroid, retinal pigment epithelium and retina (Sasaki et al., 2013; Kompella et al., 2013). Modifications of the liposome surface could enhance the chances of reaching the retina by retarding recognition and drug removal from blood circulation by phagocytic cells and promote drug binding to the specific receptors on the retinal cell surface such as transferrin (Tf)-receptors (Lajunen et al., 2014; Wang et al., 2012). Tf is a glycoprotein with a molecular weight of 80 kDa. It is an iron-transporter, which involves iron uptake in the retinal cells via endocytosis after binding to the Tf-receptor on the cell surface (Qian et al., 2002). The previous study (Lajunen et al., 2014) found that the liposomes, which had particle size lower than 100 nm and conjugated with Tf could express stronger fluorescent signals in the retina than such liposomes without Tf after they had been instilled into the eye for 15 minutes. This finding confirmed that the physicochemical properties of the liposomes affected their ability to deliver the drug specifically to the retina.

Although there are various formulations of GCV for relieving CMV retinitis available in the drug market, the ophthalmic products containing GCV-loaded liposomes (GCV-LPs) targeting the retina have not been currently available. In this study, GCV-LPs and their Tf-conjugated products (Tf-GCV-LPs) would be developed as alternative carriers of GCV for intravitreal injection and instillation into the eye.

The objectives of this study were to develop and optimize formulations of Tf-GCV-LPs, to determine their toxicity in the retinal cells and to investigate their cellular uptake by the retinal cells.

2. Materials and Methods

2.1 Chemicals

Cholesterol, 1,2-distearoyl-sn-glycero-3-phosphocholine (DSPC), 1,2-distearoyl-sn-glycero-3-phosphoethanolamine-N-[amino(polyethylene glycol)-2000] (DSPE-PEG), 1,2-distearoyl-sn-glycero-3-phosphoethanolamine-N-[maleimide (polyethylene glycol) - 2000] (DSPE-PEG-Mal) were purchased from Avanti Polar Lipids Inc. (USA). Ganciclovir (GCV) was provided by Tokyo Chemical Industry (Japan). Acetonitrile, chloroform, dichloromethane and methanol were purchased from RCL Labscan (Thailand). Cellulose dialysis tube with a molecular weight cutoff (MWCO) of 12 kDa, coumarin-6, 3-(4,5-dimethy-2-thiazolyl)-2,5-diphenyl-2H-tetrazolium bromide (MTT), dimethyl sulfoxide (DMSO), transferrin, 2-iminothiolane hydrochloride (Traut's reagent), Triton X-100 were obtained from Sigma-Aldrich (USA). Fetal bovine serum (FBS), penicillin-Streptomycin (P/S), trypan blue, trypsin-EDTA, phosphate buffer solution (PBS) (pH 7.4) and all cell culture media were supplied by Gibco (USA). Pierce's Bicinchoninic acid (BCA) protein assay kit was purchased from Thermo Fisher Scientific (USA). All other chemicals and solvents were of analytical grade and were used as received.

2.2 Preparation of GCV-Loaded Liposomes

GCV-loaded liposomes (GCV-LPs) were prepared by the reverse-phase evaporation (REV) technique following the procedure described in the previous study with some modifications (Shen and Tu, 2007). Briefly, DSPC, DSPE-PEG, DSPE-PEG-Mal and cholesterol of each formulation (Table 1) were dissolved in 30 ml of dichloromethane to obtain the organic phase. The aqueous phase (4 ml) containing GCV (2 mM) in PBS (pH 7.4) was injected into a beaker containing the organic phase. Thereafter, the mixture was homogenized by using an ultrasonic homogenizer (Biologics 150VT, USA) with a sonication intensity of 20% amplitude for 1 minute in an ice bath. The obtained water in oil emulsion was transferred to a round bottom flask. Dichloromethane consisting of the emulsion system was then evaporated in a rotary evaporator (Eyela SB-1300, Eyela, Japan) under reduced pressure at 32° C. After phase change of the emulsion was observed for 2 minutes, PBS (pH 7.4) was added to make a final volume of 40 ml, and the GCV-LPs were obtained.

The liposomes were sonicated to reduce the particle size and to obtain homogeneous particles by the ultrasonic homogenizer at 20% amplitude for 10 minutes in an ice bath. GCV-LPs were separated from the medium by using a stirred ultrafiltration cell (Millipore, USA) with an ultrafiltration membrane (10 kDa MWCO). Finally, PBS (pH

7.4) was added to re-suspend the retained GCV-LPs and to adjust the volume of GCV-LPs suspension to 1 ml. Since preservatives were not added to the formulations, all GCV-LPs were freshly prepared for each further experiment and used within 24 hours after preparation.

2.3 Preparation of Tf-Conjugated GCV-LPs

Tf-conjugated GCV-LPs (Tf-GCV-LPs) were prepared by conjugation of Tf to DSPE-PEG-Mal, a linker lipid, as described by Gijsens et al. (2002). Tf (80 µg) was added to 2 ml of borate-EDTA buffer (pH 8.5) containing 400 nmol of fresh Traut's reagent. The mixture was transferred to a lightproof bottle and shaken continuously for 1 hour at 25 °C to obtain thiolated Tf. The thiolated Tf was then concentrated by a centrifugal concentrator (Vivaspin 50 kDa of MWCO) (Satorius Filtrate B.V., Netherlands) at 2,000 rpm to make a volume of 200 µl, thereafter, 2 ml of phosphate buffer saline (PBS) (pH 8) was added and the system was concentrated again. The obtained thiolated Tf was immediately added to the GCV-LPs that had already been prepared in the previous section. The mixture was left for12 hours in a dark room at 25 °C without stirring for the complete reaction between thiolated Tf and DSPE-PEG-Mal. Finally, Tf-GCV-LPs were separated from the medium by using a centrifugal concentrator (Vivaspin 100 kDa MWCO) (Satorius Filtrate B.V., Netherlands) at 2,000 rpm to make a volume of 1ml for further experiments. All Tf-GCV-LPs were used in further experiments within 24 hours after preparation.

Table 1. Formulation compositions of GCV-LPs and Tf-GCV-LPs

Formulation	DSPC (μmol)	DSPE-PEG (μmol)	DSPE-PEG-Mal (μmol)	Cholesterol (C) (μmol)	Tf (μg)	Total phospholipids (P) (μmol)	Mole ratio of C:P
I.GCV-LPs-5.4-Mal0.2	5	0.2	0.2	3	-	5.4	0.6:1
II.GCV-LPs-4.4-Mal0.2	4	0.2	0.2	3	-	4.4	0.7:1
III.GCV-LPs-3.4-Mal0.2	3	0.2	0.2	3	-	3.4	0.9:1
IV.GCV-LPs-3.4-Mal0.1	3	0.3	0.1	3	-	3.4	0.9:1
V.GCV-LPs-3.4-Mal0.3	3	0.1	0.3	3	-	3.4	0.9:1
VI.GCV-LPs-3.4-Mal0.2-Tf	3	0.2	0.2	3	80	3.4	0.9:1
VII.GCV-LPs-3.4-Mal0.1-Tf	3	0.3	0.1	3	80	3.4	0.9:1
VIII.GCV-LPs-3.4-Mal0.3-Tf	3	0.1	0.3	3	80	3.4	0.9:1

2.4 Measurement of Particle Size, Polydispersity Index and Zeta Potential

Z-average and particle size distribution of GCV-LPs and Tf-GCV-LPs were determined immediately after they were prepared by the photon correlation spectroscopy technique via a Zetasizer Nano ZS (Malvern, UK). These parameters were reported in terms of their particle size and polydispersity index (PI), respectively. The zeta potential of these liposomes was measured by the electrophoretic light-scattering technique using the Zetasizer Nano ZS. All measurements were performed in triplicate.

2.5 Determination of Drug Entrapment Efficiency and Drug-Loading Capacity

The drug entrapment efficiency (EE) and drug-loading capacity (LC) of GCV-LPs and Tf-GCV-LPs were determined following the previous report with some modifications (Shen and Tu, 2007). Briefly, the unentrapped GCV was separated from the liposomes by using a stirred ultrafiltration cell (Millipore, USA) with an ultrafiltration membrane (MWCO 10 kDa) (Asasutjarit et al., 2015). Either GCV-LPs or Tf-GCV-LPs (1 ml) were lysed with Triton X-100 (1% w/v in 80% methanol solution) (1 ml). After mixing and centrifugation, the supernatant was chemically analyzed for GCV content by a UV-visible spectrophotometer (Shimadzu UV-Vis, Japan) at a wavelength of 254 nm (Shen and Tu, 2007). EE and LC of the liposomes were calculated using equation (1) and (2), respectively:

$$\text{EE}(\%) = \frac{\text{GCV entrapped in Tf-GCV-LPs}}{\text{total amount of GCV loaded}} \text{x}100 \quad (1)$$

$$\text{LC}(\%) = \frac{\text{GCV entrapped in Tf-GCV-LPs}}{\text{total amount of phospholipid and cholesterol}} \text{x}100 \quad (2)$$

2.6 Evaluation of Tf Conjugation Efficacy

Tf-GCV-LPs prepared in the previous experiment were concentrated to a volume of 100 µl by using a centrifugal concentrator (Vivaspin 100 kDa MWCO) (Satorius Filtrate B.V., Netherlands) at 2,000 rpm and transferred to a microfuge tube containing 400 µl of methanol. The mixture was then vortexed and centrifuged at 9,000 g (Scanspeed 1524, Labogene, Denmark) for 10 seconds. Chloroform (200 µl) was added and the sample was vortexed and centrifuged at the same condition. DI water (300 µl) was added to the centrifuge tube. The mixture was then vortexed and centrifuged at the same revolution for 1 minute. The upper phase was removed and discarded. Methanol (300 µl) was added to the centrifuge tube. The mixture was mixed and centrifuged at 9,000 g for 2

minutes. The supernatant was removed and the pellet was dried under nitrogen gas. The pellet was dispersed in PBS (pH 7.4) (20 µl). The content of Tf was determined by using a Pierce's bicinchonic acid (BCA) protein assay kit (Thermo Scientific, USA) (Anabousi et al., 2006).

2.7 Morphology Observation of GCV-LPs and Tf-GCV-LPs

The morphology of a representative of GCV-LPs and Tf-GCV-LPs were observed by the negative staining transmission electron microscopy technique (TEM) (Anabousi et al., 2005). One drop of each sample was placed on a copper grid coated carbon film. The specimens were stained with 2% w/v uranyl acetate solution and dried under room temperature after the excess liquid was removed. They were subsequently imaged by using a JEM-1400 (JEOL, Japan) transmission electron microscope at 100 kV.

2.8 Drug Release Study

The release of GCV from optimized GCV-LPs and Tf-GCV-LPs with various degrees of Tf conjugation was studied by using modified Franz diffusion cells. Briefly, one milliliter of each formulation containing GCV equivalent to 0.15 %w/v of GCV was loaded into a donor unit that was separated from a receptor unit by the cellulose dialysis membrane (MWCO 12 kDa). The receptor unit was filled with receiving solution, PBS (pH 7.4), which was stirred continuously with a magnetic stirrer and maintained at 37±1 °C. The receiving solution was withdrawn at 5, 10, 20, 30, 60 minutes, and then, every hour until 12 hours. Contents of GCV in the withdrawn receiving solution were analyzed by the UV-visible spectrophotometer (Shimadzu UV-Vis, Japan) at a wavelength of 254 nm.

2.9 FT-IR Spectroscopy Analysis

Fourier transform infrared (FT-IR) spectra of GCV, Tf, GCV-LPs, Tf-GCV-LPs and a physical mixture containing the same content of the ingredients of Tf-GCV-LPs were determined by using an FT-IR spectrometer (PerkinElmer Spectrum One, USA). Prior to the test, GCV-LPs and Tf-GCV-LPs were dried using the freeze-drying technique via an Eyela FD-1 freeze dryer (Eyela, Japan) for 24 hours without addition of any additives. Each sample was ground and mixed together with KBr powder at a ratio of 1:100. Then, it was pressed into pellets. The signal averages were obtained for 32 scans with a four cm^{-1} resolution from 4,000 to 500 cm^{-1}.

2.10 In Vitro Cytotoxicity Test by MTT Assay

The optimized Tf-GCV-LPs and GCV-LPs including GCV solution (in PBS pH 7.4) containing 0.15% w/v GCV were tested for their toxicity to the human retinal pigment epithelial cells, i.e., the ARPE-19 cells (CRL-2302; ATCC, USA). Each sample was diluted to the concentrations of 4, 40, 100, 200 and 400 µg/ml of GCV by a complete medium that contained Dulbecco's Modified Eagle Medium (DMEM), Ham's F12 nutrient mixture (F12) and fetal bovine serum (FBS). The cells were cultured in the complete medium and maintained at 37°C under 5% CO_2 atmosphere. They were seeded in 96-well plates with a density of $1x10^5$ cells/well/100 µl and incubated for 24 hours. Thereafter, each test sample (100 µl) was added to the well. The cells were incubated for 24 hours and washed twice with PBS (pH 7.4) at the end of incubation period. MTT solution in PBS (pH 7.4) (5 mg/ml) were added to each well and incubated for 4 hours. DMSO was added to dissolve the formazan crystal (100 µl/well). The optical density (OD) of each well was measured at 570 nm by a microplate reader (Fluostar Omega, BMG Labtech, Germany). The experiments were performed in three replications. Cell viability (CV) was calculated following equation (3). The test samples were considered to be totoxic to the cells if the CV (%) was less than 70%.

$$\text{CV } (\%) = \frac{\text{OD}_{\text{sample}}}{\text{OD}_{\text{control}}} \text{x}100 \qquad (3)$$

Where the OD_{sample} and $OD_{control}$ were an OD of media from the wells containing the ARPE-19 cells incubated with the samples and MTT solution and an OD of media from the wells containing the cells incubated with MTT solution without the samples, respectively.

2.11 Determination of Intracellular Uptake of Tf-GCV-LPs

The cellular uptake study of the liposomes were conducted in 6-well plates containing confluent cell layer of the ARPE-19 cells after seeding at a density of $2x10^5$ cells/well. The cells in each well were washed with PBS (pH 7.4) twice and incubated with one of the following samples, namely, 1) Tf-GCV-LPs, 2) Tf-GCV-LPs with the presence of free Tf in the medium (50 µg/ml) (Anabousi et al., 2006), 3) GCV-LPs and 4) GCV solution at a non-toxic concentration of the test samples for 24 hours. After incubation, the cells from each three-well, which were incubated with the same sample,

were pooled and transferred to new centrifuge tubes. The cells were lysed by Triton solution (1 %w/v) and freeze-thawed lysis technique. They were then centrifuged at 10,000 rpm at 4 °C for 5 minutes (Merodio et al., 2002). The supernatant was subjected to an analysis for GCV content by the high performance liquid chromatography (HPLC) technique. The samples for analysis were prepared as follows: the sample (200 µl) was mixed with 500 µl methanol that was already filled in a centrifuge tube. Thereafter, the mixture was centrifuged for 20 minutes at 60 rpm (Mikro 120 Hettich, Germany) to remove protein precipitates. The supernatant was transferred to a new centrifuge tube and dried under nitrogen gas at room temperature. The residue was dissolved in 50 µl of the mobile phase by swirl mixing for 1 minute and then injected to the HPLC instrument. The analysis of GCV content was performed by using an HPLC system (Shimadzu-SPD-20A, Japan) via a C8 column (4.6 x 150 mm, 5 µm) (Zorbax eclipse, Agilent, USA) connected to a guard column. Ten microliters of the sample were injected into the HPLC system. The sample was eluted by the mobile phase composing of 85% v/v acetonitrile and 0.05% w/v formic acid in water at a flow rate of 1.0 ml/min. A UV/visible detector was set at wavelength of 254 nm (Merodio et al., 2002).

2.12 Intracellular Uptake of Fluorescent Tf-GCV-LPs

The ARPE-19 cells were cultured in 6-well plates following the protocol described above and consequently incubated with one of the test samples as follows: 1) Tf-GCV-LPs, 2) Tf-GCV-LPs with the presence of free Tf in the medium (50 µg/ml) and 3) GCV-LPs at a non-toxic concentration of the test samples for 24 hours. All liposomes used in this study contained 0.05 µmol coumarin-6. They were prepared by using the same production process as Tf-GCV-LPs and GCV-LPs. The number of the ARPE-19 cells taking up the fluorescence liposomes was determined by the flow-cytometry technique in triplicate (Yang et al., 2009). Briefly, after incubation with the test samples, the cells were washed two times with PBS (pH 7.4) and harvested. The cell suspensions were centrifuged at 1,000 rpm for 5 minutes to remove the supernatant. The cell pellets were washed two times with cold PBS (pH 7.4) and re-suspended in 1X binding buffer to make a concentration of $1x10^5$ cells/100 µl and transferred to a 5-ml centrifuge tube. The cells were stained with propidium iodide (5 µl) (BD Pharmingen™, BD Biosciences, USA) and incubated in the dark at a room temperature for 15 minutes. The binding buffer (400 µl) was added to each tube to make a final volume of 500 µl/tube. Each cell suspension was analyzed by a flow-cytometry instrument (BD FACSVerse™, BD Biosciences, USA) at an excitation/emission wavelength of 490/520 and 535/617 nm for

coumarin-6 and propidium iodide, respectively. The fluorescent-activated cells sorting (FACS) plot was performed at least 30,000 events/sample and the data were analyzed by BD FACSVerse™ software (BD Biosciences, USA).

2.13 Determination of Inhibitory Activity of Tf-GCV-LPs on Cytomegalovirus Glycoprotein B Expression

The human-lung fibroblast cells, i.e., the MRC-5 cells (CCL-171; ATCC, USA), were used as a host of the cytomegalovirus (CMV) AD-169 (VR-538; ATCC, USA). They were cultured in 6-well plates containing complete Eagle's Minimum Essential Medium (EMEM) (2 ml) at a density of 2 x 10^5 cells/well until reaching 100% confluence. The cells were inoculated with CMV for 1 hour at a multiplicity of infection (MOI) of 0.1 pfu/cell. The unbound virus was removed; then, fresh culture medium (2 ml) was added to the wells. Twenty-four hours after inoculation, the cells in each well were incubated with one of the following test samples for 24 hour. They were 1) GCV solution, 2) Tf-GCV-LPs, 3) GCV-LPs at a concentration of 100 µg/ml of GCV, and 4) Tf-conjugated LPs without GCV (Blank Tf-GCV-LPs). Thereafter, the cells were washed twice with PBS (pH 7.4) and incubated in the fresh medium. Following a seven-day post treatment, the cells from each well were lysed and the cell proteins were extracted for the western blot analysis. Briefly, the protein extract was subjected to SDS-PAGE and transferred to a PVDF membrane. The membrane was then blocked by skim milk in Tris-buffered saline containing 0.2 % v/v Tween 20 (TBST) for 2 hours and incubated with 0.2 µg/ml mouse anti-CMV glycoprotein B (gB) monoclonal antibody (Abcam, UK) for 2 hours. The membrane was washed twice with TBST for 10 minutes and consequently incubated with rabbit anti-mouse IgG H&L (1: 100,000) that had been conjugated with horse-radish peroxidase (HRP) (Abcam, UK) for an hour. After washing the membrane with TBST, the signal was developed by the Amersham™ ECL™ Prime Western Blotting Detection Reagent (GE Healthcare, USA). The images were visualized by Amersham Imager 600 (GE Healthcare, USA). For actin loading-control detection, the membrane was stripped by a stripping solution for 45 minutes at 55 ºC. The membrane probed with 0.01 µg/ml mouse anti-actin antibody (R&D Systems, USA). Anti-mouse IgG conjugated with HRP and signal development were performed. The signal strength of each CMV gB and actin band were evaluated by the scientific image-analysis program, ImageJ (Schneider et al., 2012).

2.14 In vivo study

In vivo study of Tf-GCV-LPs was performed to determine their eye irritation potency including their distribution after being administered via either intravitreal injection or topical instillation. Male and female mice (BALB/c) those were 4 weeks old and weighed approximately 22 g were purchased from Nomura Siam International, Thailand. The procedure for use and care of the animals for this study was approved by the Animal Care Committee at Thammasat University (Protocol Number 009/2562). The animal experiment was conducted in full compliance with local, national, ethical, and regulatory principles and local licensing regulations, in accordance with the spirit of the Association for Assessment and Accreditation of Laboratory Animal Care (AAALAC) for international's expectations of animal care and use/ethics committees.

The test samples used in this study were 1) blank LPs for instillation (GCV-LPs-Blk-D), 2) blank LPs for intravitreal injection (GCV-LPs-Blk-Inj), 3) Tf-GCV-LPs for instillation (Tf-GCV-LPs-D), 4) Tf-GCV-LPs for intravitreal injection (Tf-GCV-LPs-inj), 5) GCV-LPs containing coumarin-6 for instillation (GCV-LPs-C-D), 6) GCV-LPs containing coumarin-6 for intravitreal injection (GCV-LPs-C-inj), 7) Tf-GCV-LPs containing coumarin-6 for instillation (Tf-GCV-LPs-C-D), and 8) Tf-GCV-LPs containing coumarin-6 for intravitreal injection (Tf-GCV-LPs-C-inj). Ten days prior to the *in vivo* distribution study of the liposomes, eye irritation potency of these test samples were investigated in the mice. They were divided into eight groups, those contained 2 mice/group (4 eyes). The mouse in each group received one of the test samples (5 µl) by using a needle (30G) with a syringe and a micropipette for intravitreal injection and instillation, respectively. Thereafter, the signs of eye irritation, i.e. edema of conjunctiva, redness, secretion, corneal opacity were observed at day 0, day 1, day 3 and day 7.

The *in vivo* distribution study of the liposomes was conducted at day 10 after eye irritation test. The mice were divided into 3 groups as follows:

Group 1: control group. This group consisted of one naïve mouse (2 eyes), one mouse receiving GCV-LPs-Blk-D and GCV-LPs-Blk-Inj in the left- and the right eye, respectively. Another one mouse receiving Tf-GCV-LPs-Blk-D and Tf-GCV-LPs-Blk-Inj in the left- and the right eye, respectively,

Group 2: for determination of distribution of the liposomes at 1 hour after drug administration. Group 2.1 consisted of three mice. They received GCV-LPs-C-D and CV-LPs-C-inj in the left- and the right eye, respectively. Group 2.2 consisted of three mice receiving Tf-GCV-LPs-C-D and Tf-CV-LPs-C-inj in the left- and the right eye, respectively.

Group 3: for determination of distribution of the liposomes at 3 hour after drug administration. Group 3.1 consisted of three mice. They received GCV-LPs-C-D and CV-LPs-C-inj in the left- and the right eye, respectively. Group 3.2 consisted of three mice receiving Tf-GCV-LPs-C-D and Tf-CV-LPs-C-inj in the left- and the right eye, respectively.

The intensity of fluorescent dye (coumarin-6) in the eye tissue was determined by the optical in-vivo imaging system (MS FX PRO, Bruker, Germany) and presented as %intensity change, which equaled the ratio of %intensity of the eye tissue treated with the fluorescence dye to that of the eye tissue of the naïve mouse. The conditions of the experiment were as follows: exposure time = 30 s, f-stop = 2.51, field of view = 60 mm, focal plane = 14 mm, excitation and emission wavelength = 470 and 535 nm, respectively.

2.15 Statistical Analysis

The results were presented as a mean ± standard deviation (SD). Statistical analysis for comparing treatment effects were performed by a one-way Analysis of Variance (ANOVA) with Tukey's multiple comparisons at a significant level of 0.05. Except for the *in vitro* cytotoxicity test, the comparison was performed by a two-way ANOVA to determine the effects of the test samples and their concentrations.

3. Results and Discussion

3.1 Preparation and Characterization of GCV-LPs and Tf-GCV-LPs

The physicochemical properties of GCV-LPs and Tf-GCV-LPs i.e. particles size, PI, zeta potential, EE and LC of GCV-LPs with variations in the contents of the ingredients are shown in Table 2. It was found that the particle size of the obtained liposomes was in a nanometer range of around 88-113 nm, with slightly broad particle size distribution and negative values of zeta potential between 0.3-0.4 and -31 to -34 mV, respectively. The EE and LC of these liposomes were slightly low around 32-36% and 12-16%, respectively. In particular, Tf-GCV-LPs had obviously larger particle sizes with reduction in zeta potential when compared to GCV-LPs. These results suggested that the physicochemical properties of GCV-LPs were affected by the formulation compositions.

3.1.1 Effect of Total Phospholipids Content

Table 2 shows that GCV-LPs containing various total phospholipids content with the fixed contents of cholesterol and GCV i.e. I.GCV-LPs-5.4-Mal0.2, II.GCV-LPs-4.4-Mal0.2 and III.GCV-LPs-3.4-Mal0.2 had statistical difference in particle size (*p*-value = 0.002), PI (*p*-value = 0.000), zeta potential (*p*-value = 0.000), EE (*p*-value = 0.001) and LC (*p*-value = 0.000). It was found that I.GCV-LPs-5.4-Mal0.2 containing the highest total phospholipids content (5.4 µmol) had a significantly larger particle size than that of II.GCV-LPs-4.4-Mal0.2 and III.GCV-LPs-3.4-Mal0.2, which contained a total phospholipid content of 4.4 and 3.4 µmol, respectively, (*p*-value = 0.000 and 0.000, respectively). The result suggested that the higher the total phospholipids content, the larger the particle size of GCV-LPs. This finding was consistent with the previous study that found the positive relationship of total phospholipids content and particle size of the liposomes (Shaker et al., 2017). It could be explained that the liposomes containing more content of total phospholipids had more viscosity of the organic phase of emulsions during production by the REV method (Shen ant Tu, 2007; Shaker et al., 2017). Consequently, the effective particle size reduction during production of GCV-LPs was difficult to perform. This phenomenon also led to broader particle size distribution of GCV-LPs containing higher total phospholipid content as well. Therefore, the PI value of I.GCV-LPs-5.4-Mal0.2 was higher than that of II.GCV-LPs-4.4-Mal0.2 ((*p*-value = 0.001) and III.GCV-LPs-3.4-Mal0.2 (*p*-value = 0.029), respectively.

Table 2. Physicochemical properties of GCV-LPs and Tf-GCV-LPs (mean±SD; n = 3)

Formulation	Particle size (nm)	PI	Zeta potential (mV)	%EE	%LC	%Tf conjugation
I.GCV-LPs-5.4-Mal0.2	112.7±1.8	0.44±0.02	-30.9±0.8	36.3±0.8	12.1±0.3	-
II.GCV-LPs-4.4-Mal0.2	96.3±1.7	0.38±0.01	-32.8±0.2	34.3±0.3	13.7±0.1	-
III.GCV-LPs-3.4-Mal0.2	88.7±1.5	0.32±0.05	-34.4±0.7	32.0±0.9	16.0±0.4	-
IV.GCV-LPs-3.4-Mal0.1	90.2±1.4	0.33±0.04	-34.2±0.8	31.7±1.7	15.9±0.9	-
V.GCV-LPs-3.4-Mal0.3	87.6±1.9	0.38±0.02	-33.4±1.6	32.5±0.4	16.2±0.2	-
VI.GCV-LPs-3.4-Mal0.2-Tf	94.3±2.0	0.35±0.03	-32.4±1.4	32.7±0.3	16.3±0.8	33.5±0.8
VII.GCV-LPs-3.4-Mal0.1-Tf	91.8±2.2	0.39±0.01	-32.8±0.9	32.4±0.6	16.2±1.2	27.7±0.7
VIII.GCV-LPs-3.4-Mal0.3-Tf	102.5±1.8	0.38±0.04	-31.9±0.3	33.0±0.8	15.5±0.5	35.4±0.7

The results shown in Table 2 indicated that all GCV-LPs possessed a negative value of zeta potential due to the negatively charged phospholipids, i.e., DSPE-PEG and DSPE-PEG-Mal (Eloy et al., 2014). It was found that I.GCV-LPs-5.4-Mal0.2, which contained a higher total phospholipids content than II.GCV-LPs-4.4-Mal0.2 and III.GCV-LPs-3.4-Mal0.2, respectively, had a lower absolute value of negative zeta potential than II.GCV-LPs-4.4-Mal0.2 and III.GCV-LPs-3.4-Mal0.2 at *p*-values of 0.042 and 0.002, respectively. From this finding, it was shown that DSPC, a major phospholipid of the formulation, had a neutral charge at pH 7.4, whereas, DSPE-PEG and DSPE-PEG-Mal individually had one negative charge at this pH. Therefore, the magnitudes of negative surface charge of these liposomes were derived from the amount of DSPE-PEG and DSPE-PEG-Mal. Although the zeta potential of II.GCV-LPs-4.4-Mal0.2 and III.GCV-LPs-3.4-Mal0.2 were not significantly different at a *p*-value of 0.788, their zeta potential tended to increase when the DSPC content was decreased. These findings resulted from the fact that the negative charges of the liposomal surface from both DSPE-PEG and DSPE-PEG-Mal molecules were less interfered by the small amount of DSPC (Schubert and Muller-Goymann, 2005).

The entrapment efficiencies (EE) of GCV in GCV-LPs shown in Table 2 suggested that 32-36% of loaded GCV could be entrapped in the liposomes. These low EEs of GCV-LPs were result of the hydrophilic property of GCV and small particle size of GCV-LPs leading to a small volume of the aqueous phase of these liposome vesicles (Shen and Tu, 2007; Eloy et al., 2014). The tendency of EE of I.GCV-LPs-5.4-Mal0.2, II.GCV-LPs-4.4-Mal0.2 and III.GCV-LPs-3.4-Mal0.2 showed the direct relationship with their particle sizes. As previously mentioned, there was a positive relationship between the total phospholipids content and the particle sizes of GCV-LPs; thus, the total phospholipids content also has influence on EE. Another factor that affected EE was the interaction between GCV and the compositions of lipid bilayer. Since cholesterol could suppress water penetration into the hydrocarbon chain of the phospholipids (Eloy et al., 2014), GCV would mainly interact with the polar head group of the phospholipid molecules and thus it accumulated in the aqueous core of the liposomes. Consequently, GCV was supposed to be encapsulated in the liposomes containing a high mole ratio of cholesterol to total phospholipids content (C:P) with low EE. The results shown in Table 2 pointed out the fact that III.GCV-LPs-3.4-Mal0.2 containing the highest mole ratio of C:P at 0.9:1 could encapsulate GCV less than II.GCV-LPs-4.4-Mal0.2 (*p*-value = 0.013) and I.GCV-LPs-5.4-Mal0.2 (*p*-value = 0.001), which contained a mole ratio of C:P at 0.7:1 and 0.6:1, respectively. These results thus agreed with the aforementioned

assumption. On the contrary, the LC of GCV-LPs decreased with an increase in the total phospholipids content. It was found that LC of I.GCV-LPs-5.4-Mal0.2 was significantly lower than that of II.GCV-LPs-4.4-Mal0.2 (*p*-value = 0.001) and III.GCV-LPs-3.4-Mal0.2 (*p*-value = 0.000), respectively. This result was a consequence of the lowest ratio of the amount GCV entrapped in the liposomes to the amount of total phospholipids and cholesterol for encapsulation of GCV. This result confirmed that I.GCV-LPs-5.4-Mal0.2 could entrap larger amount of GCV than that of II.GCV-LPs-4.4-Mal0.2 and III.GCV-LPs-3.4-Mal0.2 because it contained larger amount of phospholipid and cholesterol in the vesicles.

As previously mentioned, the nanoparitcles with a size less than 100 nm were suitable as targeted drug delivery system for both intravitreal injection and topical instillation. Thus, III.GCV-LPs-3.4-Mal0.2, which had the smallest particle size with the average particle size less than 100 nm was chosen as a prototype of GCV-LPs and used for Tf conjugation to prepare Tf-GCV-LPs.

3.1.2 Effect of the DSPE-PEG and DSPE-PEG-Mal Content

To prepare Tf-GCV-LPs with various degrees of Tf conjugation on their surfaces, the content of PEGylated phospholipids, in particular DSPE-PEG-Mal, were varied. In this study, DSPE-PEG was used as a stabilizer because it could increase physical stability through steric effects, increase solubility and reduce immunogenicity in the body. It could also provide a stealth effect; thus, the obtained liposomes would have the ability to escape from the reticuloendothelial system (Kim et al., 2012) whereas DSPE-PEG-Mal was used as a linker phospholipid that contained a maleimide group for conjugation to thiolated Tf (Gijsens et al., 2002). The total amount of DSPE-PEG and DSPE-PEG-Mal in GCV-LPs was fixed at 0.4 μmol (as shown in Table 1) with the same content of cholesterol as III.GCV-LPs-3.4-Mal0.2. The physicochemical properties of IV.GCV-LPs-3.4-Mal0.1 and V.GCV-LPs-3.4-Mal0.3 were compared to those of III.GCV-LPs-3.4-Mal0.2. It is pertinent to note that particle size, PI, zeta potential, EE and LC of these three GCV-LPs were not statistically different at *p*-value of 0.320, 0.970, 0.663, 0.738, and 0.740, respectively. Thus, it could be concluded that a change in the small content of DSPE-PEG-Mal and DSPE-PEG at a constant total amount of these PEGylated phospholipids did not cause any obvious alteration in the physicochemical properties of GCV-LPs. It can be explained by the similarity in chemical structure of DSPE-PEG and DSPE-PEG-Mal that would not cause any obvious changes in the liposomes properties.

3.1.3 Effect of Tf Conjugation

Tf-GCV-LPs were prepared with different percentage of Tf conjugation on the liposomal surface through variations in the DSPE-PEG-Mal content. The results shown in Table 2 suggest that the higher the DSPE-PEG-Mal content, the higher the percentage of Tf conjugation. Thus, it was established as the fact that the higher DSPE-PEG-Mal content in Tf-GCV-LPs provided more maleimide molecules to couple the thiolated Tf. Among three formulations of VI.GCV-LPs-3.4-Mal0.2-Tf, VII.GCV-LPs-3.4-Mal0.1-Tf and VIII.GCV-LPs-3.4-Mal0.3-Tf; VIII.GCV-LPs-3.4-Mal0.3-Tf that contained the highest content of DSPE-PEG-Mal and thus had more Tf content on the liposomal surfaces than that of the former two formulations at *p*-values of 0.046 and 0.000, respectively.

Comparison of physicochemical properties of these Tf-GCV-LPs indicated that VIII.GCV-LPs-3.4-Mal0.3-Tf had larger particle size than that of VI.GCV-LPs-3.4-Mal0.2-Tf (*p*-value= 0.016) and VII.GCV-LPs-3.4-Mal0.1-Tf (*p*-value= 0.004), whereas the latter two formulations had statistically comparable particle size (*p*-value= 0.484). Although the particle size of Tf-GCV-LPs tended to be larger than that of GCV-LPs containing the same content DSPE-PEG and DSPE-PEG-Tf as seen in Table 2, only VIII.GCV-LPs-3.4-Mal0.3-Tf had a statistically larger particle size than that of V.GCV-LPs-3.4-Mal0.3 (*p*-value of 0.000). These results suggested that conjugation of Tf on the liposomal surface up to around 35% caused a significant change in particle size when compared to their prototypes prior to conjugation. This finding was consistent with the previous studies reporting that conjugation of Tf to PEGylated liposomes sometimes increased the hydrodynamic size representing the size of the particle (Chen et al., 2016) because of a change in the spatial structure of the DSPE-PEG molecules (Chen et al., 2011). Note that the zeta potential of Tf-GCV-LPs tended to decrease with an increase in %Tf conjugation because of the interference of Tf on the net charge of liposomal surface. However, a statistical comparison of these three formulations for PI, zeta potential, EE and LC of Tf-GCV-LPs containing various degrees of Tf did not show significant difference at *p*-values of 0.524, 0.060, 0.932, 0.913, respectively. Furthermore, a statistical comparison of these parameters before- and after conjugation to Tf of GCV-LPs indicated the similarity of their values at *p*-value $>$ 0.05. These results suggested that conjugation of Tf on the liposomal surface up to 35% did not cause significantly different PI, zeta potential, EE and LC. Since VI.GCV-LPs-3.4-Mal0.2-Tf had particle sizes less than 100 nm with optimal degree of Tf conjugation, it was selected for the cellular uptake study of the ARPE-19 cells.

3.2 Morphology of GCV-LPs and Tf-GCV-LPs

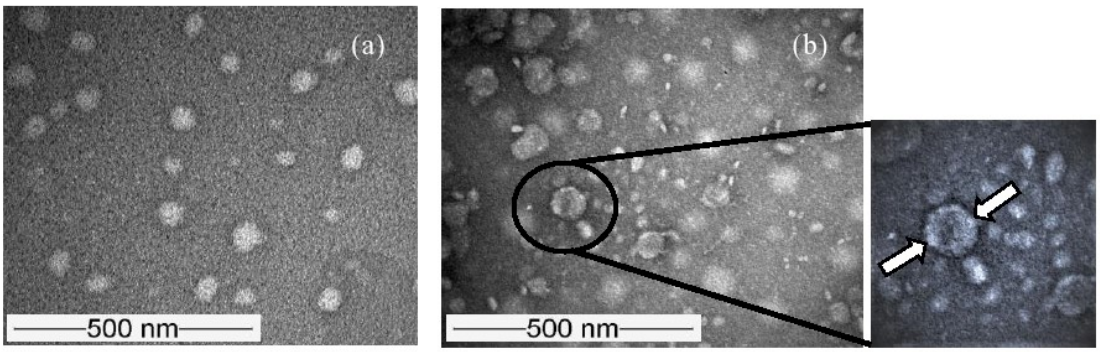

Fig. 1 TEM photographs: (a) III.GCV-LPs-3.4-Mal0.2 and (b) VI.GCV-LPs-3.4-Mal0.2-Tf.

TEM photographs of the representative of GCV-LPs and Tf-GCV-LPs, i.e., III.GCV-LPs-3.4-Mal0.2 and VI.GCV-LPs-3.4-Mal0.2-Tf are shown in Fig. 1 (a) and (b), respectively. The pictures showed that both GCV-LPs and Tf-GCV-LPs had spherical shape with particle sizes less than 100 nm. The pictures showed a slightly broad particle size distribution of both liposomes that were consistent with PI determined by the photon correlation technique. Fig. 1 (b) showed small structures of Tf on the liposomal surface of VI.GCV-LPs-3.4-Mal0.2-Tf, in addition, these small structures were also found in the space between Tf-GCV-LPs. Meanwhile, they were absent on III.GCV-LPs-3.4-Mal0.2 surface and the space between GCV-LPs as shown in Fig. 1 (a). These findings agreed with the TEM photographs of Tf conjugated liposomes reported in the previous publication (Anabousi et al., 2006) and confirmed the conjugation of Tf to the liposomal surface.

3.3 Drug Release Study

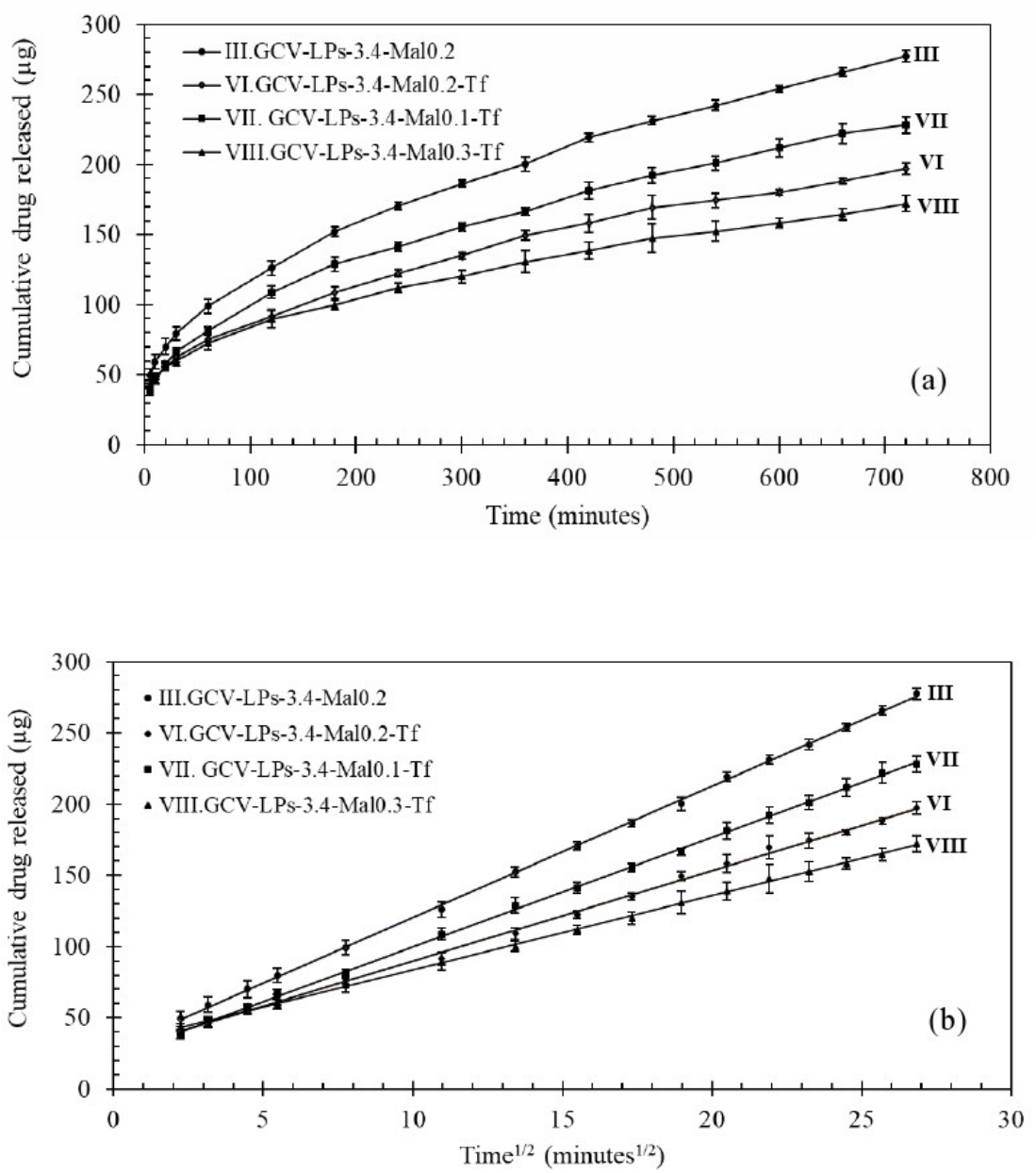

Fig. 2 Release profiles of GCV: (a) plots of cumulative drug released against time and (b) plots of cumulative drug released against time$^{1/2}$.

A drug release study of III.GCV-LPs-3.4-Mal0.2, VI.GCV-LPs-3.4-Mal0.2-Tf, VII.GCV-LPs-3.4-Mal0.1-Tf and VIII.GCV-LPs-3.4-Mal0.3-Tf was performed to determine the release kinetic of GCV and the effect of Tf conjugation percentage on GCV release from the liposomes. *In vitro* release profiles shown in Fig. 2 (a) and (b) indicated that the release kinetic of GCV from III.GCV-LPs-3.4-Mal0.2, VI.GCV-LPs-3.4-Mal0.2-Tf, VII.GCV-LPs-3.4-Mal0.1-Tf and VIII.GCV-LPs-3.4-Mal0.3-Tf followed the Higuchi's model with an r^2 of 0.9996, 0.9985, 0.9996 and 0.9995, respectively. This finding suggested that diffusion of GCV molecules was the main factor controlling drug release of GCV from these liposomes (Haidar et al., 2008). This released was the result of the presence of PEG grafted onto the liposomal surfaces and the interaction between GCV and PEG as seen in the case of III.GCV-LPs-3.4-Mal0.2. In addition, these results indicated that Tf conjugation to the liposomes markedly affected the release rate of GCV. It was found that the release rate of GCV from VIII.GCV-LPs-3.4-Mal0.3-Tf (5.21±0.17 μg/minute$^{1/2}$) that conjugated to Tf with the highest percentage conjugation was less than that of VI.GCV-LPs-3.4-Mal0.2-Tf (6.34±0.29 μg/minute$^{1/2}$), VII.GCV-LPs-3.4-Mal0.1-Tf (7.71±0.16 μg/minute$^{1/2}$) and III.GCV-LPs-3.4-Mal0.2 (9.22±0.25 μg/minute$^{1/2}$) at a *p*-value of 0.001, 0.000 and 0.000, respectively. This result implied that Tf could impede diffusion of GCV resulting in slow release rates and a prolonged release of GCV over 12 hours.

3.4 FT-IR Spectroscopy Analysis

The interactions between GCV and the components consisting of the liposomes were determined by using FT-IR spectroscopy technique. The FT-IR spectra of GCV and Tf are shown in Fig. 3 (a) and (b), respectively. The FT-IR spectrum of GCV exhibits its characteristic bands at wavenumbers of 1,180-1,223 cm^{-1}, which represented the C-O-C asymmetric stretch, 1,305 cm^{-1} for C-N stretch. It also shows important bands at 2,942 cm^{-1}, 3,170 cm^{-1}, 3,319 cm^{-1} and 3,417 cm^{-1} responding to the stretch of aliphatic C-H, aromatic C-H, N-H and O-H, respectively (Sarbajna et al., 2011). The FT-IR spectrum of Tf shows the bands of tyrosine at 1,163 cm^{-1}, 1,240 cm^{-1}, 1,517cm^{-1}. It also shows the band of amide group I at a wavenumber of 1,656 cm^{-1} and N-H stretch at 3,307 cm^{-1} (Duca et al., 2018). The FT-IR spectrum of a physical mixture of Tf, GCV, DSPE-PEG-Mal, DSPC and cholesterol at the same weight ratio as the compositions consisting of the obtained VI.GCV-LPs-3.4-Mal0.2-Tf is presented in Fig. 3 (c).

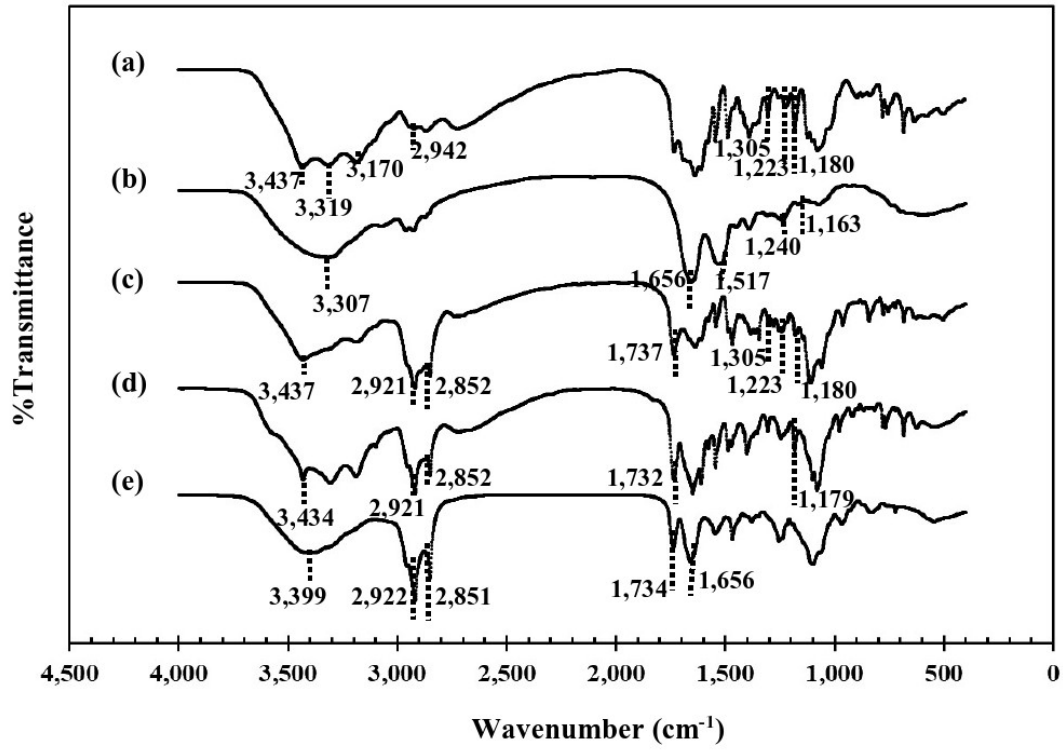

Fig. 3 FT-IR spectra: (a) GCV; (b) Tf; (c) a physical mixture of Tf, GCV, DSPE-PEG-Mal, DSPC and cholesterol; (d) III.GCV-LPs-3.4-Mal0.2 and (e) VI.GCV-LPs-3.4-Mal0.2-Tf.

It illustrated the characteristic bands of the phospholipids at a wavenumber of 1,737 cm^{-1} that was assigned for the C=O stretch of the ester bond between the fatty acid chain and the head group. The strong bands at 2,852 cm^{-1} and 2,921 cm^{-1} responded to the CH_2 symmetric and symmetric stretch modes, respectively, in the phospholipids and cholesterol molecules (Briuglia et al., 2015). Furthermore, this spectrum also showed the same characteristic bands of GCV at wavenumbers of 1,180-1,223 cm^{-1}, 1,305 cm^{-1} and 3,437 cm^{-1} as shown in Fig. 3 (a). These results implied that there was no significant interaction between GCV and the compositions consisting of the physical mixture. However, the characteristic bands of Tf could not be observed in the FT-IR spectrum because of the small amount of Tf in the formulation. Fig. 3 (d) shows some trivial shifts of the characteristic bands of GCV from wavenumbers of 1,180 cm^{-1} and 3,437 cm^{-1} to 1,179 cm^{-1} and 3,434 cm^{-1}, respectively. Furthermore, the bands at wavenumbers of 1,223 cm^{-1} and 1,305 cm^{-1}, which were found in the FT-IR spectrum of standard GCV (Fig. 3 (a)) and that of the physical mixture (Fig. 3 (b)) were absent in the

FT-IR spectrum of III.GCV-LPs-3.4-Mal0.2. This phenomenon also occurred with the characteristic band of the phospholipid that shifted from the wavenumber of 1,737 cm^{-1} to 1,732 cm^{-1}. This pattern suggested that there were some interactions between the ingredients comprising III.GCV-LPs-3.4-Mal0.2 and GCV molecules (34). Fig. 4 (e) indicated that there were strong interactions between GCV and the ingredients consisting of VI.GCV-LPs-3.4-Mal0.2-Tf, such as hydrogen bonds. It caused some trivial shifts of the characteristic band of the phospholipids and cholesterol including the absence of the important characteristic bands of GCV and Tf. These interactions thus significantly affected the release rate of GCV from the liposomes conjugated to various Tf contents as reported in the previous section.

3.5 In Vitro Cytotoxicity Test by MTT Assay

Since VI.GCV-LPs-3.4-Mal0.2-Tf had optimal %Tf conjugation with acceptable particle size, PI, zeta potential and EE, it was selected for the cellular uptake study in the ARPE-19 cells and thus determined a maximum concentration that did not cause toxicity towards the cells. In this study, III.GCV-LPs-3.4-Mal0.2 and GCV solution were also subjected to the test to determine the effect of the formulation compositions on the cytotoxicity to the ARPE-19 cells. The concentrations of the test samples were calculated based on the concentration of GCV entrapped in the liposomes. Fig. 4 shows that the CV (%) of the ARPE-19 cells those exposed to the test samples containing 2-200 µg/ml of GCV were more than 70%. The results clearly indicated that the ARPE-19 cells could tolerate all test samples at the entire concentrations of GCV consisting of the formulations. Therefore, it could be concluded that VI.GCV-LPs-3.4-Mal0.2-Tf, III.GCV-LPs-3.4-Mal0.2 and GCV solution were safe for the ARPE-19 cells.

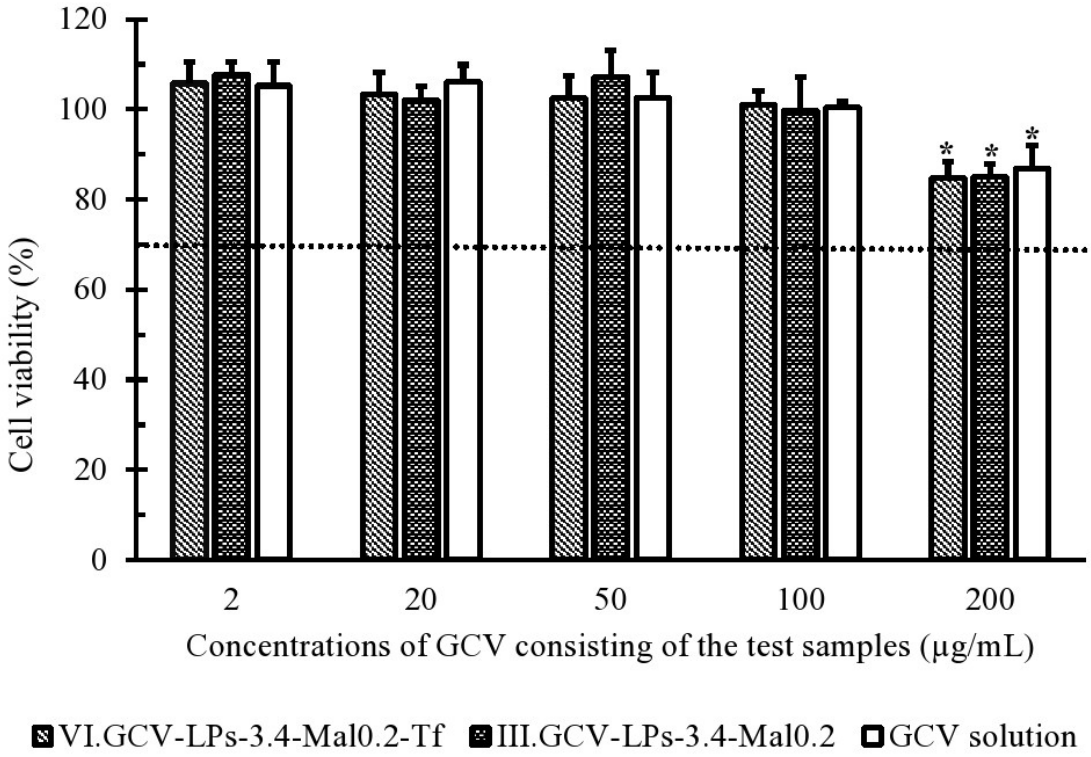

Fig. 4 Cell viability (%) of the ARPE-19 cells after incubation with various concentrations of GCV consisting of VI.GCV-LPs-3.4-Mal0.2-Tf, III.GCV-LPs-3.4-Mal0.2 and GCV solution for 24 hours (mean±SD; n=3).

The CV of the cells incubated with these three samples were comparable for each GCV concentration (*p*-value = 0.411), it suggested that the formulations of GCV i.e. VI.GCV-LPs-3.4-Mal0.2-Tf, III.GCV-LPs-3.4-Mal0.2 and GCV solution did not significantly affect the CV of the ARPE-19 cells. However, the CV of the ARPE-19 cells was markedly decreased to around 80% when they were incubated with VI.GCV-LPs-3.4-Mal0.2-Tf, III. GCV-LPs-3.4-Mal0.2 and GCV solution containing the highest GCV concentration (200 µg/ml) (*p*-value = 0.000, 0.000 and 0.000, respectively). These results might come from the higher concentration of the ingredients consisting of the formulations such as phospholipids and GCV leading to an inappropriate environment for cell growth. In addition, GCV is generally toxic to the viral infected cells and the rapidly propagating cells i.e. blood cells and their precursors; sometimes, it could cause adverse effects to the DNA during the DNA synthesis process of the normal cell because its molecular structure is similar to guanosine (Janoly-Dumenil et al., 2009). To avoid any toxicity from overly high concentrations of the formulations, test samples containing GCV at a concentration equivalent to 100 µg/ml were selected for further studies.

3.6 Intracellular Uptake Study of Tf-GCV-LPs in the ARPE-19 Cells by HPLC Method

The study of the intracellular uptake of VI.GCV-LPs-3.4-Mal0.2-Tf with and without the presence of free Tf in the medium, III.GCV-LPs-3.4-Mal0.2 and GCV solution in the ARPE-19 cells were performed by incubation of the cells with the test samples for 24 hours at a concentration equivalent to 100 µg/ml of GCV consisting of the formulation. The cells were extracted and chemically analyzed for GCV concentration by the HPLC technique.

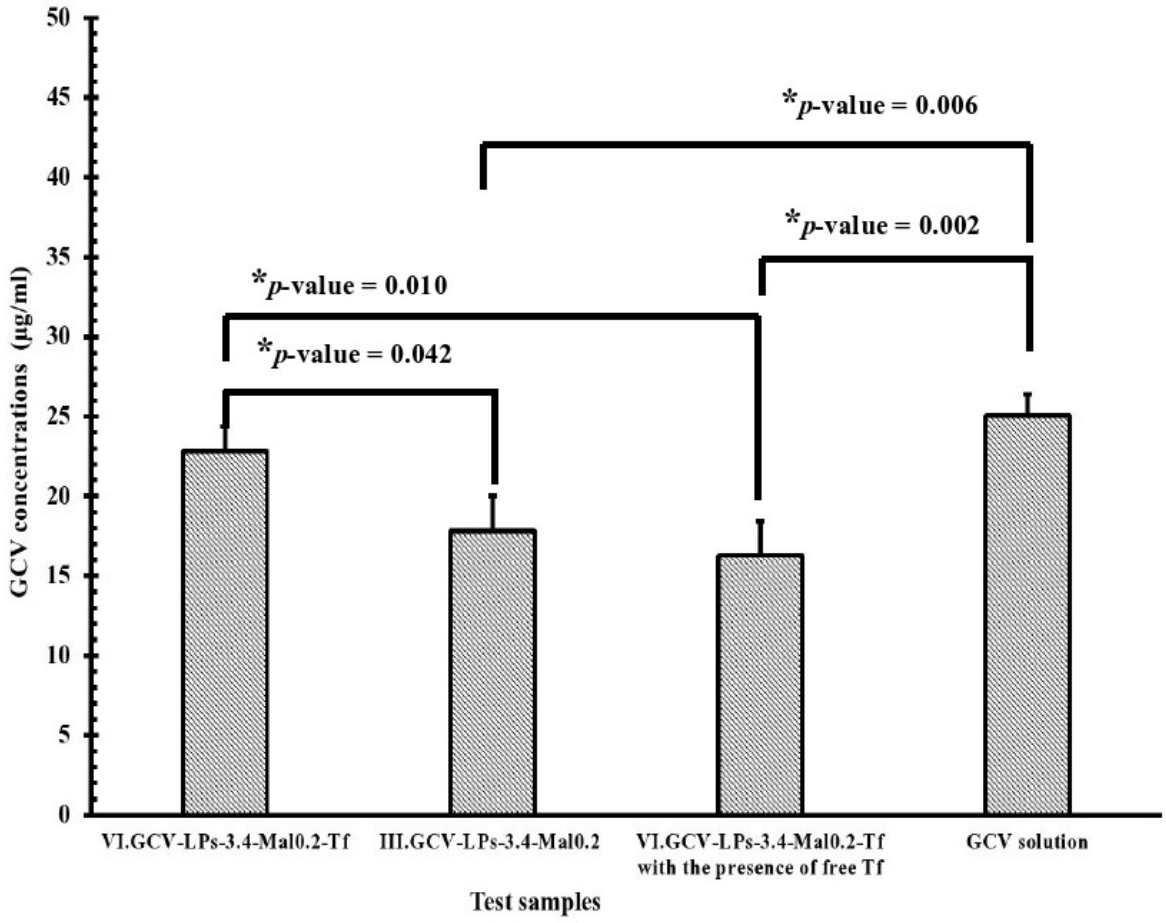

Fig. 5 GCV concentrations in the ARPE-19 cells after incubation with VI.GCV-LPs-3.4-Mal0.2-Tf, III.GCV-LPs-3.4-Mal0.2, VI.GCV-LPs-3.4-Mal0.2-Tf with the presence of free Tf and GCV solution for 24 hours, which were analyzed by HPLC technique (mean±SD; n=3).

Fig. 5 contains an illustration showing that the concentration of GCV from the cells, which were incubated with VI.GCV-LPs-3.4-Mal0.2-Tf, was significantly higher than that of the GCV from the cells incubated with III.GCV-LPs-3.4-Mal0.2 and VI.GCV-LPs-3.4-Mal0.2-Tf with the presence of free Tf at *p*-values of 0.042 and 0.010, respectively. By contrast, the intracellular concentrations of GCV taken up from III.GCV-LPs-3.4-Mal0.2 and VI.GCV-LPs-3.4-Mal0.2-Tf with the presence of free Tf were not significantly different at a *p*-value of 0.743. These results implied that Tf conjugation to GCV-LP surface could facilitate the cellular internalization of GCV properly. In addition, the presence of free Tf in the cell culture medium obviously decreased the intracellular uptake of VI.GCV-LPs-3.4-Mal0.2-Tf. This effect was caused by the free Tf competitively binding to the Tf receptors (TfRs) on the cell surface and blocked the TfRs before binding to Tf on the surface of VI.GCV-LPs-3.4-Mal0.2-Tf. It thus confirmed the fact that VI.GCV-LPs-3.4-Mal0.2-Tf could be taken up into the ARPE-19 cells by TfRs-mediated endocytosis (Anabousi et al., 2006).

The statistical comparison between the concentrations of GCV extracted from the cells, which had been incubated with VI.GCV-LPs-3.4-Mal0.2-Tf and GCV solution suggested that they were comparable at a *p*-value of 0.501. This finding might result from the cellular absorption of GCV molecules from GCV solution through diffusion and in particular purine nucleobase and nucleoside transporters (Perrottet et al., 2009). Since intracellular accumulation of the GCV molecules from GCV solution did not need the complicated drug release process, the absorption rate of GCV into the cells was higher than that of the liposomal GCV. Consequently, the concentration of GCV in the ARPE-19 cells treated with GCV solution was higher than that of the GCV in the cells incubated with III.GCV-LPs-3.4-Mal0.2 and VI.GCV-LPs-3.4-Mal0.2-Tf with the presence of free Tf at a *p*-value of 0.006 and 0.002, respectively.

Although the results suggested that the concentration of GCV taken up from GCV solution was comparable to that of GCV from VI.GCV-LPs-3.4-Mal0.2-Tf, the GCV solution was not appropriate for ophthalmic drug delivery. In particular, the drug-targeting posterior eye segment that was aimed to administer by either intravitreal or topical instillation because of rapid elimination from the targeting sites (Al-Halafi, 2014; Chen, 2015). Therefore, VI.GCV-LPs-3.4-Mal0.2-Tf capable of delivering GCV into the cells was accepted for these purposes.

3.7 Intracellular Uptake of Fluorescent Tf-GCV-LPs in the ARPE-19 Cells

The intracellular uptake study of fluorescent VI.GCV-LPs-3.4-Mal0.2-Tf, III.GCV-LPs-3.4-Mal0.2 and VI.GCV-LPs-3.4-Mal0.2-Tf with the presence of free Tf were conducted to determine the number of living ARPE-19 cells, which could take up these fluorescent liposomes into the cells. The quadrant LR (Courmarin-6^{+}, Propidium iodide^{-}) of fluorescent-activated cells-sorting (FACS) plots depicted in Fig. 6 (a)-(c) shows that the number of the living ARPE-19 cells that took up the fluorescent liposomes were around 80-90% of the cell population.

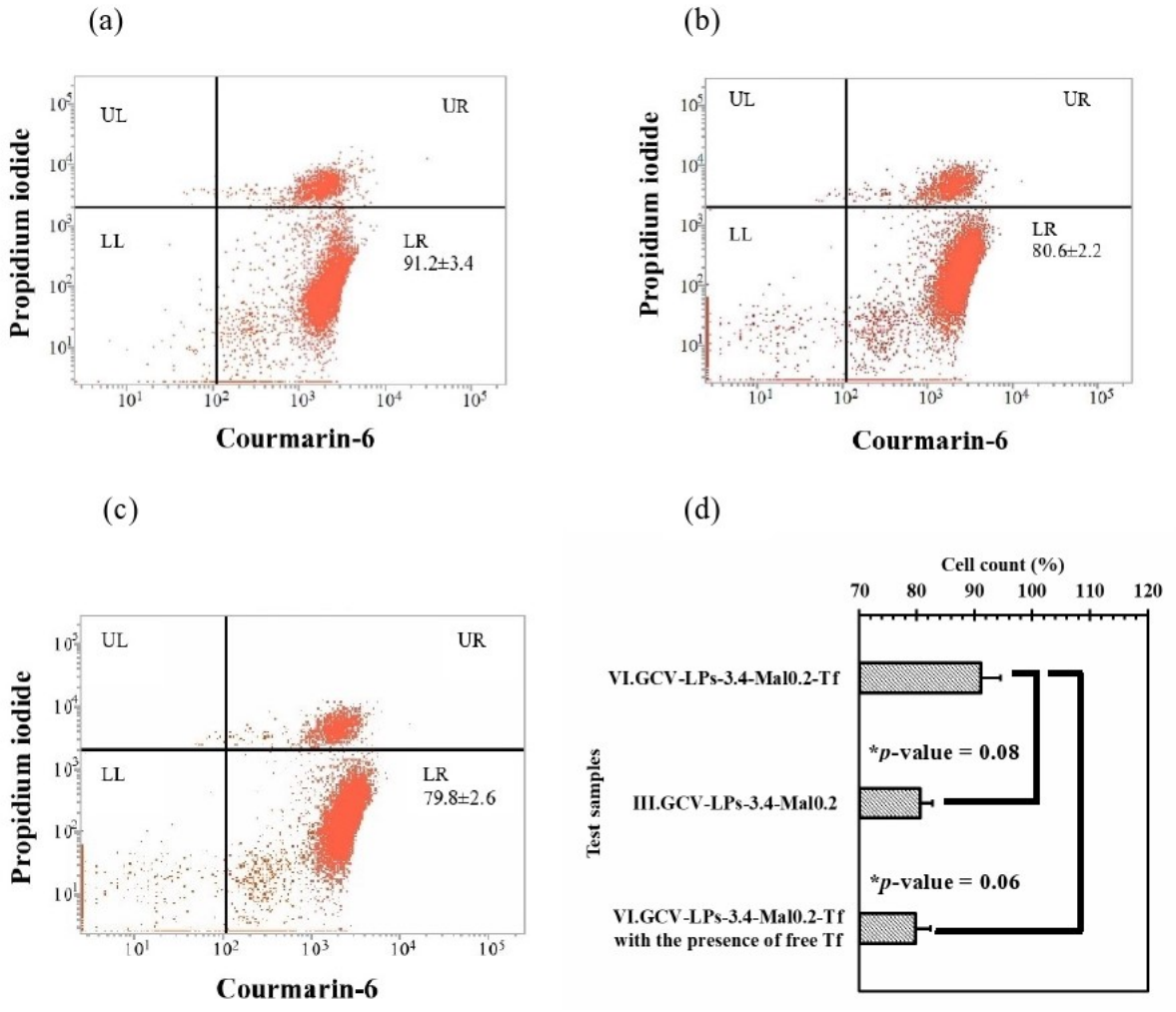

Fig. 6 Number of the living ARPE-19 cells taking up fluorescent Tf-GCV-LPs: (a)-(c) FACs plots of number of the living ARPE-19 cells taking up VI.GCV-LPs-3.4-Mal0.2-Tf, III.GCV-LPs-3.4-Mal0.2 and VI.GCV- LPs-3.4-Mal0.2-Tf with the presence of free Tf, respectively; (d) comparison of numbers of the living ARPE-19 cells taking up fluorescent Tf-GCV-LPs after incubation for 24 hours (mean±SD; n=3).

This outcome suggested that after incubation for 24 hours, all fluorescent liposomes could be taken up by the ARPE-19 cells. The uptake levels of the cells incubated with VI.GCV-LPs-3.4-Mal0.2-Tf, III.GCV-LPs-3.4-Mal0.2 and VI.GCV-LPs-3.4-Mal0.2-Tf with the presence of free Tf as shown in Fig. 6 (d) illustrated that they were statistically different and depended on Tf conjugation and free Tf in the medium. Fig. 6 (a) shows that the number of the living ARPE-19 cells taking up fluorescent VI.GCV-LPs-3.4-Mal0.2-Tf (without free Tf) was higher than that of the living cells that took up fluorescent III.GCV-LPs-3.4-Mal0.2 (Fig. 6 (b)) and fluorescent VI.GCV-LPs-3.4-Mal0.2-Tf with the presence of free Tf (Fig. 6 (c)) at a *p*-value of 0.08 and 0.06, respectively. These findings were in good agreement with the results of intracellular uptake study of Tf-GCV-LPs by HPLC method and confirmed that the cellular internalization via TfRs-mediated endocytosis facilitated the uptake of VI.GCV-LPs-3.4-Mal0.2-Tf into the ARPE-19 cells. Note that III.GCV-LPs-3.4-Mal0.2 did not contained Tf on the surface; it could be internalized into the cells by 80.6% of the cell population. This finding indicated that III.GCV-LPs-3.4-Mal0.2 could be internalized by the cells with other less effective endocytosis pathways (Eloy et al., 2014). For the case of VI.GCV-LPs-3.4-Mal0.2-Tf with the presence of free Tf, it could be internalized into the cells by 79.8% of the cell population which was comparable to that of III.GCV-LPs-3.4-Mal0.2 (*p*-value =0.934). This was due to the fact that TfRs were blocked by the free Tf leading to unreachable binding sites for the targeted ligand on the surface of VI.GCV-LPs-3.4-Mal0.2-Tf (Chen et al., 2016). However, VI.GCV-LPs-3.4-Mal0.2-Tf with the presence of Tf would bind to the TfRs when the new TfRs have been presented on the cell surface once the blocking Tf was taken up via endocytosis and the recycling process of TfRs was complete (Qian et al., 2002).

3.8 Inhibitory Activity of Tf-GCV-LPs on CMV Glycoprotein B Expression

To determine the activity of Tf-GCV-LPs against CMV, the MRC-5 cells were used as host cells for CMV infection because of their effective permissiveness to CMV infection and replication (Merodio et al., 2002). The MRC-5 cells were incubated with VI.GCV-LPs-3.4-Mal0.2-Tf at a concentration equivalent to 100 µg/ml of GCV consisting of the formulation, which was not toxic to the MRC-5 cells (data not shown). The signal strength of the expressed CMV glycoprotein B (CMV gB) from the western blot assay was then quantified and normalized by the signal strength of the actin of the MRC-5 cells as shown in Fig. 7 (a) and (b) (Schneider et al., 2012).

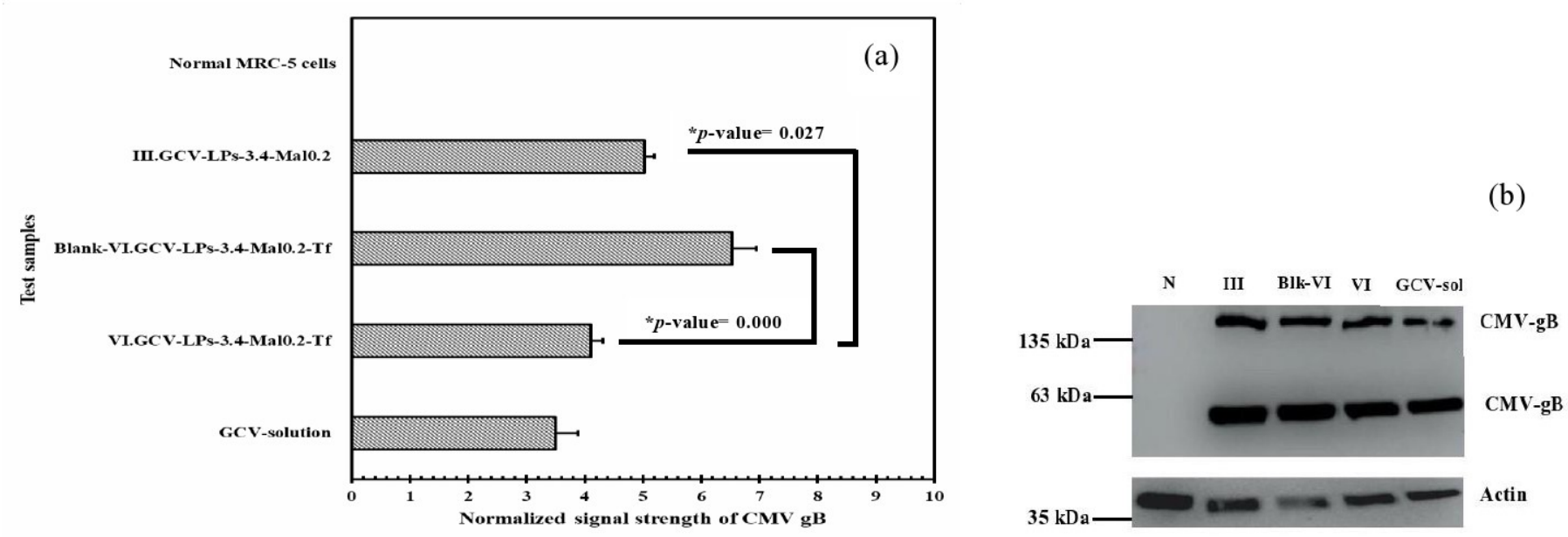

Fig. 7 Normalized signal strengths of CMV gB from the MRC-5 cells: (a) comparison of signal strengths of CMV gB from the normal MRC-5 cells and the MRC-5 cells after CMV infection and incubation with III.GCV-LPs-3.4-Mal0.2, Blank-VI.GCV- LPs-3.4-Mal0.2-Tf, VI.GCV- LPs-3.4-Mal0.2-Tf and GCV solution (mean±SD; n=3); (b) CMV gB from the western blot assay. Lane N: the normal MRC-5 cells; Lane III, Blk-VI, VI, GCV-sol: CMV gB from the infected MRC-5 cell that were incubated with III.GCV-LPs-3.4-Mal0.2, Blank-VI.GCV- LPs-3.4-Mal0.2-Tf, VI.GCV- LPs-3.4-Mal0.2-Tf and GCV solution, respectively.

The infected MRC-5 cells were incubated with one of the following test samples, namely, III.GCV-LPs-3.4-Mal0.2, Blank-VI.GCV-LPs-3.4-Mal0.2-Tf (without GCV), VI.GCV-LPs-3.4-Mal0.2-Tf and GCV solution to investigate the effect of formulation compositions on anti-CMV activity of the liposomes. Their normalized signal strengths of the expressed CMV gB representing the quantity of CMV were reported.

Two factions of CMV gB from the western blot assay, which is an important glycoprotein of CMV for fusion to the plasma membrane of the host cells during cellular entry process (Wille et al., 2013), could be found in only infected MRC-5 cells as can be seen in in Fig. 7 (b). The CMV gB could not, however, be found in the normal MRC-5 cells that were not infected by CMV (Lane N). Fig. 7 (a) indicated that the normalized signal strength of CMV gB from the cells treated with VI.GCV-LPs-3.4-Mal0.2-Tf was significantly lower than the normalized signal strength of CMV gB from the cells treated with III.GCV-LPs-3.4-Mal0.2 and Blank-VI.GCV-LPs-3.4-Mal0.2-Tf at a *p*-value of 0.027 and 0.000, respectively. This finding pointed out that VI.GCV-LPs-3.4-Mal0.2-Tf had a higher potential for inhibiting the expression of CMV gB in the infected cell than the latter two test samples. This result was due to the effective cellular internalization of VI.GCV-LPs-3.4-Mal0.2-Tf by the cells, which was facilitated by the Tf grafted on the liposome surface. After the specific binding of Tf to TfRs, the complexes of Tf-TfRs were clustered into clathrin-coated pits. They were then internalized and enclosed with endocytic vesicles (Qian et al., 2002). The GCV encapsulated in the liposomes was thus protected from the endosome environment, allowing a controlled release into the cells. It was in good agreement with the previous studies showing that delivery of doxorubicin encapsulated in Tf-conjugated liposomes could increase the uptake rate into the tumor cells and that it selectively enhanced cytotoxicity to the cancerous human pulmonary (Anabousi et al., 2006) and hepatoma (Li et al., 2009) epithelial cell lines. The lower potency of III.GCV-LPs-3.4-Mal0.2 for inhibition of CMV gB expression was the result of the PEGylated phospholipids without conjugation. They could reduce the uptake of the liposomes into the cells through sterically impeding the access to specific receptors on the cell surface (Anabousi et al., 2006) resulting in less effective cellular internalization by the cells as mentioned in the previous section. Since Blank-VI.GCV-LPs-3.4-Mal0.2-Tf did not contained GCV, the infected cells incubated with these liposomes showed the highest signal strength of CMV gB. This result strongly supported that the anti-CMV activity of VI.GCV-LPs-3.4-Mal0.2-Tf was from the GCV.

The comparison between signal strengths of CMV gB from incubation with VI.GCV-LPs-3.4-Mal0.2-Tf and GCV solution demonstrated that they were statistically

comparable at a *p*-value of 0.153. This finding resulted from GCV molecules from GCV solution could penetrate into the infected cells properly through a diffusion process and nucleoside transporters as previously mentioned. More importantly, the GCV molecules in the infected cells would be rapidly phosphorylated by the protein kinase of CMV without the drug release process unlike the liposomal GCV. Therefore, GCV solution could eradiate CMV effectively resulting in a comparable signal strength of CMV gB to that obtained from the infected cells treated with VI.GCV-LPs-3.4-Mal0.2-Tf.

3.9 In vivo study

3.9.1 Eye irritation test of GCV-LPs and Tf-GCV-LPs

The results of the *in vivo* study indicated that all liposomes delivered by topical instillation did not cause any signs of eye irritation during the entire experiment period. Unfortunately, intravitreal injection of all liposomes caused significantly enlargement of the eye balls. This result was due to increase in the volume of the vitreous humor after injection of the test samples. However, the size of the eye ball was gradually decreased in the next days and completely recovered at day 7 after injection. Furthermore, intravitreal injection of these test samples did not cause the signs of eye irritation during the entire experiment as well.

3.9.2 *In vivo* distribution study of GCV-LPs and Tf-GCV-LPs

The results of *in vivo* distribution study of GCV-LPs and Tf-GCV-LPs are shown in Fig. 8 and 9.

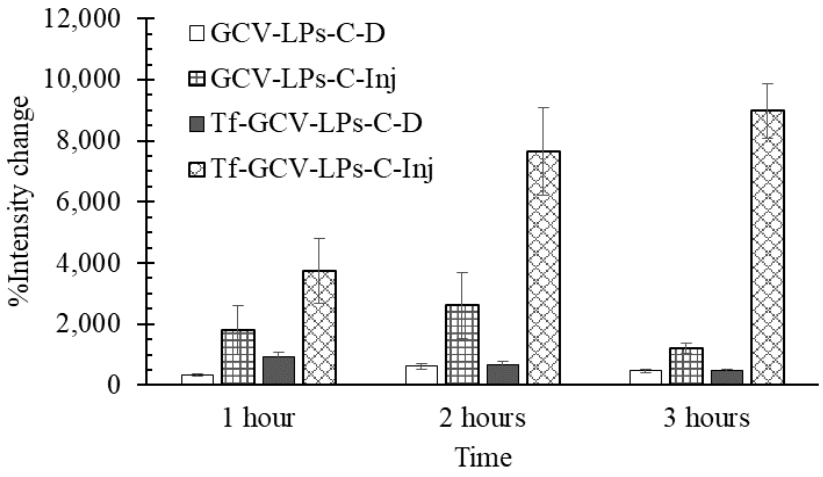

Fig. 8 %Intensity change of the fluorescent dye in the eye after treatment with the fluorescent liposomes at various times.

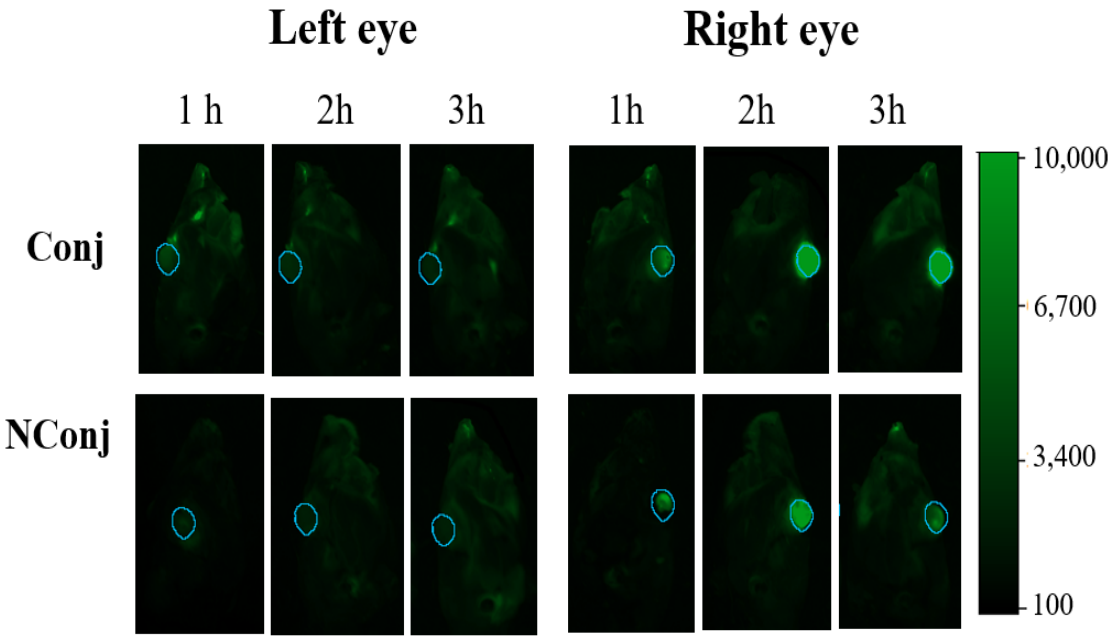

Fig. 9 Intensity of the fluorescent dye in the eye after treatment with the fluorescent liposomes at various times: left and right eye represented the drug administration via instillation and intravitreal injection, repectively.

They illustrated that %intensity change of the fluorescent signal in the eye receiving Tf-GCV-LPs-C-Inj was higher than that of the eye receiving GCV-LPs-C-Inj, Tf-GCV-LPs-C-D and GCV-LPs-C-D, respectively at 1, 2, 3 hours. Therefore, intravitreal injection of the fluorescent liposomes, in particular the fluorescent liposomes conjugated with Tf could promote distribution of the fluorescence dye in eye more than instillation of these liposomes. Furthermore, liposomes conjugated with Tf also increased accumulation time of the fluorescent dye in the eye.

4. Conclusions

Formulations of GCV-LPs and Tf-GCV-LPs were developed for drug delivery of the GCV targeting posterior eye segment by intravitreal injection and topical instillation. Thus, they should have particle size smaller than 100 nm with a surface modification in order to increase cell-uptake efficiency. It was found that the physicochemical properties of GCV-LPs, i.e., particle size, PI, zeta potential, EE(%) and LC(%) were affected by the formulation compositions. The results indicated that an increase in total phospholipids led to an increase in particle size, PI and EE(%) of GCV-LPs. Unfortunately, the higher total of phospholipids that consisted of the formulation caused lower values of zeta potential and LC (%) of GCV-LPs. Modification of DSPE-PEG and DSPE-PEG-Mal at a constant total content of these PEGylated phospholipids did not cause any obvious change in particle size, PI, zeta potential, EE(%) or LC(%) of GCV-LPs. However, GCV-LPs containing more DSPE-PEG-Mal content was able to conjugate to more Tf and had larger particle sizes than that of GCV-LPs, which contained less DSPE-PEG-Mal content. In this study, the conjugation of GCV-LPs to Tf up to 35% could not significantly alter their PI, zeta potential, EE(%) and LC(%) when compared to those of GCV-LPs before conjugation to Tf. The drug release kinetic of GCV from GCV-LPs and Tf-GCV-LPs were consistent with the Higuchi's model, with high values of r^2. This finding indicated that the interactions between GCV and liposomal vesicles that were confirmed by FT-IR spectroscopy analysis. *In vitro* cytotoxicity test of GCV-LPs and Tf-GCV-LPs suggested that they were safe for the ARPE-19 cells with percentage cell viability of 80-100%. The results of intracellular uptake of the optimized Tf-GCV-LPs in the ARPE-19 cells indicated that they were taken up by the cells via TfRs-mediated endocytosis. Furthermore, they could inhibit expression of CMV gB after infection effectively. Therefore, the optimized Tf-GCV-LPs, which were developed in this study, could be accepted as a potential drug delivery system for targeted GCV delivery to the retina for treatment of CMV retinitis.

Acknowledgments

The authors gratefully acknowledge the financial supports by The Thailand Research Fund (TRF) and Thammasat University for the Research Career Development Grant: grant No. RSA6080034.

5. References

Al-Halafi, A.M., 2014. Nanocarriers of nanotechnology in retinal diseases. Saudi. J. Ophthalmol. 28, 304-309.

Anabousi, S., Laue, M., Lehr, C.M., Bakowsky, U., Ehrhardt, C., 2005. Assessing transferrin modification of liposomes by atomic force microscopy and transmission electron microscopy. Eur. J. Pharm. Biopharm. 60, 295-303.

Anabousi, S., Bakowsky, U., Schneider, M., Huwer, H., Lehr, C.M., Ehrhardt, C., 2006. *In vitro* assessment of transferrin-conjugated liposomes as drug delivery systems for inhalation therapy of lung cancer. Eur. J. Pharm. Sci. 29, 367-374.

Asasutjarit, R., Theerachayanan, T., Kewsuwan, P., Veeranodha, S., Fuongfuchat, A., Ritthidej, G.C., 2015. Development and evaluation of diclofenac sodium loaded-N-trimethyl chitosan nanoparticles for ophthalmic use. AAPS PharmSciTech. 16, 1013-1024.

Bochot, A., Fattal, E., 2012. Liposomes for intravitreal drug delivery: a state of the art. J. Control. Release. 161, 628-34.

Briuglia, M.L., Rotella, C., McFarlane, A., Lamprou, D.A., 2015. Influence of cholesterol on liposome stability and on in vitro drug release. Drug. Deliv. Transl. Res. 5, 231-242.

Chen, C.W., Lu, D.W., Yeh, M.K., Shiau, C.Y., Chiang, C.H., 2011. Novel RGD-lipid conjugate-modified liposomes for enhancing siRNA delivery in human retinal pigment epithelial cells. Int. J. Nanomedicine. 6, 2567-2580.

Chen, H., 2015. Recent developments in ocular drug delivery. J. Drug. Target. 23, 597-604.

Chen, Z.L., Huang, M., Wang, X.R., Fu, J., Han, M., Shen, Y.Q., et al., 2016. Transferrin-modified liposome promotes alpha-mangostin to penetrate the blood-brain barrier. Nanomedicine. 12, 421-430.

Diebold, Y., Calonge, M., 2010. Applications of nanoparticles in ophthalmology. Prog. Retin. Eye. Res. 29, 596-609.

Duca, G., Anghel, L., Erhan, R.V., 2018. Structural aspects of lactoferrin and serum transferrin observed by FT-IR spectroscopy. Chem. J. Mold. 13, 111-116.

Eloy, J.O., Claro de Souza, M., Petrilli, R., Barcellos, J.P., Lee, R.J., Marchetti, J.M., Liposomes as carriers of hydrophilic small molecule drugs: strategies to enhance encapsulation and delivery. Colloids. Surf. B., Biointerfaces. 123, 345-363.

Gijsens, A., Derycke, A., Missiaen, L., De Vos, D., Huwyler, J., Eberle, A., et al., 2002. Targeting of the photocytotoxic compound AlPcS4 to Hela cells by transferrin

conjugated PEG-liposomes. Int. J. Cancer. 101, 78-85.

Haidar, Z.S., Hamdy, R.C., Tabrizian, M., 2008. Protein release kinetics for core-shell hybrid nanoparticles based on the layer-by-layer assembly of alginate and chitosan on liposomes. Biomaterials. 29, 1207-1215.

Janoly-Dumenil, A., Rouvet, I., Bleyzac, N., Bertrand, Y., Aulagner, G., Zabot, M.T., 2009. Effect of duration and intensity of ganciclovir exposure on lymphoblastoid cell toxicity. Antivir. Chem. Chemother. 19, 257-262.

Jiang, S., Franco, Y.L., Zhou, Y., Chen, J., 2018. Nanotechnology in retinal drug delivery. Int. J. Ophthalmol. 11, 1038-1044.

Kapanigowda, U.G., Nagaraja, S.H., Ramaiah, B., Boggarapu, P.R., 2015. Improved intraocular bioavailability of ganciclovir by mucoadhesive polymer based ocular microspheres: development and simulation process in Wistar rats. Daru. 23:49.

Kim, T.H., Jo, Y.G., Jiang, H.H., Lim, S.M., Youn, Y.S., Lee, S., et al., 2012. PEG-transferrin conjugated TRAIL (TNF-related apoptosis-inducing ligand) for therapeutic tumor targeting. J. Control. Release. 162, 422-428.

Kompella, U.B., Amrite, A.C., Pacha, R.R., Durazo, S.A., 2013. Nanomedicines for back of the eye drug delivery, gene delivery, and imaging. Prog. Retin. Eye. Res. 36, 172-98.

Lajunen, T., Hisazumi, K., Kanazawa, T., Okada, H., Seta, Y., Yliperttula, M., et al., 2014. Topical drug delivery to retinal pigment epithelium with microfluidizer produced small liposomes. Eur. J. Pharm. Sci. 62, 23-32.

Lee, J.H., Agarwal, A., Mahendradas, P., Lee, C.S., Gupta, V., Pavesio, C.E., et al., 2017. Viral posterior uveitis. Surv. Ophthalmol. 62, 404-445.

Li, X., Ding, L., Xu, Y., Wang, Y., Ping, Q., 2009. Targeted delivery of doxorubicin using stealth liposomes modified with transferrin. Int. J. Pharm. 373, 116-123.

Merodio, M., Espuelas, M.S., Mirshahi, M., Arnedo, A., Irache, J.M., 2002. Efficacy of ganciclovir- loaded nanoparticles in human cytomegalovirus (HCMV)-infected cells. J. Drug. Target. 10, 231-238.

Moussa, K., Doan, T., Stewart, J.M., Shantha, J., Gonzales, J., Acharya, N., et al., 2018. Cytomegalovirus retinitis associated with occlusive vasculopathy in an elderly, human immunodeficiency virus-negative man. Retin. Case. Brief. Rep. 12, S114-S117.

Patel, A., Cholkar, K., Agrahari, V., Mitra, A.K., 2013. Ocular drug delivery systems: An overview. World. J. Pharmacol. 2, 47-64.

Perrottet, N., Decosterd, L.A., Meylan, P., Pascual, M., Biollaz, J., Buclin, T., 2009.

Valganciclovir in adult solid organ transplant recipients: pharmacokinetic and pharmacodynamic characteristics and clinical interpretation of plasma concentration measurements. Clin. Pharmacokinet. 48, 399-418.

Qian, Z.M., Li, H., Sun, H., Ho, K., 2002. Targeted drug delivery via the transferrin receptor-mediated endocytosis pathway. Pharmacol. Rev. 54, 561-587.

Sahin, A., Hamrah, P., 2012. Acute Herpetic Keratitis: What is the Role for Ganciclovir Ophthalmic Gel? Ophthalmol. Eye. Dis. 4, 23-34.

Sakurai, E., Ozeki, H., Kunou, N., Ogura, Y., 2001. Effect of particle size of polymeric nanospheres on intravitreal kinetics. Ophthalmic. Res. 33, 31-36.

Sarbajna, R.M., Preetam, A., Devi, A.S., Suryanarayana, M.V., Sethi, M., Dutta, D., 2011. Studies on Crystal Modifications of Ganciclovir. Mol. Cryst. Liq. Cryst. 537, 141-154.

Sasaki, H., Karasawa, K., Hironaka, K., Tahara, K., Tozuka, Y., Takeuchi, H., 2013. Retinal drug delivery using eyedrop preparations of poly-L-lysine-modified liposomes. Eur. J. Pharm. Biopharm. 83, 364-369.

Schneider, C.A., Rasband, W.S., Eliceiri, K.W., 2012. NIH Image to ImageJ: 25 years of Image analysis. Nat. Methods. 9, 671-675.

Schubert, M.A., Muller-Goymann, C.C., 2005. Characterisation of surface-modified solid lipid nanoparticles (SLN): influence of lecithin and nonionic emulsifier. Eur. J. Pharm. Biopharm. 61, 77-86.

Shaker, S., Gardouh, A.R., Ghorab, M.M., 2017. Factors affecting liposomes particle size prepared by ethanol injection method. Res. Pharm. Sci. 12, 346-352.

Shen, Y., Tu, J., 2007. Preparation and ocular pharmacokinetics of ganciclovir liposomes. AAPS. J. 9, E371-E377.

Teoh, S.C., Ou, X., Lim, T.H., 2012. Intravitreal ganciclovir maintenance injection for cytomegalovirus retinitis: efficacy of a low-volume, intermediate-dose regimen. Ophthalmology. 119, 588-595.

Veloso, A.A.Jr., Zhu, Q., Herrero-Vanrell, R., Refojo, M.F. 1997. Ganciclovir-loaded polymer microspheres in rabbit eyes inoculated with human cytomegalovirus. Invest. Ophthalmol. Vis. Sci. 38, 665-675.

Wang, W., Zhou, F., Ge, L., Liu, X., Kong, F., 2012. Transferrin-PEG-PE modified dexamethasone conjugated cationic lipid carrier mediated gene delivery system for tumor-targeted transfection. Int. J. Nanomedicine. 7, 2513-2522.

Wille, P.T., Wisner, T.W., Ryckman, B., Johnson, D.C., 2013. Human cytomegalovirus

(HCMV) glycoprotein gB promotes virus entry in trans acting as the viral fusion protein rather than as a receptor-binding protein. MBio. 4, e00332-13.

Yang, X., Koh, C.G., Liu, S., Pan, X., Santhanam, R., Yu, B., et al., 2009. Transferrin receptor-targeted lipid nanoparticles for delivery of an antisense oligodeoxyribonucleotide against Bcl-2. Mol. Pharm. 6, 221-230.

Output จากโครงการวิจัยที่ได้รับทุนจาก สกว.

สัญญาเลขที่ RSA6080034 **ชื่อโครงการ** การพัฒนาลิโพโซมแกนไซโคลเวียร์มุ่งเป้าสู่ดวงตาส่วนหลังด้วยการหยอดตา

หัวหน้าโครงการ รองศาสตราจารย์ ดร. รัฐพล อาษาสุจริต

หน่วยงาน คณะเภสัชศาสตร์ มหาวิทยาลัยธรรมศาสตร์

โทรศัพท์ 081-8312902 **โทรสาร** 02-5643156 **อีเมล์** rathapona@hotmail.com; rathapon@tu.ac.th

1. ผลงานตีพิมพ์ในวารสารวิชาการนานาชาติ

1) Asasutjarit, R., Managit, C., Phanaksri, T., Treesuppharat, W, Fuongfuchat, A. Formulation development and in vitro evaluation of transferrin-conjugated liposomes as a carrier of ganciclovir targeting the retina. **Int J Pharm**. 2020; 577:119084. **(Published)-***รายละเอียดอยู่ในรายงานฉบับสมบูรณ์*

2) Asasutjarit, R., Sookdee, P., Veeranondha, S., Fuongfuchat, A., Itharat, A. Application of Film-forming solution as a transdermal delivery system of piperine-rich herbal mixture extract for anti-inflammation. **Heliyon**. xxx; x(x):xxx. **(Under Review for the 3rd Revised Version)** –*รายละเอียดอยู่ในรายงานฉบับสมบูรณ์ โดยในงานวิจัยนี้ ได้มีการประเมินการก่อระคายเคืองดวงตาของผลิตภัณฑ์ตาม OECD guideline โดยศึกษาความเป็นพิษในเซลล์กระจกตา SIRC cells ด้วย short time exposure (STE) test*

2. การนำผลงานวิจัยไปใช้ประโยชน์

- เชิงวิชาการ (มีการพัฒนาการเรียนการสอน/สร้างนักวิจัยใหม่)

: การสร้างนักวิจัยใหม่ ระดับปริญญาโท: นางสาวนวรัตน์ สุกใส คณะเภสัชศาสตร์ ม.ธรรมศาสตร์

3. การเสนอผลงานในที่ประชุมวิชาการ

Oral presentation

: Rathapon Asasutjarit, Kriyapa Lairungruang, Papawee Sookdee, Chittima Managit, Teva Phanaksri, and Worapapar Treesuppharat. ***In vitro* Evaluation of Liposomal Ganciclovir Targeting the Retinal Cells.** The Euroscicon Conference on Nanoscience and Graphene Nanotechnology 2019. ANA Crowne Plaza Narita Hotel, Tokyo, Japan. 25-27 November 2019.-*รายละเอียดอยู่ในรายงานฉบับสมบูรณ์*

ภาคผนวก

1. ผลงานตีพิมพ์ในวารสารวิชาการนานาชาติ

1) Asasutjarit, R., Managit, C., Phanaksri, T., Treesuppharat, W, Fuongfuchat, A. Formulation development and in vitro evaluation of transferrin-conjugated liposomes as a carrier of ganciclovir targeting the retina. **Int J Pharm**. 2020; 577:119084. **(Published)-***รายละเอียดอยู่ในรายงานฉบับสมบูรณ์*

2) Asasutjarit, R., Sookdee, P., Veeranondha, S., Fuongfuchat, A., Itharat, A. Application of Film-forming solution as a transdermal delivery system of piperine-rich herbal mixture extract for anti-inflammation. **Heliyon**. xxx; x(x):xxx. **(Under Review for the 3rd Revised Version)** –*รายละเอียดอยู่ในรายงานฉบับสมบูรณ์ โดยในงานวิจัยนี้ ได้มีการประเมินการก่อระคายเคืองดวงตาของผลิตภัณฑ์ตาม OECD guideline โดยศึกษาความเป็นพิษในเซลล์กระจกตา SIRC cells ด้วย short time exposure (STE) test*

3. การเสนอผลงานในที่ประชุมวิชาการ

Oral presentation

: Rathapon Asasutjarit, Kriyapa Lairungruang, Papawee Sookdee, Chittima Managit, Teva Phanaksri, and Worapapar Treesuppharat. ***In vitro* Evaluation of Liposomal Ganciclovir Targeting the Retinal Cells.** The Euroscicon Conference on Nanoscience and Graphene Nanotechnology 2019. ANA Crowne Plaza Narita Hotel, Tokyo, Japan. 25-27 November 2019.-*รายละเอียดอยู่ในรายงานฉบับสมบูรณ์*

International Journal of Pharmaceutics 577 (2020) 119084

Contents lists available at ScienceDirect

International Journal of Pharmaceutics

journal homepage: www.elsevier.com/locate/ijpharm

Formulation development and *in vitro* evaluation of transferrin-conjugated liposomes as a carrier of ganciclovir targeting the retina

Rathapon Asasutjarit[a,*], Chittima Managit[b], Teva Phanaksri[c], Worapapar Treesuppharat[d], Asira Fuongfuchat[e]

[a] Novel Drug Delivery Systems Development Center, Department of Pharmaceutical Sciences, Faculty of Pharmacy, Thammasat University, Pathum Thani 12120, Thailand
[b] Department of Pharmaceutical Technology, Faculty of Pharmacy, Srinakharinwirot University, Nakhon Nayok 26120, Thailand
[c] Chulabhorn International College of Medicine, Thammasat University, Pathum Thani 12120, Thailand
[d] Drug Discovery and Development Center, Thammasat University, 12120, Thailand
[e] National Metal and Materials Technology Center, National Science and Technology Development Agency (NSTDA), Thailand Science Park, Pathum Thani 12120, Thailand

ARTICLE INFO

Keywords:
Ganciclovir
Liposomes
Transferrin
Ophthalmic drug delivery
Targeted drug delivery
Retina
Cytomegalovirus

ABSTRACT

Ganciclovir (GCV) is an antiviral drug approved for treatment of cytomegalovirus (CMV) retinitis. It can be delivered to the eye via systemic administrations. However, local delivery of GCV that targets the retina is considered as an alternative to increase efficacy of the treatment and lessen side effects. Thus, this study aimed to develop formulations of transferrin (Tf)-conjugated liposomes containing GCV (Tf-GCV-LPs) for intravitreal injection and topical instillation. Tf-GCV-LPs were prepared by the reverse-phase evaporation technique and then conjugated to Tf. Their physicochemical properties were evaluated. The optimized formulation was selected and subjected to the cytotoxicity test, cellular uptake study in the human retinal pigment epithelial cells (the ARPE-19 cells) and antiviral activity evaluation. The results showed that physicochemical properties of Tf-GCV-LPs were affected by formulation compositions. The optimized Tf-GCV-LPs had a particle size lower than 100 nm with a negative value of zeta potential. They were safe for the ARPE-19 cells. These Tf-GCV-LPs were taken up by these cells via Tf receptors-mediated endocytosis and showed inhibitory activity on CMV in the infected cells. Therefore, the optimized Tf-GCV-LPs could be accepted as a promising drug delivery system for targeted GCV delivery to the retina in the treatment of CMV retinitis.

1. Introduction

Ganciclovir (GCV) is an antiviral drug that has been currently approved for treatment of cytomegalovirus (CMV) retinitis in the immunocompromised patients (Moussa et al., 2018; Kapanigowda et al., 2015). It shows excellent activity against CMV with an IC_{50} of 900 ng/ml (Shen and Tu, 2007). Nowadays, administration of GCV through oral, intravenous, intravitreal routes and scleral implant are accepted for the clinical treatments of CMV retinitis (Patel et al., 2013). Unfortunately, they sometimes cause complications, poor patient compliance, and eventually, unsuccessful treatment. The drug itself has poor ocular bioavailability, the physicians have to prescribe high doses of either oral GCV or GCV intravenous injections for their patients. Consequently, severe systemic adverse reactions, such as neutropenia and thrombocytopenia from bone marrow suppression by GCV, are usually found in these patients (Teoh et al., 2012; Shen and Tu, 2007; Veloso et al., 1997). Although an intravitreal injection that locally delivers the drug to the posterior eye segment can reduce such systemic side effects, it leads to pain, hemorrhage in the eye, retinal detachment and endophthalmitis (Veloso et al., 1997). The frequency and the volume of intravitreal injection were recommended to be lessened to minimize the risk of these adverse effects (Teoh et al., 2012). For an implant, it can prolong the duration of the action of GCV against CMV in the retina for 5–8 months. Nevertheless, it requires surgical

Abbreviations: C, cholesterol; CMV, cytomegalovirus; CV, cell viability; DSPC, 1,2-distearoyl-*sn*-glycero-3-phosphocholine; DSPE-PEG, 1,2-distearoyl-*sn*-glycero-3-phosphoethanolamine-N-[amino(polyethylene glycol)-2000]; DSPE-PEG-Mal, 1,2-distearoyl-*sn*-glycero-3-phosphoethanolamine-N-[maleimide (polyethylene glycol) − 2000]; DMEM, Dulbecco's modified Eagle medium; EE, entrapment efficiency; FBS, fetal bovine serum; F12, Ham's F12 nutrient mixture; gB, glycoprotein B; GCV, ganciclovir; GCV-LPs, ganciclovir-loaded liposomes; LC, drug-loading capacity; Mol, mole; MWCO, molecular weight cutoff; OD, optical density; P, phospholipids; PBS, phosphate buffer saline; REV, reverse-phase evaporation; Tf, transferrin; Tf-GCV-LPs, transferrin-conjugated liposomes containing ganciclovir

* Corresponding author.
E-mail address: rathapon@tu.ac.th (R. Asasutjarit).

https://doi.org/10.1016/j.ijpharm.2020.119084
Received 28 October 2019; Received in revised form 29 December 2019; Accepted 22 January 2020
Available online 25 January 2020
0378-5173/

procedures to implant and to remove after the drug was exhausted. The implant always causes hemorrhage and retinal detachment as well as endophthalmitis (Patel et al., 2013; Veloso et al., 1997). Presently, the demand of the GCV implant has been decreased; and it will no longer be available in the drug market soon (Lee et al., 2017).

To date, around 90% of marketed ophthalmic products have been formulated in forms of topical eye drops because they are easy to use by the patients themselves by simply instilling into the eye with accurate doses (Patel et al., 2013). However, these conventional dosage forms cannot efficiently relieve the disease symptoms in the posterior eye segment, particularly the retina, because of rapid elimination from the eye surface and anatomical barriers of the eye (Chen, 2015). It was reported that the eye drops were dissipated within the first 15–30 s after instillation into the eyes and less than 5% of the applied drug reached intraocular tissues (Diebold and Calonge, 2010). Therefore, the GCV eye drop solution (0.15% w/w), which has been approved for clinical applications, is suitable for only treatment of viral infection in the anterior eye segment (Sahin and Hamrah, 2012).

Liposomes are one of the promising drug delivery systems, which are widely investigated for targeted drug delivery (Lajunen et al., 2014; Sasaki et al., 2013). They are lipid bilayer vesicles, which are composed mainly of phospholipids and cholesterol (Patel et al., 2013). The surface-modified liposomes can improve physicochemical properties of the drug and facilitate the drug absorption through the ocular tissue giving the higher drug bioavailability in the posterior eye segment (Al-Halafi, 2014; Lajunen et al., 2014; Sasaki et al., 2013). They can control and sustain drug release to the targeted ocular tissue leading to decrease in frequency of drug administrations (Kompella et al., 2013). More importantly, these liposomes can selectively deliver the drug to the retina by either intravitreal injection (Bochot and Fattal, 2012) or instillation into the eye (Lajunen et al., 2014; Sasaki et al., 2013). For the intravitreal injection, the particle size of the surface-modified liposomes should be large enough to avoid rapid leakage into the blood vessel. At the same time, it should be small enough for injection and penetration through the ocular barrier (Jiang et al., 2018). Sakurai et al. (2001) reported that the nanoparticles possessing a size smaller than 200 nm could move toward the retina and retain in the retina for 2 months after intravitreal injection. Meanwhile, the larger particles (200 nm–2 μm) mostly distributed in the vitreous cavity. For topical instillation targeting the posterior eye segment, the surface-modified liposomes having particle sizes no greater than 100 nm were potential drug carriers (Sasaki et al., 2013). They could permeate across the arteries in conjunctiva and ciliary body, and then, distributed to the sclera, choroid, retinal pigment epithelium and retina (Kompella et al., 2013; Sasaki et al., 2013). Modifications of the liposome surface could enhance the chances of reaching the retina by retarding recognition and drug removal from blood circulation by phagocytic cells. They can also promote drug binding to the specific receptors on the retinal cell surface such as transferrin (Tf)-receptors (Lajunen et al., 2014; Wang et al., 2012). Tf is a glycoprotein with a molecular weight of 80 kDa. It is an iron-transporter, which involves iron uptake in normal cells such as the retinal cells and the cancer cells via endocytosis after binding to the Tf-receptor on the cell surface (Qian et al., 2002). Although efficacy of Tf-conjugated liposomes as a carrier for anticancer drug delivery has been extensively studied and reported in numerous publications (Wang et al., 2012; Anabousi et al., 2006; Gijsens et al., 2002; Qian et al., 2002), fewer applications of such liposomes in ophthalmic drug delivery have been found. One of the previous studies by Lajunen et al. (2014) found that the Tf-conjugated liposomes prepared by the microfluidization and having particle size lower than 100 nm could express stronger fluorescent signals in the retina than non-conjugated liposomes at 15 min after instillation to the eye. This particular study demonstrated a potential of Tf-conjugated liposomes as targeted drug delivery system for the retina.

Even if various formulations of GCV for treatment of CMV retinitis can be found in the drug market, the ophthalmic products containing GCV-loaded liposomes (GCV-LPs) that target the retina have not been currently available. In this study, GCV-LPs and their Tf-conjugated products (Tf-GCV-LPs) were thus developed as alternative carriers of GCV for intravitreal injection and instillation into the eye.

The objectives of this study were to develop and optimize formulations of Tf-GCV-LPs, to determine their toxicity in the retinal cells and to investigate their cellular uptake by the retinal cells.

2. Materials and methods

2.1. Chemicals

Cholesterol, 1,2-distearoyl-*sn*-glycero-3-phosphocholine (DSPC), 1,2-distearoyl-*sn*-glycero-3-phosphoethanolamine-N-[amino(polyethylene glycol)-2000] (DSPE-PEG), 1,2-distearoyl-*sn*-glycero-3-phosphoethanolamine-N-[maleimide (polyethylene glycol) − 2000] (DSPE-PEG-Mal) were purchased from Avanti Polar Lipids Inc. (USA). Ganciclovir (GCV) was provided by Tokyo Chemical Industry (Japan). Acetonitrile, chloroform, dichloromethane and methanol were purchased from RCL Labscan (Thailand). Cellulose dialysis tube with a molecular weight cutoff (MWCO) of 12 kDa, coumarin-6, 3-(4,5-dimethy-2-thiazolyl)-2,5-diphenyl-2H-tetrazolium bromide (MTT), dimethyl sulfoxide (DMSO), transferrin, 2-iminothiolane hydrochloride (Traut's reagent), Triton X-100 were obtained from Sigma-Aldrich (USA). Fetal bovine serum (FBS), penicillin-Streptomycin (P/S), trypan blue, trypsin-EDTA, phosphate buffer solution (PBS) (pH 7.4) and all cell culture media were supplied by Gibco (USA). Pierce's Bicinchoninic acid (BCA) protein assay kit was purchased from Thermo Fisher Scientific (USA). All other chemicals and solvents were of analytical grade and were used as received.

2.2. Preparation of GCV-loaded liposomes

GCV-loaded liposomes (GCV-LPs) were prepared by the reverse-phase evaporation (REV) technique following the procedure described in the previous study with some modifications (Shen and Tu, 2007). Briefly, DSPC, DSPE-PEG, DSPE-PEG-Mal and cholesterol of each formulation (Table 1) were dissolved in 30 ml of dichloromethane to obtain the organic phase. The aqueous phase (4 ml) containing GCV (2 mg) in PBS (pH 7.4) was injected into a beaker containing the

Table 1
Formulation compositions of GCV-LPs and Tf-GCV-LPs.

Formulation	DSPC (μmol)	DSPE-PEG (μmol)	DSPE-PEG-Mal (μmol)	Cholesterol (C) (μmol)	Tf (μg)	Total phospholipids (P) (μmol)	Mol ratio of C:P
I.GCV-LPs-5.4-Mal0.2	5	0.2	0.2	3	–	5.4	0.6:1
II.GCV-LPs-4.4-Mal0.2	4	0.2	0.2	3	–	4.4	0.7:1
III.GCV-LPs-3.4-Mal0.2	3	0.2	0.2	3	–	3.4	0.9:1
IV.GCV-LPs-3.4-Mal0.1	3	0.3	0.1	3	–	3.4	0.9:1
V.GCV-LPs-3.4-Mal0.3	3	0.1	0.3	3	–	3.4	0.9:1
VI.GCV-LPs-3.4-Mal0.2-Tf	3	0.2	0.2	3	80	3.4	0.9:1
VII.GCV-LPs-3.4-Mal0.1-Tf	3	0.3	0.1	3	80	3.4	0.9:1
VIII.GCV-LPs-3.4-Mal0.3-Tf	3	0.1	0.3	3	80	3.4	0.9:1

organic phase. Thereafter, the mixture was homogenized by using an ultrasonic homogenizer (Biologics 150VT, USA) with a sonication intensity of 20% amplitude for 1 min in an ice bath. The obtained water in oil emulsion was transferred to a round bottom flask. Dichloromethane consisting of the emulsion system was then evaporated in a rotary evaporator (Eyela SB-1300, Eyela, Japan) under reduced pressure at 32 °C. After phase change of the emulsion was observed for 2 min, PBS (pH 7.4) was added to make a final volume of 40 ml, and the GCV-LPs were obtained.

The liposomes were sonicated to reduce the particle size and to obtain homogeneous particles by the ultrasonic homogenizer at 20% amplitude for 10 min in an ice bath. GCV-LPs were separated from the medium by using a stirred ultrafiltration cell (Millipore, USA) with an ultrafiltration membrane (10 kDa MWCO). Finally, PBS (pH 7.4) was added to re-suspend the retained GCV-LPs and to adjust the volume of GCV-LPs suspension to 1 ml. Since preservatives were not added to the formulations, all GCV-LPs were freshly prepared for each further experiment and used within 24 h after preparation.

2.3. Preparation of Tf-Conjugated GCV-LPs

Tf-conjugated GCV-LPs (Tf-GCV-LPs) were prepared by conjugation of Tf to DSPE-PEG-Mal, a linker lipid, as described by Gijsens et al. (2002). Tf (80 μg) was added to 2 ml of borate-EDTA buffer (pH 8.5) containing 400 nmol of fresh Traut's reagent. The mixture was transferred to a lightproof bottle and shaken continuously for 1 h at 25 °C to obtain thiolated Tf. The thiolated Tf was then concentrated by a centrifugal concentrator (Vivaspin 50 kDa of MWCO) (Satorius Filtrate B.V., Netherlands) at 2000 rpm to make a volume of 200 μl, thereafter, 2 ml of phosphate buffer saline (PBS) (pH 8) was added and the system was concentrated again. The obtained thiolated Tf was immediately added to the GCV-LPs that had already been prepared in the previous section. The mixture was left for12 hours in a dark room at 25 °C without stirring for the complete reaction between thiolated Tf and DSPE-PEG-Mal. Finally, Tf-GCV-LPs were separated from the medium by using a centrifugal concentrator (Vivaspin 100 kDa MWCO) (Satorius Filtrate B.V., Netherlands) at 2000 rpm to make a volume of 1 ml for further experiments. All Tf-GCV-LPs were used in further experiments within 24 h after preparation.

2.4. Measurement of particle size, polydispersity index and zeta potential

Z-average and particle size distribution of GCV-LPs and Tf-GCV-LPs were determined immediately after they were prepared without further dilution by the photon correlation spectroscopy technique via a Zetasizer Nano ZS (Malvern, UK). These parameters were reported in terms of their particle size and polydispersity index (PI), respectively. The zeta potential of these liposomes was measured by the electrophoretic light-scattering technique using the Zetasizer Nano ZS (Manca et al., 2016). All measurements were performed in triplicate.

2.5. Determination of drug entrapment efficiency and drug-loading capacity

The drug entrapment efficiency (EE) and drug-loading capacity (LC) of GCV-LPs and Tf-GCV-LPs were determined following the previous report with some modifications (Shen and Tu, 2007). Briefly, the unentrapped GCV was separated from the liposomes by using a stirred ultrafiltration cell (Millipore, USA) with an ultrafiltration membrane (MWCO 10 kDa) (Asasutjarit et al., 2015). Either GCV-LPs or Tf-GCV-LPs (1 ml) were lysed with Triton X-100 (1% w/v in 80% methanol solution) (1 ml). After mixing and centrifugation, the supernatant was chemically analyzed for GCV content by a UV–visible spectrophotometer (Shimadzu UV–Vis, Japan) at a wavelength of 254 nm (Shen and Tu, 2007). EE and LC of the liposomes were calculated using Eqs. (1) and (2), respectively:

$$EE\ (\%) = \frac{\text{GCV entrapped in the liposomes}}{\text{total amount of GCV loaded}} \times 100 \quad (1)$$

$$LC\ (\%) = \frac{\text{GCV entrapped in the liposomes}}{\text{total amount of phospholipid and cholesterol}} \times 100 \quad (2)$$

2.6. Evaluation of Tf conjugation efficacy

Tf-GCV-LPs prepared in the previous experiment were concentrated to a volume of 100 μl by using a centrifugal concentrator (Vivaspin 100 kDa MWCO) (Satorius Filtrate B.V., Netherlands) at 2000 rpm and transferred to a microfuge tube containing 400 μl of methanol. The mixture was then vortexed and centrifuged at 9000*g* (Scanspeed 1524, Labogene, Denmark) for 10 s. Chloroform (200 μl) was added and the sample was vortexed and centrifuged at the same condition. DI water (300 μl) was added to the centrifuge tube. The mixture was then vortexed and centrifuged at the same revolution for 1 min. The upper phase was removed and discarded. Methanol (300 μl) was added to the centrifuge tube. The mixture was mixed and centrifuged at 9000*g* for 2 min. The supernatant was removed and the pellet was dried under nitrogen gas. The pellet was dispersed in PBS (pH 7.4) (20 μl). The content of Tf was determined by using a Pierce's bicinchonic acid (BCA) protein assay kit (Thermo Scientific, USA) (Anabousi et al., 2006).

2.7. Morphology observation of GCV-LPs and Tf-GCV-LPs

The morphology of a representative of GCV-LPs and Tf-GCV-LPs were observed by the negative staining transmission electron microscopy technique (TEM) (Anabousi et al., 2005). One drop of each sample was placed on a copper grid coated carbon film. The specimens were stained with 2% w/v uranyl acetate solution and dried under room temperature after the excess liquid was removed. They were subsequently imaged by using a JEM-1400 (JEOL, Japan) transmission electron microscope at 100 kV. More than 100 particles were observed and the best representative area was selected to report.

2.8. Drug release study

The release of GCV from optimized GCV-LPs and Tf-GCV-LPs with various degrees of Tf conjugation was studied by using modified Franz diffusion cells. Briefly, one milliliter of each formulation containing GCV equivalent to 0.15 %w/v of GCV was loaded into a donor unit that was separated from a receptor unit by the cellulose dialysis membrane with MWCO of 12 kDa. The receptor unit was filled with receiving solution, PBS (pH 7.4), which was stirred continuously with a magnetic stirrer and maintained at 37 ± 1 °C. The receiving solution was withdrawn at 5, 10, 20, 30, 60 min, and then, every hour until 12 h. Contents of GCV in the withdrawn receiving solution were analyzed by the UV–visible spectrophotometer (Shimadzu UV–Vis, Japan) at a wavelength of 254 nm.

2.9. FT-IR spectroscopy analysis

Fourier transform infrared (FT-IR) spectra of GCV, Tf, GCV-LPs, Tf-GCV-LPs and a physical mixture containing the same content of the ingredients of Tf-GCV-LPs were determined by using an FT-IR spectrometer (PerkinElmer Spectrum One, USA). Prior to the test, GCV-LPs and Tf-GCV-LPs were dried using the freeze-drying technique via an Eyela FD-1 freeze dryer (Eyela, Japan) for 24 h without addition of any additives. Each sample was ground and mixed together with KBr powder at a ratio of 1:100. Then, it was pressed into pellets. The signal averages were obtained for 32 scans with a four cm^{-1} resolution from 4000 to 500 cm^{-1}.

2.10. In vitro cytotoxicity test by MTT assay

The optimized Tf-GCV-LPs and GCV-LPs including GCV solution (in PBS pH 7.4) containing 0.15% w/v GCV were tested for their toxicity to the human retinal pigment epithelial cells, i.e., the ARPE-19 cells (CRL-2302; ATCC, USA). Each sample was diluted to the concentrations of 4, 40, 100, 200 and 400 μg/ml of GCV by a complete medium that contained Dulbecco's Modified Eagle Medium (DMEM), Ham's F12 nutrient mixture (F12) and fetal bovine serum (FBS). The cells were cultured in the complete medium and maintained at 37 °C under 5% CO_2 atmosphere. They were seeded in 96-well plates with a density of 1×10^5 cells/well/100 μl and incubated for 24 h. Thereafter, each test sample (100 μl) was added to the well. The cells were incubated for 24 h and washed twice with PBS (pH 7.4) at the end of incubation period. MTT solution in PBS (pH 7.4) (0.5 mg/ml) (Manconi et al., 2017) were added to each well and incubated for 4 h. DMSO was added to dissolve the formazan crystal (100 μl/well). The optical density (OD) of each well was measured at 570 nm by a microplate reader (Fluostar Omega, BMG Labtech, Germany). The experiments were performed in three replications. Cell viability (CV) was calculated following Eq. (3). The test samples were considered to be totoxic to the cells if the CV (%) was less than 70%.

$$CV\ (\%) = \frac{OD_{sample}}{OD_{control}} \times 100 \quad (3)$$

where the OD_{sample} and $OD_{control}$ were an OD of media from the wells containing the ARPE-19 cells incubated with the samples and MTT solution and an OD of media from the wells containing the cells incubated with MTT solution without the samples, respectively.

2.11. Determination of intracellular uptake of Tf-GCV-LPs by HPLC method

The cellular uptake study of the liposomes were conducted in 6-well plates containing confluent cell layer of the ARPE-19 cells after seeding at a density of 2×10^5 cells/well. The cells in each well were washed with PBS (pH 7.4) twice and incubated with one of the following samples, namely, (1) Tf-GCV-LPs, (2) Tf-GCV-LPs with the presence of free Tf in the medium (50 μg/ml) (Anabousi et al., 2006), (3) GCV-LPs and (4) GCV solution at a non-toxic concentration of the test samples for 24 h. After incubation, the cells from each three-well, which were incubated with the same sample, were pooled and transferred to new centrifuge tubes. The cells were lysed by Triton solution (1 %w/v) and freeze-thawed lysis technique. They were then centrifuged at 10000 rpm at 4 °C for 5 min (Merodio et al., 2002). The supernatant was subjected to an analysis for GCV content by the high performance liquid chromatography (HPLC) technique. The samples for analysis were prepared as follows: the sample (200 μl) was mixed with 500 μl methanol that was already filled in a centrifuge tube. Thereafter, the mixture was centrifuged for 20 min at 60 rpm (Mikro 120 Hettich, Germany) to remove protein precipitates. The supernatant was transferred to a new centrifuge tube and dried under nitrogen gas at room temperature. The residue was dissolved in 50 μl of the mobile phase by swirl mixing for 1 min and then injected to the HPLC instrument. The analysis of GCV content was performed by using an HPLC system (Shimadzu-SPD-20A, Japan) via a C8 column (4.6 × 150 mm, 5 μm) (Zorbax eclipse, Agilent, USA) connected to a guard column. Ten microliters of the sample were injected into the HPLC system. The sample was eluted by the mobile phase composing of 85% v/v acetonitrile and 0.05% w/v formic acid in water at a flow rate of 1.0 ml/min. A UV/visible detector was set at wavelength of 254 nm (Merodio et al., 2002).

2.12. Intracellular uptake of fluorescent Tf-GCV-LPs

The ARPE-19 cells were cultured in 6-well plates following the protocol described above and consequently incubated with one of the test samples as follows: (1) Tf-GCV-LPs, (2) Tf-GCV-LPs with the presence of free Tf in the medium (50 μg/ml) and (3) GCV-LPs at a non-toxic concentration of the test samples for 24 h. All liposomes used in this study contained 0.05 μmol coumarin-6 for tracking the liposome vesicles after they were incubated with the cells. They were prepared by using the same production process as Tf-GCV-LPs and GCV-LPs. The number of the ARPE-19 cells taking up the fluorescence liposomes was determined by the flow-cytometry technique in triplicate (Yang et al., 2009). Briefly, after incubation with the test samples, the cells were washed two times with PBS (pH 7.4) and harvested. The cell suspensions were centrifuged at 1000 rpm for 5 min to remove the supernatant. The cell pellets were washed two times with cold PBS (pH 7.4) and re-suspended in 1X binding buffer to make a concentration of 1×10^5 cells/100 μl and transferred to a 5-ml centrifuge tube. The cells were stained with propidium iodide (5 μl) (BD Pharmingen™, BD Biosciences, USA) and incubated in the dark at a room temperature for 15 min. The binding buffer (400 μl) was added to each tube to make a final volume of 500 μl/tube. Each cell suspension was analyzed by a flow-cytometry instrument (BD FACSVerse™, BD Biosciences, USA) at an excitation/emission wavelength of 490/520 and 535/617 nm for coumarin-6 and propidium iodide, respectively. The fluorescent-activated cells sorting (FACS) plot was performed at least 30,000 events/sample and the data were analyzed by BD FACSVerse™ software (BD Biosciences, USA).

2.13. Determination of inhibitory activity of Tf-GCV-LPs on cytomegalovirus glycoprotein B expression

The human-lung fibroblast cells, i.e., the MRC-5 cells (CCL-171; ATCC, USA), were used as a host of the cytomegalovirus (CMV) AD-169 (VR-538; ATCC, USA). They were cultured in 6-well plates containing complete Eagle's Minimum Essential Medium (EMEM) (2 ml) at a density of 2×10^5 cells/well until reaching 100% confluence. The cells were inoculated with CMV for 1 h at a multiplicity of infection (MOI) of 0.1 pfu/cell. The unbound virus was removed; then, fresh culture medium (2 ml) was added to the wells. Twenty-four hours after inoculation, the cells in each well were incubated with one of the following test samples for 24 h. They were (1) GCV solution, (2) Tf-GCV-LPs, (3) GCV-LPs at a concentration of 100 μg/ml of GCV, and (4) Tf-conjugated LPs without GCV (Blank Tf-GCV-LPs). Thereafter, the cells were washed twice with PBS (pH 7.4) and incubated in the fresh medium. Following a seven-day post treatment, the cells from each well were lysed and the cell proteins were extracted for the western blot analysis. Briefly, the protein extract was subjected to SDS-PAGE and transferred to a PVDF membrane. The membrane was then blocked by skim milk in Tris-buffered saline containing 0.2% v/v Tween 20 (TBST) for 2 h and incubated with 0.2 μg/ml mouse anti-CMV glycoprotein B (gB) monoclonal antibody (Abcam, UK) for 2 h. The membrane was washed twice with TBST for 10 min and consequently incubated with rabbit anti-mouse IgG H&L (1: 100,000) that had been conjugated with horse-radish peroxidase (HRP) (Abcam, UK) for an hour. After washing the membrane with TBST, the signal was developed by the Amersham™ ECL™ Prime Western Blotting Detection Reagent (GE Healthcare, USA). The images were visualized by Amersham Imager 600 (GE Healthcare, USA). For actin loading-control detection, the membrane was stripped by a stripping solution for 45 min at 55 °C. The membrane probed with 0.01 μg/ml mouse anti-actin antibody (R&D Systems, USA). Anti-mouse IgG conjugated with HRP and signal development were performed. The signal strength of each CMV gB and actin band were evaluated by the scientific image-analysis program, ImageJ (Schneider et al., 2012).

2.14. Statistical analysis

The results were presented as a mean ± standard deviation (SD). Statistical analysis for comparing treatment effects were performed by a one-way Analysis of Variance (ANOVA) with Tukey's multiple comparisons at a significant level of 0.05. Except for the *in vitro* cytotoxicity

Table 2
Physicochemical properties of GCV-LPs and Tf-GCV-LPs (mean ± SD; n = 3).

Formulation	Particle size (nm)	PI	Zeta potential (mV)	%EE	%LC	%Tf conjugation
I.GCV-LPs-5.4-Mal0.2	112.7 ± 1.8	0.44 ± 0.02	−30.9 ± 0.8	36.3 ± 0.8	12.1 ± 0.3	–
II.GCV-LPs-4.4-Mal0.2	96.3 ± 1.7	0.38 ± 0.01	−32.8 ± 0.2	34.3 ± 0.3	13.7 ± 0.1	–
III.GCV-LPs-3.4-Mal0.2	88.7 ± 1.5	0.32 ± 0.05	−34.4 ± 0.7	32.0 ± 0.9	16.0 ± 0.4	–
IV.GCV-LPs-3.4-Mal0.1	90.2 ± 1.4	0.33 ± 0.04	−34.2 ± 0.8	31.7 ± 1.7	15.9 ± 0.9	–
V.GCV-LPs-3.4-Mal0.3	87.6 ± 1.9	0.38 ± 0.02	−33.4 ± 1.6	32.5 ± 0.4	16.2 ± 0.2	–
VI.GCV-LPs-3.4-Mal0.2-Tf	94.3 ± 2.0	0.35 ± 0.03	−32.4 ± 1.4	32.7 ± 0.3	16.3 ± 0.8	33.5 ± 0.8
VII.GCV-LPs-3.4-Mal0.1-Tf	91.8 ± 2.2	0.39 ± 0.01	−32.8 ± 0.9	32.4 ± 0.6	16.2 ± 1.2	27.7 ± 0.7
VIII.GCV-LPs-3.4-Mal0.3-Tf	102.5 ± 1.8	0.38 ± 0.04	−31.9 ± 0.3	33.0 ± 0.8	15.5 ± 0.5	35.4 ± 0.7

test, the comparison was performed by a two-way ANOVA to determine the effects of the test samples and their concentrations.

3. Results and discussion

3.1. Preparation and characterization of GCV-LPs and Tf-GCV-LPs

The physicochemical properties of GCV-LPs and Tf-GCV-LPs i.e. particle size, PI, zeta potential, EE and LC of GCV-LPs with variations in the contents of the ingredients are shown in Table 2. It was found that the particle size of all liposomes was in a nanometer range of around 88–113 nm with negative values of zeta potential between −31 and −34 mV. Particle size distribution was found to be slightly broad (PI ~ 0.3–0.4). This result was due to low efficiency of the particle size reduction performed by the ultrasonication technique (Asasutjarit et al., 2019). The EE and LC of these liposomes were moderately low around 32–36% and 12–16%, respectively.

In particular, Tf-GCV-LPs had obviously larger particle sizes when compared to those of GCV-LPs. These results suggested that the physicochemical properties of GCV-LPs were affected by the formulation compositions.

3.1.1. Effect of total phospholipids and PEGylated phospholipid contents

Tables 1 and 2 show that GCV-LPs containing various total phospholipids content with the fixed contents of cholesterol and GCV i.e. I.GCV-LPs-5.4-Mal0.2, II.GCV-LPs-4.4-Mal0.2 and III.GCV-LPs-3.4-Mal0.2 had statistical difference in particle size (p-value = 0.002), PI (p-value = 0.000), zeta potential (p-value = 0.000), EE (p-value = 0.001) and LC (p-value = 0.000). The results indicated that the higher the total phospholipids content, the larger the particle size of GCV-LPs. The formulations with high content of total phospholipids have been reported to give more viscous organic phase of emulsions during production by the REV method (Shaker et al., 2017; Shen and Tu, 2007). Consequently, the effective particle size reduction during production of GCV-LPs was difficult to perform. This phenomenon led to the broader particle size distribution as well. The PI value of I.GCV-LPs-5.4-Mal0.2 was thus higher than that of II.GCV-LPs-4.4-Mal0.2 ((p-value = 0.001) and III.GCV-LPs-3.4-Mal0.2 (p-value = 0.029), respectively.

Apart from the total phospholipid content, the contents of PEGylated phospholipids, i.e. DSPE-PEG and DSPE-PEG-Mal, were also varied to investigate their effect on liposome properties. DSPE-PEG was a stabilizer of the liposomes because it could increase physical stability through steric effects, increase solubility and reduce immunogenicity in the body. It could also provide a stealth effect; thus, the obtained liposomes would have the ability to escape from the reticuloendothelial system (Kim et al., 2012). While DSPE-PEG-Mal is a linker phospholipid that contained a maleimide group for conjugation to thiolated Tf (Gijsens et al., 2002). The difference in DSPE-PEG-Mal contents led to various degrees of Tf conjugation on the surface of Tf-GCV-LPs. In this study, the total amount of PEGylated phosphates was fixed at 0.4 μmol (as shown in Table 1). The physicochemical properties of III.GCV-LPs-3.4-Mal0.2 to V.GCV-LPs-3.4-Mal0.3 were compared. It was found that the particle size, PI, zeta potential, EE and LC of these three GCV-LPs were not statistically different at p-value of 0.320, 0.970, 0.663, 0.738, and 0.740, respectively. Thus, minor difference in chemical structure of DSPE-PEG and DSPE-PEG-Mal did not cause any obvious changes in the properties of GCV-LPs.

All GCV-LPs possessed a negative value of zeta potential due to the negatively charged phospholipids, i.e., DSPE-PEG and DSPE-PEG-Mal (Eloy et al., 2014). I.GCV-LPs-5.4-Mal0.2, which contained a higher total phospholipids content than II.GCV-LPs-4.4-Mal0.2 and III.GCV-LPs-3.4-Mal0.2, respectively, had a lower absolute value of negative zeta potential than such liposomes at p-values of 0.042 and 0.002, respectively. However, the zeta potential of II.GCV-LPs-4.4-Mal0.2 and III.GCV-LPs-3.4-Mal0.2 were not significantly different at a p-value of 0.788. These findings elucidated that contribution of DSPE-PEG and DSPE-PEG-Mal molecules to surface charges was interfered by the content of DSPC (Schubert and Muller-Goymann, 2005).

The entrapment efficiencies (EE) of GCV in GCV-LPs shown in Table 2 suggested that 32–36% of loaded GCV could be entrapped in the liposomes. These low EEs of GCV-LPs were results of the hydrophilic property of GCV and small particle size of GCV-LPs leading to a small volume of the aqueous phase of these liposome vesicles (Eloy et al., 2014; Shen and Tu, 2007). As previously mentioned, there was a positive relationship between the total phospholipids content and the particle sizes of GCV-LPs; thus, the total phospholipids content also had influence on EE. III.GCV-LPs-3.4-Mal0.2 which contains the lowest total phospholipids and the highest mole ratio of cholesterol to total phospholipids content (C:P) could encapsulate GCV less than II.GCV-LPs-4.4-Mal0.2 (p-value = 0.013) and I.GCV-LPs-5.4-Mal0.2 (p-value = 0.001). Therefore, not only the particle size, the C:P also affected the EE. Since cholesterol could suppress water penetration into the hydrocarbon chain of the phospholipids (Eloy et al., 2014), GCV would mainly interact with the polar head group of the phospholipid molecules and accumulated only in the aqueous core of the liposomes.

On the contrary, the LC of GCV-LPs decreased with an increase in the total phospholipids content. This result was a consequence of the lowest ratio of the amount GCV entrapped in the liposomes to the amount of total phospholipids and cholesterol for encapsulation of GCV.

3.1.2. Effect of Tf conjugation

Tf-GCV-LPs were prepared with different percentage of Tf conjugation on the liposomal surface through variations in the DSPE-PEG-Mal content. The results shown in Table 2 suggested that among three formulations, i.e. VI.GCV-LPs-3.4-Mal0.2-Tf, VII.GCV-LPs-3.4-Mal0.1-Tf and VIII.GCV-LPs-3.4-Mal0.3-Tf, VIII.GCV-LPs-3.4-Mal0.3-Tf with the highest content of DSPE-PEG-Mal had more Tf content on the liposomal surfaces than that of the former two formulations at p-values of 0.046 and 0.000, respectively. This finding was a result from the higher DSPE-PEG-Mal content that provided more maleimide molecules to couple the thiolated Tf.

The physicochemical properties shown in Table 2 indicated that VIII.GCV-LPs-3.4-Mal0.3-Tf had larger particle size than that of VI.GCV-LPs-3.4-Mal0.2-Tf (p-value = 0.016) and VII.GCV-LPs-3.4-Mal0.1-Tf (p-

value = 0.004), whereas the latter two formulations had statistically comparable particle size (p-value = 0.484). Only VIII.GCV-LPs-3.4-Mal0.3-Tf which contained Tf around 35% had a statistically larger particle size than that of the non-conjugated liposomes (p-value of 0.000). This finding was consistent with the previous studies reporting that conjugation of Tf to PEGylated liposomes sometimes increased the hydrodynamic size representing the size of the particle because of a change in the spatial structure of the DSPE-PEG molecules (Chen et al., 2011). Comparison of these three formulations for PI, zeta potential, EE and LC of Tf-GCV-LPs containing various degrees of Tf did not show significant difference at p-values of 0.524, 0.060, 0.932, 0.913, respectively. Furthermore, a statistical comparison of these parameters before- and after conjugation to Tf of GCV-LPs indicated the similarity of their values at p-value $^{>}$ 0.05.

As previously mentioned, the nanoparticles with a size less than 100 nm were suitable as targeted drug delivery system for both intravitreal injection and topical instillation. Thus, VI.GCV-LPs-3.4-Mal0.2-Tf, which had the small particle size with the average particle size less than 100 nm, was selected for the further studies.

3.2. Morphology of GCV-LPs and Tf-GCV-LPs

TEM photographs of the representative of GCV-LPs and Tf-GCV-LPs, i.e., III.GCV-LPs-3.4-Mal0.2 and VI.GCV-LPs-3.4-Mal0.2-Tf are shown in Fig. 1(a) and (b), respectively. The pictures showed that both GCV-LPs and Tf-GCV-LPs were small unilamellar vesicles. They had spherical shape with particle sizes of less than 100 nm. These pictures also elucidated a slightly broad particle size distribution of both liposomes that were consistent with PI determined by the photon correlation technique. Fig. 1(b) showed small structures of Tf on the liposomal surface of VI.GCV-LPs-3.4-Mal0.2-Tf, in addition, these small structures were also found in the space between Tf-GCV-LPs. Meanwhile, they were absent on III.GCV-LPs-3.4-Mal0.2 surface and the space between GCV-LPs as shown in Fig. 1(a). These findings agreed with the TEM photographs of Tf conjugated liposomes reported in the previous publications (Chen et al., 2016; Anabousi et al., 2006) and confirmed the conjugation of Tf to the liposomal surface.

3.3. Drug release study

A drug release study of III.GCV-LPs-3.4-Mal0.2, VI.GCV-LPs-3.4-Mal0.2-Tf, VII.GCV-LPs-3.4-Mal0.1-Tf and VIII.GCV-LPs-3.4-Mal0.3-Tf was performed to determine the release kinetic of GCV and the effect of Tf conjugation percentage on GCV release from the liposomes. In vitro release profiles shown in Fig. 2(a) and (b) indicated that the release kinetic of GCV from III.GCV-LPs-3.4-Mal0.2, VI.GCV-LPs-3.4-Mal0.2-Tf, VII.GCV-LPs-3.4-Mal0.1-Tf and VIII.GCV-LPs-3.4-Mal0.3-Tf followed the Higuchi's model with an r^2 of 0.9996, 0.9985, 0.9996 and 0.9995, respectively. This finding suggested that diffusion of GCV molecules was the main factor controlling drug release of GCV from these liposomes (Haidar et al., 2008). This release was the result of the presence of PEG grafted onto the liposomal surfaces and the interaction between GCV and PEG as seen in the case of III.GCV-LPs-3.4-Mal0.2. In addition, these results indicated that Tf conjugation to the liposomes markedly affected the release rate of GCV. It was found that the release rate of GCV from VIII.GCV-LPs-3.4-Mal0.3-Tf (5.21 ± 0.17 μg/minute$^{1/2}$) that conjugated to Tf with the highest percentage conjugation was less than that of VI.GCV-LPs-3.4-Mal0.2-Tf (6.34 ± 0.29 μg/minute$^{1/2}$), VII.GCV-LPs-3.4-Mal0.1-Tf (7.71 ± 0.16 μg/minute$^{1/2}$) and III.GCV-LPs-3.4-Mal0.2 (9.22 ± 0.25 μg/minute$^{1/2}$) at a p-value of 0.001, 0.000 and 0.000, respectively. This result implied that Tf could impede diffusion of GCV resulting in slow release rates and a prolonged release of GCV over 12 h.

3.4. FT-IR spectroscopy analysis

The interactions between GCV and the components consisting of the liposomes were determined by using FT-IR spectroscopy technique. The FT-IR spectra of GCV and Tf are shown in Fig. 3(a) and (b), respectively. The FT-IR spectrum of GCV exhibits its characteristic bands at wavenumbers of 1180–1223 cm^{-1}, which represented the C—O—C asymmetric stretch, 1305 cm^{-1} for C—N stretch. It also shows important bands at 2942 cm^{-1}, 3170 cm^{-1}, 3319 cm^{-1} and 3437 cm^{-1} responding to the stretch of aliphatic C—H, aromatic C—H, N—H and O—H, respectively (Sarbajna et al., 2011). The FT-IR spectrum of Tf shows the bands of tyrosine at 1163 cm^{-1}, 1240 cm^{-1}, 1517 cm^{-1}. It also shows the band of amide group I at a wavenumber of 1656 cm^{-1} and N—H stretch at 3307 cm^{-1} (Duca et al., 2018). The FT-IR spectrum of a physical mixture of Tf, GCV, DSPE-PEG-Mal, DSPC and cholesterol at the same weight ratio as the compositions consisting of the obtained VI.GCV-LPs-3.4-Mal0.2-Tf is presented in Fig. 3(c). It illustrates the characteristic bands of the phospholipids at a wavenumber of 1737 cm^{-1} that was assigned for the C═O stretch of the ester bond between the fatty acid chain and the head group. The strong bands at 2852 cm^{-1} and 2921 cm^{-1} responded to the CH_2 symmetric and symmetric stretch modes, respectively, in the phospholipids and cholesterol molecules (Briuglia et al., 2015). Furthermore, this spectrum also showed the same characteristic bands of GCV at wavenumbers of 1180–1223 cm^{-1}, 1305 cm^{-1} and 3437 cm^{-1} as shown in Fig. 3(a). These results implied that there was no significant interaction between GCV and the compositions consisting of the physical mixture. However, the characteristic bands of Tf could not be observed in the FT-IR spectrum because of the small amount of Tf in the formulation. Fig. 3(d) shows some trivial shifts of the characteristic bands of GCV from wavenumbers of 1180 cm^{-1} and 3437 cm^{-1} to 1179 cm^{-1} and 3434 cm^{-1}, respectively. Furthermore, the bands at wavenumbers of 1223 cm^{-1} and 1305 cm^{-1}, which were found in the FT-IR spectrum of standard GCV (Fig. 3(a)) and that of the physical mixture (Fig. 3(b)) were absent in the FT-IR spectrum of III.GCV-LPs-3.4-Mal0.2. This phenomenon also occurred with the characteristic band of the phospholipid that shifted

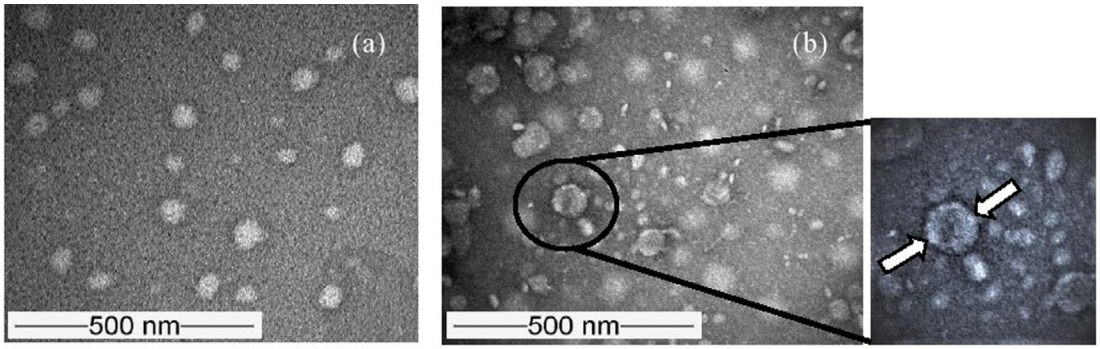

Fig. 1. TEM photographs: (a) III.GCV-LPs-3.4-Mal0.2 and (b) VI.GCV-LPs-3.4-Mal0.2-Tf.

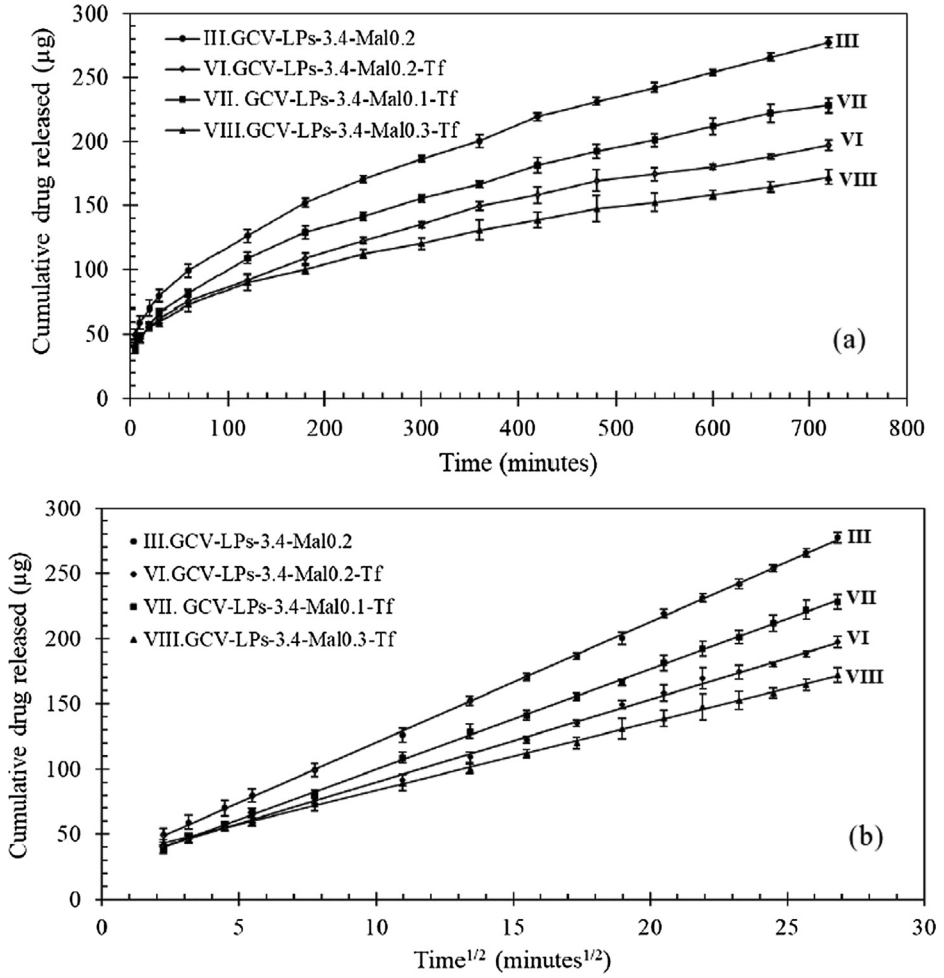

Fig. 2. Release profiles of GCV: (a) plots of cumulative drug released against time and (b) plots of cumulative drug released against time$^{1/2}$.

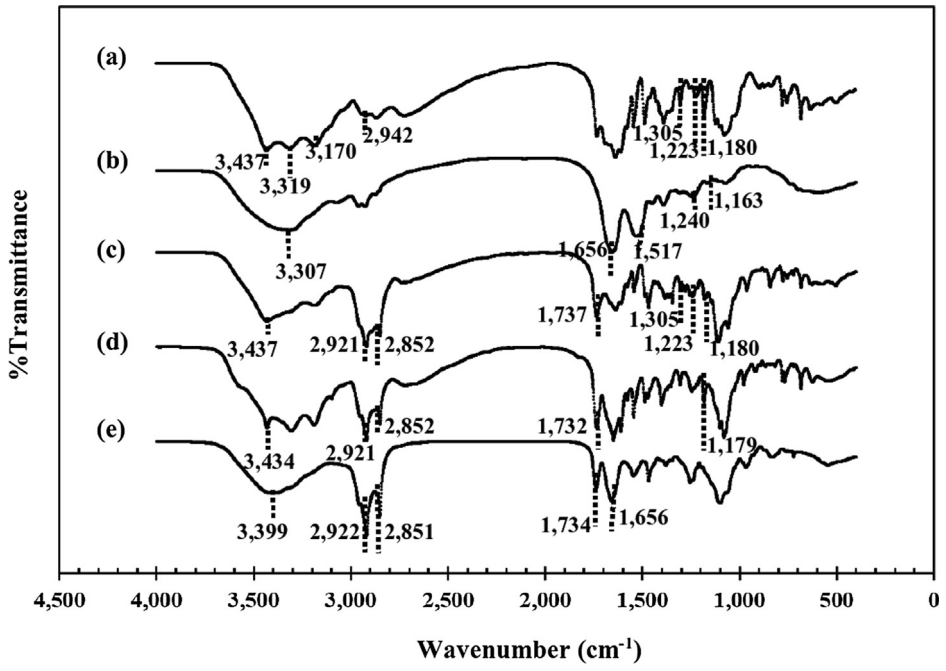

Fig. 3. FT-IR spectra: (a) GCV; (b) Tf; (c) a physical mixture of Tf, GCV, DSPE-PEG-Mal, DSPC and cholesterol; (d) III.GCV-LPs-3.4-Mal0.2 and (e) VI.GCV-LPs-3.4-Mal0.2-Tf.

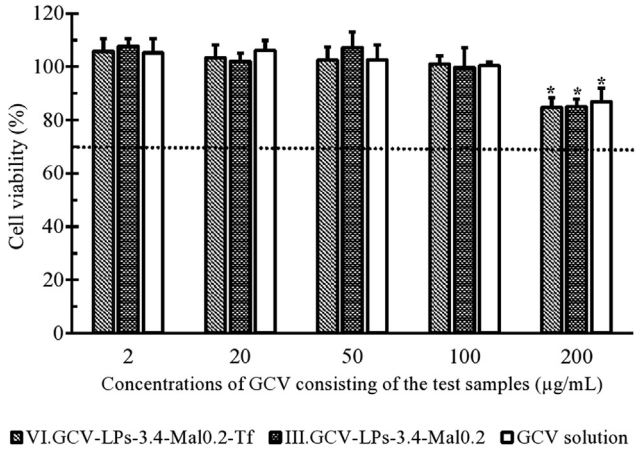

Fig. 4. Cell viability (%) of the ARPE-19 cells after incubation with various concentrations of GCV consisting of VI.GCV-LPs-3.4-Mal0.2-Tf, III.GCV-LPs-3.4-Mal0.2 and GCVsolution for 24 h (mean ± SD; n = 3) (*significantly different from the other concentrations at a *p*-value < 0.05).

from the wavenumber of 1737 cm^{-1} to –1732 cm^{-1}. The pattern of this FT-IR spectrum suggested that there were some interactions between the ingredients comprising III.GCV-LPs-3.4-Mal0.2 and GCV molecules. Fig. 3(e) indicated that there were strong interactions between GCV and the ingredients consisting of VI.GCV-LPs-3.4-Mal0.2-Tf, such as hydrogen bonds. It caused some trivial shifts of the characteristic band of the phospholipids and cholesterol including the absence of the important characteristic bands of GCV and Tf. These interactions thus significantly affected the release rate of GCV from the liposomes conjugated to various Tf contents as reported in the previous section.

3.5. In vitro cytotoxicity test by MTT assay

Since VI.GCV-LPs-3.4-Mal0.2-Tf had optimal %Tf conjugation with acceptable particle size, PI, zeta potential and EE, it was selected for the cellular uptake study in the ARPE-19 cells and thus determined a maximum concentration that did not cause toxicity towards the cells. In this study, III.GCV-LPs-3.4-Mal0.2 and GCV solution were also subjected to the test to determine the effect of the formulation compositions on the cytotoxicity to the ARPE-19 cells. The concentrations of the test samples were calculated based on the concentration of GCV entrapped in the liposomes. Fig. 4 shows that the CV (%) of the ARPE-19 cells those exposed to the test samples containing 2–200 µg/ml of GCV were more than 70%. The results clearly indicated that the ARPE-19 cells could tolerate all test samples at the entire concentrations of GCV consisting of the formulations. Therefore, it could be concluded that VI.GCV-LPs-3.4-Mal0.2-Tf, III.GCV-LPs-3.4-Mal0.2 and GCV solution were safe for the ARPE-19 cells.

The CV of the cells incubated with these three samples were comparable for each GCV concentration (*p*-value = 0.411), it suggested that the formulations of GCV i.e. VI.GCV-LPs-3.4-Mal0.2-Tf, III.GCV-LPs-3.4-Mal0.2 and GCV solution did not significantly affect the CV of the ARPE-19 cells. However, the CV of the ARPE-19 cells was markedly decreased to around 80% when they were incubated with VI.GCV-LPs-3.4-Mal0.2-Tf, III. GCV-LPs-3.4-Mal0.2 and GCV solution containing the highest GCV concentration (200 µg/ml) (*p*-value = 0.000). These results might come from the higher concentration of the ingredients consisting of the formulations such as phospholipids and GCV leading to an inappropriate environment for cell growth. In addition, GCV is generally toxic to the viral infected cells and the rapidly propagating cells i.e. blood cells and their precursors; sometimes, it could cause adverse effects to the DNA during the DNA synthesis process of the normal cell because its molecular structure is similar to guanosine (Janoly-Dumenil et al., 2009). To avoid any toxicity from overly high concentrations of the formulations, test samples containing GCV at a concentration equivalent to 100 µg/ml were selected for further studies.

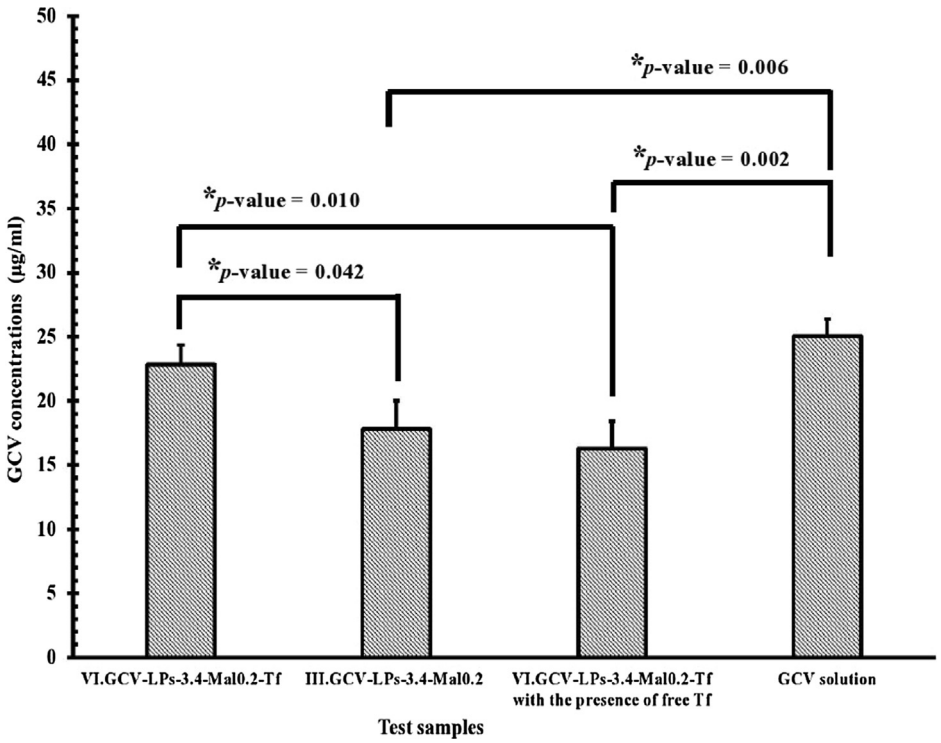

Fig. 5. GCV concentrations in the ARPE-19 cells after incubation with VI.GCV-LPs-3.4-Mal0.2-Tf, III.GCV-LPs-3.4-Mal0.2, VI.GCV-LPs-3.4-Mal0.2-Tf with the presence of free Tf and GCV solution for 24 h, which were analyzed by HPLC technique (mean ± SD; n = 3) (*significantly different at a *p*-value < 0.05).

3.6. Intracellular uptake study of Tf-GCV-LPs in the ARPE-19 cells by HPLC method

The study of the intracellular uptake of VI.GCV-LPs-3.4-Mal0.2-Tf with and without the presence of free Tf in the medium, III.GCV-LPs-3.4-Mal0.2 and GCV solution in the ARPE-19 cells were performed by incubation of the cells with the test samples at a concentration equivalent to 100 μg/ml of GCV for 24 h. The cells were extracted and chemically analyzed for GCV concentration by the HPLC technique. Fig. 5 contains an illustration showing that the concentration of GCV from the cells, which were incubated with VI.GCV-LPs-3.4-Mal0.2-Tf, was significantly higher than that of the GCV from the cells incubated with III.GCV-LPs-3.4-Mal0.2 and VI.GCV-LPs-3.4-Mal0.2-Tf with the presence of free Tf at *p*-values of 0.042 and 0.010, respectively. By contrast, the intracellular concentrations of GCV taken up from III.GCV-LPs-3.4-Mal0.2 and VI.GCV-LPs-3.4-Mal0.2-Tf with the presence of free Tf were not significantly different at a *p*-value of 0.743. These results implied that Tf conjugation to GCV-LP surface could facilitate the cellular internalization of GCV. In addition, the presence of free Tf in the cell culture medium obviously decreased the intracellular uptake of VI.GCV-LPs-3.4-Mal0.2-Tf. This effect was caused by the free Tf competitively binding to the Tf receptors (TfRs) on the cell surface and blocked the TfRs before binding to Tf on the surface of VI.GCV-LPs-3.4-Mal0.2-Tf. It thus confirmed the fact that VI.GCV-LPs-3.4-Mal0.2-Tf could be taken up into the ARPE-19 cells by TfRs-mediated endocytosis (Anabousi et al., 2006).

The statistical comparison between the concentrations of GCV extracted from the cells, which had been incubated with VI.GCV-LPs-3.4-Mal0.2-Tf and GCV solution suggested that they were comparable at a *p*-value of 0.501. This finding might result from the cellular absorption of GCV molecules from GCV solution through diffusion and in particular purine nucleobase and nucleoside transporters (Perrottet et al., 2009). Since intracellular accumulation of the GCV molecules from GCV solution did not need the complicated drug release process, the absorption rate of GCV into the cells was higher than that of the liposomal GCV. Consequently, the concentration of GCV in the ARPE-19 cells treated with GCV solution was higher than that of the GCV in the cells incubated with III.GCV-LPs-3.4-Mal0.2 and VI.GCV-LPs-3.4-Mal0.2-Tf with the presence of free Tf at a *p*-value of 0.006 and 0.002, respectively.

Although the results suggested that the concentration of GCV taken up from GCV solution was comparable to that of GCV from VI.GCV-LPs-3.4-Mal0.2-Tf, the GCV solution was not appropriate for ophthalmic drug delivery. In particular, the drug-targeting posterior eye segment that aimed to administer by either intravitreal or topical instillation because of rapid elimination from the targeting sites (Chen, 2015; Al-Halafi, 2014). Therefore, VI.GCV-LPs-3.4-Mal0.2-Tf capable of delivering GCV into the cells was accepted for these purposes.

3.7. Intracellular uptake of fluorescent Tf-GCV-LPs in the ARPE-19 cells

The intracellular uptake study of fluorescent VI.GCV-LPs-3.4-Mal0.2-Tf, III.GCV-LPs-3.4-Mal0.2 and VI.GCV-LPs-3.4-Mal0.2-Tf with the presence of free Tf were conducted to determine the number of living ARPE-19 cells, which could take up these fluorescent liposomes into the cells. The quadrant LR (Courmarin-6$^+$, Propidium iodide$^-$) of fluorescent-activated cells-sorting (FACS) plots depicted in Fig. 6(a)–(c) shows that the number of the living ARPE-19 cells that took up the fluorescent liposomes were around 80–90% of the cell population. This outcome suggested that after incubation for 24 h, all fluorescent liposomes could be taken up by the ARPE-19 cells. The uptake levels of the cells incubated with VI.GCV-LPs-3.4-Mal0.2-Tf, III.GCV-LPs-3.4-Mal0.2 and VI.GCV-LPs-3.4-Mal0.2-Tf with the presence of free Tf as shown in Fig. 6(d) illustrated that they were statistically different and depended on Tf conjugation and free Tf in the medium. Fig. 6(a) shows that the number of the living ARPE-19 cells taking up fluorescent VI.GCV-LPs-3.4-Mal0.2-Tf (without free Tf) was higher than that of the living cells that took up fluorescent III.GCV-LPs-3.4-Mal0.2 (Fig. 6(b)) and fluorescent VI.GCV-LPs-3.4-Mal0.2-Tf with the presence of free Tf (Fig. 6(c)) at a *p*-value of 0.008 and 0.006, respectively. These findings were in good agreement with the results of intracellular uptake study of Tf-GCV-LPs by HPLC method and confirmed that the cellular internalization via TfRs-mediated endocytosis facilitated the uptake of VI.GCV-LPs-3.4-Mal0.2-Tf into the ARPE-19 cells. Note that III.GCV-LPs-3.4-Mal0.2 did not contained Tf on the surface; it could be internalized into the cells by 80.6% of the cell population. This finding indicated that III.GCV-LPs-3.4-Mal0.2 could be internalized by the cells with other less effective endocytosis pathways (Eloy et al., 2014). For the case of VI.GCV-LPs-3.4-Mal0.2-Tf with the presence of free Tf, it could be internalized into the cells by 79.8% of the cell population which was comparable to that of III.GCV-LPs-3.4-Mal0.2 (*p*-value = 0.934). This was due to the fact that TfRs were blocked by the free Tf leading to unreachable binding sites for the targeted ligand on the surface of VI.GCV-LPs-3.4-Mal0.2-Tf (Chen et al., 2016). However, VI.GCV-LPs-3.4-Mal0.2-Tf with the presence of Tf would bind to the TfRs when the new TfRs had been presented on the cell surface once the blocking Tf was taken up via endocytosis and the recycling process of TfRs was complete (Qian et al., 2002).

3.8. Inhibitory activity of Tf-GCV-LPs on CMV glycoprotein B expression

To determine the activity of Tf-GCV-LPs against CMV, the MRC-5 cells were used as host cells for CMV infection because of their effective permissiveness to CMV infection and replication (Merodio et al., 2002). The infected MRC-5 cells were incubated with GCV-LPs and Tf-GCV-LPs at a concentration equivalent to 100 μg/ml of GCV, which was not toxic to the MRC-5 cells (data not shown). The signal strength of the expressed CMV glycoprotein B (CMV gB) from the western blot assay representing the quantity of CMV was then quantified and normalized by the signal strength of the actin of the MRC-5 cells as shown in Fig. 7(a) and (b) (Schneider et al., 2012).

Two factions of CMV gB, which is an important glycoprotein of CMV for fusion to the plasma membrane of the host cells during cellular entry process (Wille et al., 2013), could be found in only infected MRC-5 cells as can be seen in in Fig. 7(b): Lane III, Blk-VI, VI, GCV-sol. However, it could not be found in the normal MRC-5 cells that were not infected by CMV (Lane N).

Fig. 7(a) indicated that the normalized signal strength of CMV gB from the cells treated with VI.GCV-LPs-3.4-Mal0.2-Tf was significantly lower than the normalized signal strength of CMV gB from the cells treated with III.GCV-LPs-3.4-Mal0.2 and Blank-VI.GCV-LPs-3.4-Mal0.2-Tf (without GCV) at a *p*-value of 0.027 and 0.000, respectively. This finding pointed out that VI.GCV-LPs-3.4-Mal0.2-Tf had a higher potential for inhibiting the expression of CMV gB in the infected cell than the latter two test samples. This result was due to the effective cellular internalization of VI.GCV-LPs-3.4-Mal0.2-Tf by the cells, which was facilitated by the Tf grafted on the liposome surface. After the specific binding of Tf to TfRs, the complexes of Tf-TfRs were clustered into clathrin-coated pits. They were then internalized and enclosed with endocytic vesicles (Qian et al., 2002). The GCV encapsulated in the liposomes was thus protected from the endosome environment, allowing a controlled release into the cells. It was in good agreement with the previous studies showing that delivery of doxorubicin encapsulated in Tf-conjugated liposomes could increase the uptake rate into the tumor cells and that it selectively enhanced cytotoxicity to the cancerous human pulmonary (Anabousi et al., 2006) and hepatoma (Li et al., 2009) epithelial cell lines. The lower potency of III.GCV-LPs-3.4-Mal0.2 for inhibition of CMV gB expression was the result of the PEGylated phospholipids without conjugation. They could reduce the uptake of the liposomes into the cells through sterically impeding the access to specific receptors on the cell surface (Anabousi et al., 2006) resulting in less effective cellular internalization by the cells as

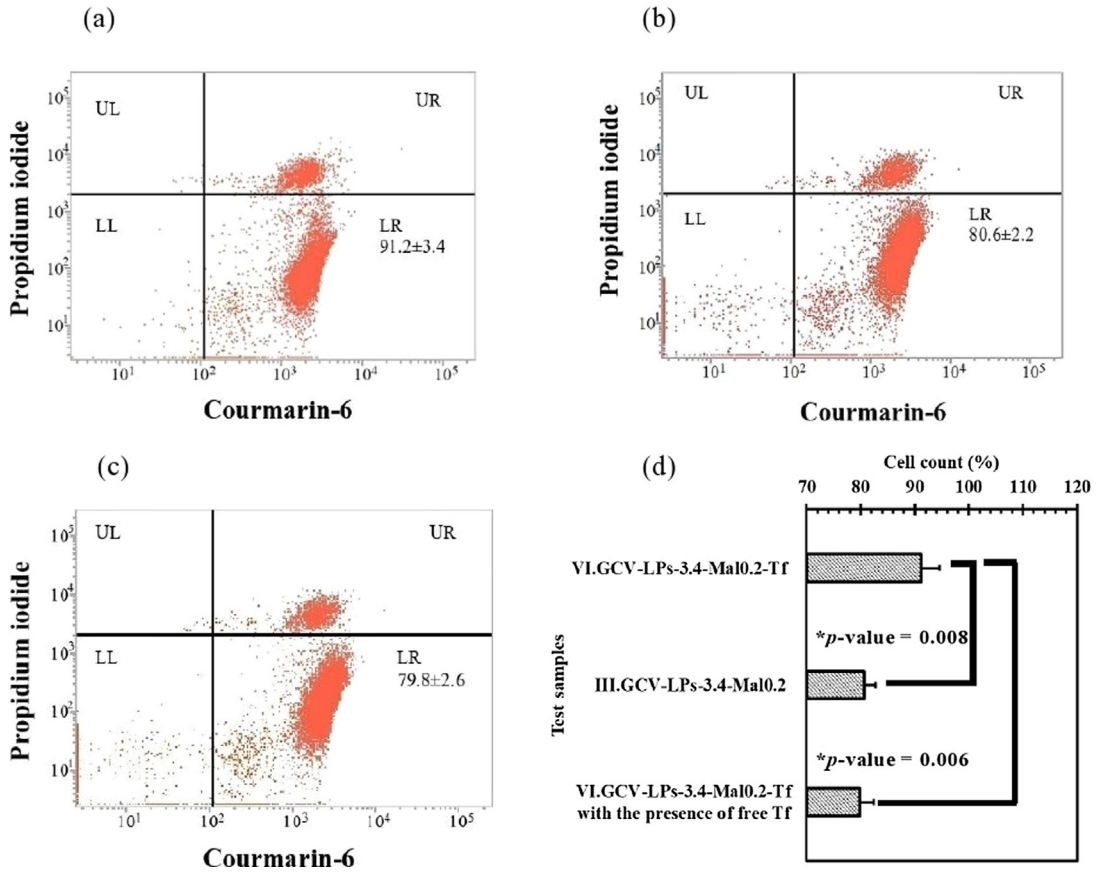

Fig. 6. Number of the living ARPE-19 cells taking up fluorescent Tf-GCV-LPs: (a)-(c) FACs plots of number of the living ARPE-19 cells taking up VI.GCV-LPs-3.4-Mal0.2-Tf, III.GCV-LPs-3.4-Mal0.2 and VI.GCV-LPs-3.4-Mal0.2-Tf with the presence of free Tf, respectively; (d) comparison of numbers of the living ARPE-19 cells taking up fluorescent Tf-GCV-LPs after incubation for 24 h (mean ± SD; n = 3) (*significantly different at a *p*-value < 0.05).

mentioned in the previous section. Since Blank-VI.GCV-LPs-3.4-Mal0.2-Tf did not contained GCV, the infected cells incubated with these liposomes showed the highest signal strength of CMV gB. This result strongly supported that the anti-CMV activity of VI.GCV-LPs-3.4-Mal0.2-Tf was from the GCV.

The comparison between signal strengths of CMV gB from incubation with VI.GCV-LPs-3.4-Mal0.2-Tf and GCV solution demonstrated that they were statistically comparable at a *p*-value of 0.153. This finding resulted from GCV molecules from GCV solution could penetrate into the infected cells properly through a diffusion process and nucleoside transporters as previously mentioned. More importantly, the GCV molecules in the infected cells would be rapidly phosphorylated by the protein kinase of CMV without the drug release process unlike the liposomal GCV. Therefore, GCV solution could eradiate CMV effectively resulting in a comparable signal strength of CMV gB to that obtained from the infected cells treated with VI.GCV-LPs-3.4-Mal0.2-Tf.

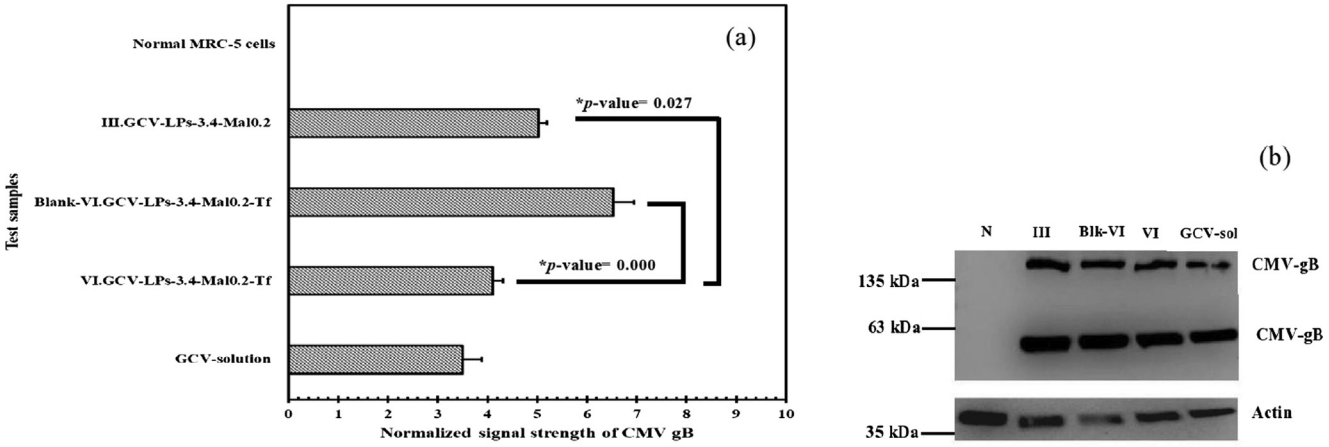

Fig. 7. Normalized signal strengths of CMV gB from the MRC-5 cells: (a) comparison of signal strengths of CMV gB from the normal MRC-5 cells and the MRC-5 cells after CMV infection and incubation with III.GCV-LPs-3.4-Mal0.2, Blank-VI.GCV-LPs-3.4-Mal0.2-Tf, VI.GCV-LPs-3.4-Mal0.2-Tf and GCV solution (mean ± SD; n = 3); (b) CMV gB from the western blot assay. Lane N: the normal MRC-5 cells; Lane III, Blk-VI, VI, GCV-sol: CMV gB from the infected MRC-5 cell that were incubated with III.GCV-LPs-3.4-Mal0.2, Blank-VI.GCV-LPs-3.4-Mal0.2-Tf, VI.GCV-LPs-3.4-Mal0.2-Tf and GCV solution, respectively (*significantly different at a *p*-value < 0.05).

4. Conclusions

Formulations of Tf-GCV-LPs were developed for drug delivery of the GCV targeting posterior eye segment by intravitreal injection and topical instillation. Thus, they should have particle size smaller than 100 nm with a surface modification in order to increase cell-uptake efficiency. It was found that the physicochemical properties of GCV-LPs, i.e., particle size, PI, zeta potential, EE(%) and LC(%) were affected by the formulation compositions. The results indicated that an increase in total phospholipids led to an increase in particle size, PI and EE(%) of GCV-LPs. Unfortunately, the higher total of phospholipids that consisted of the formulation caused lower values of zeta potential and LC (%) of GCV-LPs. Modification of DSPE-PEG and DSPE-PEG-Mal at a constant total content of these PEGylated phospholipids did not cause any obvious change in particle size, PI, zeta potential, EE(%) and LC(%) of GCV-LPs. However, GCV-LPs containing more DSPE-PEG-Mal content was able to conjugate to more Tf resulting in the larger particle size of Tf-GV-LPs. In this study, the conjugation of GCV-LPs to Tf up to 35% could not significantly alter their PI, zeta potential, EE(%) and LC(%) when compared to those of GCV-LPs before conjugation to Tf. The drug release kinetic of GCV from GCV-LPs and Tf-GCV-LPs were consistent with the Higuchi's model, with high values of r^2. This finding indicated that the interactions between GCV and liposomal vesicles that were confirmed by FT-IR spectroscopy analysis. In vitro cytotoxicity test of GCV-LPs and Tf-GCV-LPs suggested that they were safe for the ARPE-19 cells with percentage cell viability of 80–100%. The results of intracellular uptake of the optimized Tf-GCV-LPs in the ARPE-19 cells indicated that they were taken up by the cells via TfRs-mediated endocytosis. Furthermore, they could inhibit expression of CMV gB after infection effectively. Therefore, the optimized Tf-GCV-LPs, which were developed in this study, could be accepted as a potential drug delivery system for targeted GCV delivery to the retina for treatment of CMV retinitis.

CRediT authorship contribution statement

Rathapon Asasutjarit: Funding acquisition, Conceptualization, Investigation, Data curation, Project administration, Writing - original draft. **Chittima Managit:** Conceptualization, Investigation, Data curation. **Teva Phanaksri:** Conceptualization, Investigation, Data curation, Writing - original draft. **Worapapar Treesuppharat:** Conceptualization, Investigation, Data curation. **Asira Fuongfuchat:** Conceptualization, Investigation, Data curation, Writing - review & editing.

Declaration of Competing Interest

The authors declare that they have no known competing financial interests or personal relationships that could have appeared to influence the work reported in this paper.

Acknowledgements

The authors gratefully acknowledge the financial supports by The Thailand Research Fund (TRF) and Thammasat University for the Research Career Development Grant: grant No. RSA6080034.

Appendix A. Supplementary material

Supplementary data to this article can be found online at https://doi.org/10.1016/j.ijpharm.2020.119084.

References

Al-Halafi, A.M., 2014. Nanocarriers of nanotechnology in retinal diseases. Saudi J. Ophthalmol. 28, 304–309.
Anabousi, S., Laue, M., Lehr, C.M., Bakowsky, U., Ehrhardt, C., 2005. Assessing transferrin modification of liposomes by atomic force microscopy and transmission electron microscopy. Eur. J. Pharm. Biopharm. 60, 295–303.
Anabousi, S., Bakowsky, U., Schneider, M., Huwer, H., Lehr, C.M., Ehrhardt, C., 2006. *In vitro* assessment of transferrin-conjugated liposomes as drug delivery systems for inhalation therapy of lung cancer. Eur. J. Pharm. Sci. 29, 367–374.
Asasutjarit, R., Theerachayanan, T., Kewsuwan, P., Veeranodha, S., Fuongfuchat, A., Ritthidej, G.C., 2015. Development and evaluation of diclofenac sodium loaded-N-trimethyl chitosan nanoparticles for ophthalmic use. AAPS PharmSciTech. 16, 1013–1024.
Asasutjarit, R., Meesomboon, T., Adulheem, P., Kittiwisut, S., Sookdee, P., Samosornsuk, W., et al., 2019. Physicochemical properties of alpha-mangostin loaded nanomeulsions prepared by ultrasonication technique. Heliyon. 5, e02465.
Bochot, A., Fattal, E., 2012. Liposomes for intravitreal drug delivery: a state of the art. J. Control. Release. 161, 628–634.
Briuglia, M.L., Rotella, C., McFarlane, A., Lamprou, D.A., 2015. Influence of cholesterol on liposome stability and on in vitro drug release. Drug. Deliv. Transl. Res. 5, 231–242.
Chen, C.W., Lu, D.W., Yeh, M.K., Shiau, C.Y., Chiang, C.H., 2011. Novel RGD-lipid conjugate-modified liposomes for enhancing siRNA delivery in human retinal pigment epithelial cells. Int. J. Nanomed. 6, 2567–2580.
Chen, H., 2015. Recent developments in ocular drug delivery. J. Drug. Target. 23, 597–604.
Chen, Z.L., Huang, M., Wang, X.R., Fu, J., Han, M., Shen, Y.Q., et al., 2016. Transferrin-modified liposome promotes alpha-mangostin to penetrate the blood-brain barrier. Nanomedicine 12, 421–430.
Diebold, Y., Calonge, M., 2010. Applications of nanoparticles in ophthalmology. Prog. Retin. Eye. Res. 29, 596–609.
Duca, G., Anghel, L., Erhan, R.V., 2018. Structural aspects of lactoferrin and serum transferrin observed by FT-IR spectroscopy. Chem. J. Mold. 13, 111–116.
Eloy, J.O., Claro de Souza, M., Petrilli, R., Barcellos, J.P., Lee, R.J., Marchetti, J.M., 2014. Liposomes as carriers of hydrophilic small molecule drugs: strategies to enhance encapsulation and delivery. Colloids Surf. B Biointerfaces 123, 345–363.
Gijsens, A., Derycke, A., Missiaen, L., De Vos, D., Huwyler, J., Eberle, A., et al., 2002. Targeting of the photocytotoxic compound AlPcS4 to Hela cells by transferrin conjugated PEG-liposomes. Int. J. Cancer 101, 78–85.
Haidar, Z.S., Hamdy, R.C., Tabrizian, M., 2008. Protein release kinetics for core-shell hybrid nanoparticles based on the layer-by-layer assembly of alginate and chitosan on liposomes. Biomaterials 29, 1207–1215.
Janoly-Dumenil, A., Rouvet, I., Bleyzac, N., Bertrand, Y., Aulagner, G., Zabot, M.T., 2009. Effect of duration and intensity of ganciclovir exposure on lymphoblastoid cell toxicity. Antivir. Chem. Chemother. 19, 257–262.
Jiang, S., Franco, Y.L., Zhou, Y., Chen, J., 2018. Nanotechnology in retinal drug delivery. Int. J. Ophthalmol. 11, 1038–1044.
Kapanigowda, U.G., Nagaraja, S.H., Ramaiah, B., Boggarapu, P.R., 2015. Improved intraocular bioavailability of ganciclovir by mucoadhesive polymer based ocular microspheres: development and simulation process in Wistar rats. Dar. 23, 49.
Kim, T.H., Jo, Y.G., Jiang, H.H., Lim, S.M., Youn, Y.S., Lee, S., et al., 2012. PEG-transferrin conjugated TRAIL (TNF-related apoptosis-inducing ligand) for therapeutic tumor targeting. J. Control. Release. 162, 422–428.
Kompella, U.B., Amrite, A.C., Pacha, R.R., Durazo, S.A., 2013. Nanomedicines for back of the eye drug delivery, gene delivery, and imaging. Prog. Retin. Eye. Res. 36, 172–198.
Lajunen, T., Hisazumi, K., Kanazawa, T., Okada, H., Seta, Y., Yliperttula, M., et al., 2014. Topical drug delivery to retinal pigment epithelium with microfluidizer produced small liposomes. Eur. J. Pharm. Sci. 62, 23–32.
Lee, J.H., Agarwal, A., Mahendradas, P., Lee, C.S., Gupta, V., Pavesio, C.E., et al., 2017. Viral posterior uveitis. Surv. Ophthalmol. 62, 404–445.
Li, X., Ding, L., Xu, Y., Wang, Y., Ping, Q., 2009. Targeted delivery of doxorubicin using stealth liposomes modified with transferrin. Int. J. Pharm. 373, 116–123.
Manca, M.L., Matricardi, P., Cencetti, C., Peris, J.E., Melis, V., Carbone, C., et al., 2016. Combination of argan oil and phospholipids for the development of an effective liposome-like formulation able to improve skin hydration and allantoin dermal delivery. Int. J. Pharm. 505, 204–211.
Manconi, M., Manca, M.L., Valenti, D., Escribano, E., Hillaireau, H., Fadda, A.M., et al., 2017. Chitosan and hyaluronan coated liposomes for pulmonary administration of curcumin. Int. J. Pharm. 525, 203–210.
Merodio, M., Espuelas, M.S., Mirshahi, M., Arnedo, A., Irache, J.M., 2002. Efficacy of ganciclovir- loaded nanoparticles in human cytomegalovirus (HCMV)-infected cells. J. Drug. Target. 10, 231–238.
Moussa, K., Doan, T., Stewart, J.M., Shantha, J., Gonzales, J., Acharya, N., et al., 2018. Cytomegalovirus retinitis associated with occlusive vasculopathy in an elderly, human immunodeficiency virus-negative man. Retin. Case. Brief. Rep. 12, S114–S117.
Patel, A., Cholkar, K., Agrahari, V., Mitra, A.K., 2013. Ocular drug delivery systems: an overview. World. J. Pharmacol. 2, 47–64.
Perrottet, N., Decosterd, L.A., Meylan, P., Pascual, M., Biollaz, J., Buclin, T., 2009. Valganciclovir in adult solid organ transplant recipients: pharmacokinetic and pharmacodynamic characteristics and clinical interpretation of plasma concentration measurements. Clin. Pharmacokinet. 48, 399–418.
Qian, Z.M., Li, H., Sun, H., Ho, K., 2002. Targeted drug delivery via the transferrin receptor-mediated endocytosis pathway. Pharmacol. Rev. 54, 561–587.
Sahin, A., Hamrah, P., 2012. Acute herpetic keratitis: what is the role for ganciclovir ophthalmic gel? Ophthalmol. Eye. Dis. 4, 23–34.
Sakurai, E., Ozeki, H., Kunou, N., Ogura, Y., 2001. Effect of particle size of polymeric nanospheres on intravitreal kinetics. Ophthalmic. Res. 33, 31–36.

Sarbajna, R.M., Preetam, A., Devi, A.S., Suryanarayana, M.V., Sethi, M., Dutta, D., 2011. Studies on crystal modifications of ganciclovir. Mol. Cryst. Liq. Cryst. 537, 141–154.
Sasaki, H., Karasawa, K., Hironaka, K., Tahara, K., Tozuka, Y., Takeuchi, H., 2013. Retinal drug delivery using eyedrop preparations of poly-L-lysine-modified liposomes. Eur. J. Pharm. Biopharm. 83, 364–369.
Schneider, C.A., Rasband, W.S., Eliceiri, K.W., 2012. NIH Image to ImageJ: 25 years of Image analysis. Nat. Methods 9, 671–675.
Schubert, M.A., Muller-Goymann, C.C., 2005. Characterisation of surface-modified solid lipid nanoparticles (SLN): influence of lecithin and nonionic emulsifier. Eur. J. Pharm. Biopharm. 61, 77–86.
Shaker, S., Gardouh, A.R., Ghorab, M.M., 2017. Factors affecting liposomes particle size prepared by ethanol injection method. Res. Pharm. Sci. 12, 346–352.
Shen, Y., Tu, J., 2007. Preparation and ocular pharmacokinetics of ganciclovir liposomes. AAPS. J. 9, E371–E377.
Teoh, S.C., Ou, X., Lim, T.H., 2012. Intravitreal ganciclovir maintenance injection for cytomegalovirus retinitis: efficacy of a low-volume, intermediate-dose regimen. Ophthalmology 119, 588–595.
Veloso Jr., A.A., Zhu, Q., Herrero-Vanrell, R., Refojo, M.F., 1997. Ganciclovir-loaded polymer microspheres in rabbit eyes inoculated with human cytomegalovirus. Invest. Ophthalmol. Vis. Sci. 38, 665–675.
Wang, W., Zhou, F., Ge, L., Liu, X., Kong, F., 2012. Transferrin-PEG-PE modified dexamethasone conjugated cationic lipid carrier mediated gene delivery system for tumor-targeted transfection. Int. J. Nanomed. 7, 2513–2522.
Wille, P.T., Wisner, T.W., Ryckman, B., Johnson, D.C., 2013. Human cytomegalovirus (HCMV) glycoprotein gB promotes virus entry in trans acting as the viral fusion protein rather than as a receptor-binding protein. MBio. 4, e00332–e413.
Yang, X., Koh, C.G., Liu, S., Pan, X., Santhanam, R., Yu, B., et al., 2009. Transferrin receptor-targeted lipid nanoparticles for delivery of an antisense oligodeoxyribonucleotide against Bcl-2. Mol. Pharm. 6, 221–230.

Heliyon

Application of Film-forming solution as a transdermal delivery system of piperine-rich herbal mixture extract for anti-inflammation

--Manuscript Draft--

Manuscript Number:	HELIYON-D-20-01008R3
Article Type:	Original Research Article
Section/Category:	Pharmaceutical Science, Pharmacology, Toxicology
Keywords:	Film; Polymer solution; Transdermal drug delivery; Skin permeation; Piperine; Traditional medicine; Anti-inflammatory activity; Eye irritation; Skin toxicity
Manuscript Classifications:	50.150: Materials Application; 60.140: Natural product chemistry; 60.200: Pharmaceutical chemistry; 110.250: Pharmaceutical Science; 130.280: Pharmacology; 130.400: Alternative Medicine
Corresponding Author:	Rathapon Asasutjarit Thammasat University A. Klongluang, Pathum Thani THAILAND
First Author:	Rathapon Asasutjarit
Order of Authors:	Rathapon Asasutjarit
	Papawee Sookdee
	Sukitaya Veeranodha
	Asira Fuongfuchat
	Arunporn Itharat
Abstract:	Piperine-rich herbal mixture (PHM) used in this study is a traditional Thai medicine that contains 21 oriental herbs. It is called “Sahastara remedy” and is officially included in the Thai National List of Essential Medicine since A.D. 2011. PHM has been used orally to relieve muscle and bone pains. It contains Piper nigrum fruits as a major constituent and also Piper retrofractum fruits, PHM thus has anti-inflammatory activities that mostly come from the bioactivities of piperine consisting of these pepper fruits. Unfortunately, PHM usually causes gastrointestinal side effects. Consequently, a topical product containing an alcoholic extract of PHM (PHM-E), i.e., film-forming solution (FFS) was developed to overcome this drawback. The aims of this study were to investigate the anti-inflammatory activity of PHM-E, to evaluate physicochemical properties and the anti-inflammatory activity of FFS containing PHM-E (PHM-E FFS). Anti-inflammatory activities of PHM-E were investigated in the RAW 264.7 cells. Physicochemical properties, in vitro toxicities and anti-inflammatory activities of PHM-E FFS including its dry film (PHM-E film) were determined. PHM-E showed anti-inflammatory activities with dose dependent manners via inhibition of nitric oxide and prostaglandin E 2 production by the RAW 264.7 cells and promotion of the cell phenotype polarization from M1 to M2. PHM-E FFS had low viscosity and exhibited the Newtonian behavior. It provided elastic PHM-E film with low tensile strength. The release profile of piperine from PHM-E film followed a zero-kinetic model. PHM-E FFS demonstrated compatibility with the skin cells, minimal ocular irritant when accidentally splashing into the eye and moderate-to-high potency for inhibition of inflammatory symptoms in the rats. PHM-E FFS thus had potential for use in the further clinical study to investigate its efficacy and safety in patients.
Suggested Reviewers:	Sewan Theeramankong sewan_t@yahoo.com
	Walaisiri Muangsiri walaisiri@yahoo.com
	Worapapar Treesuppharat g4736963@gmail.com
	Chittima Manakit chittimm@g.swu.ac.th

Opposed Reviewers:	

Cover letter

This manuscript has not been previously published in any language, anywhere and it is not under simultaneous consideration by another journal.

Rathapon Asasutjarit

Recommended reviewers

1. Sewan Theeramankong, *E-mail address*: sewan_t@yahoo.com
2. Walaisiri Muangsiri, *E-mail address*: walaisiri@yahoo.com
3. Worapapar Treesuppharat, *E-mail address*: g4736963@gmail.com
4. Chittima Manakit, *E-mail address*: chittimm@g.swu.ac.th

Response to reviewers

Ms. Ref. No.: HELIYON-D-20-01008R2

Title: Application of Film-forming solution as a transdermal delivery system of piperine-rich herbal mixture extract for anti-inflammation

Journal: Heliyon

Dear editor,

We modified the manuscript according to the reviewers' suggestions. The detailed corrections and explanations are listed point by point as follows:

Editor and Reviewer comments:

Reviewer #1: The formulation proposed by the authors is interesting and their manuscript is well organised. The study is well designed but it lacks a skin permeation study. My suggestion is to add these data or revise the manuscript according to my comments below.

Methods:

Results: Why did the authors do not carry out skin permeation studies with the formulation and the control? I would like to suggest to reduce the number of Figures. Results of Figure 5 could be described in the text. Figure 4 could be added to the Supplementary Material. Were the data of Figure 6b modelled according to any equation? It seems like the data were linearised, but it is not clear in the Figure caption.

Interpretation: The in vitro studies were carried out with fibroblast. How can be the authors be sure about the permeation of piperine to reach the dermis?

Other comments: In the title, the authors claim the transdermal use of the developed formulation. However, they did not carry out skin permeation studies. Therefore, I would like to suggest to include these data or revised the title and the conclusion. In the conclusion they stated that the formulation has potential for being used in a clinical study... however, for being used in a clinical study, at least the drug permeation and the effective permeation of pipeline across the stratum corneum and epidermis should be demonstrated.

Response:

1. The skin permeation study of piperine from PHM-E FFS was performed according to the suggestion. The obtained results confirmed that piperine from PHM-E FFS could permeate through the skin, which were consistent with the results of *in vivo* anti-inflammatory test of PHM-E FFS as previously reported in the manuscript.

The detail of the methods and results were added to the manuscript as follows:

Methods

2.2.10. In vitro skin permeation study of PHM-E film

Skin permeation of piperine from PHM-E films was investigated in triplicate by using modified Franz diffusion cells and the skin from newborn pigs those died naturally after birth. The skin was supplied by a local pig farm. It was removed subcutaneous fat and then cut into 2x2 cm before storage at -18 °C. One hour prior to the experiment, the skin was equilibrated in PBS (pH 7.4) at 37 °C [15]. PHM-E films with the size of 2x2 cm, which covered the diffusion area (1.78 cm^2), were placed on the epidermis of the skin and faced to the donor unit. Then, they were put on the receptor unit containing ethanol (10% v/v) in PBS (pH 7.4), which was a receiving solution and was under stirring by a magnetic stirrer with temperature control at 37±1 °C. The receiving solutions were withdrawn at 1, 2, 3, 4, 6, 8, 10, 12, 14, 16, 18, 20 and 24 hours. Thereafter, the fresh solutions were replaced to maintain constant volume of the receiving solution. The piperine content in the receiving solutions was determined by the HPLC technique. The flux of piperine through the skin was calculated according to Fick's first law of diffusion [15].

Results and discussion

3.8 *In vitro skin permeation study of PHM-E film*

The skin permeation profile of piperine from PHM-E film is presented in Fig. 5 (a). It shows the non-steady state of skin permeation of piperine at the first 3 hours of the experiment, and then the steady state of skin permeation of piperine as seen in the linear portion of the plot. The lag time of skin permeation of piperine, which was determined by extrapolating the linear portion of the steady state permeation profile to the time axis (Fig. 5 (b)), was 57.6±0.5 min (0.96±0.01 hour). It indicated that the concentration gradient of piperine in the skin reached equilibrium at around 1 hour after the beginning of the experiment.

The linear portion of the permeation profile shown in Fig. 5 (b) was described by Equation (8). It was used for determination of the flux of piperine according to Fick's first law of diffusion [15].

Piperine permeated content = 0.55(Time) – 0.52; $r^2 = 0.9977$ Equation (8)

It was found that the flux of piperine through the skin was 0.31±0.04 µg/cm^2·hour. This result implied that approximately 0.31 µg of piperine from PHM-E film could permeate through a unit cross section of the skin in an hour.

Fig. 5

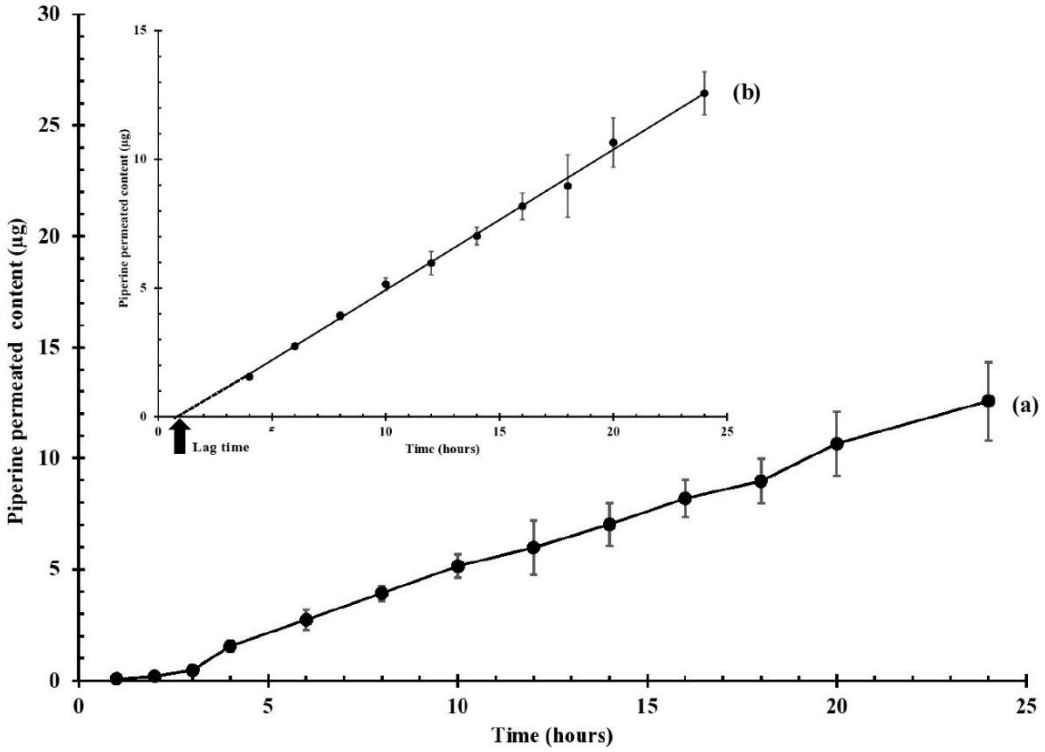

Fig. 5 Skin permeation profile of piperine from PHM-E film (mean±SD; n=3): (a) piperine permeated content against time; (b) linear relationship between piperine permeated content and time during 4-24 hours.

2. Fig.4 and 5 in the revised manuscript (R2) were removed. The results shown in these figures were described in the text as follows:

3.5. Rheological evaluation of Base FFS and PHM-E FFS

The study of rheological properties showed the linear relationship between shear stress and shear rate of Base FFS and PHM-E FFS, which are represented by the Equation (5) and (6), respectively.

Shear stress $_{\text{Base FFS}}$ = 0.087xShear rate $_{\text{Base FFS}}$; r^2= 0.9998 Equation (5)

Shear stress $_{\text{PHM-E FFS}}$ = 0.056xShear rate $_{\text{PHM-E FFS}}$; r^2= 0.9997 Equation (6)

3.6. Characterization of Base film and PHM-E film

The study of mechanical properties indicated that PHM-E film possessed an obviously lower tensile strength (0.99±0.09 MPa) than that of Base film (4.04±0.04 MPa) at a *p*-value of 0.000. It is possible that PHM-E reduced intermolecular forces between polymer chains and numbers of polymer-polymer contact leading to a decrease in the rigidity of the three-dimensional network in PHM-E film [32-34]. On the contrary, PHM-E film had significantly a greater percentage elongation at break (5.33±0.12%) than that of Base film (3.13±0.06%) at a *p*-value of 0.000. Thus, PHM-E had a plasticizing effect on the films [35]. The results from this study also showed that PHM-E film had a higher tackiness (18.05±0.05 gf) than that of Base film (13.97±0.05 gf) at a *p*-value of 0.000.

3. The data shown in Fig. 6 (b) : the linear portion of the Piperine release profile was described by the Equation (7). This equation was added to the manuscript.

Piperine released content = 0.19(Time) – 11.07; r^2 = 0.9928 Equation (7)

We really appreciate the reviewers' and the editor's valuable comments and kind suggestions.
Kindly inform us if there is any further concern. We are willing to respond promptly.
The manuscript has been resubmitted to your journal. We look forward to your positive response.

Best regards,
Rathapon Asasutjarit

1. Introduction

Inflammation is a pathophysiological response of living tissues to injuries, chemicals, irradiations, microbial infections and immune reactions. Its important signs are swelling, erythema, increased heat and pain at inflamed organs [1-3]. Recently, Global Burden of Disease 2016 (GBD 2016): Disease and Injury Incidence and Prevalence Collaborators [4] reported that during A.D. 2006-2016, the percentage changes of Years Lived with Disability (YLDs) of patients suffering from osteoarthritis (OA), low back pain and neck pain in 195 countries and territories grouped within 21 regions were increases of 31.5%, 18.0% and 21.9%, respectively. OA, in particular, causes knee pain and lower extremity disability in older adults and thus, lower quality of life [5].

Non-steroidal anti-inflammatory drugs (NSAIDs) are a group of acidic substances used for relieving inflammatory symptoms, pain and fever. They inhibit functions of cyclooxygenase enzymes (COXs) leading to blocking the synthesis process of prostaglandins. NSAIDs are used worldwide by more than 30 million people [6]. Around 59% of OA patients were treated with NSAIDs [7]. Some NSAIDs cause gastrointestinal and renal adverse reactions because of their inhibitory effect on COX-1, while their therapeutic effects are mainly from the inhibitory activity on COX-2 [6]. Thus, a search for new anti-inflammatory substances with fewer side effects is necessary, especially for those substances that can be administered by topical application for local effect to avoid systemic adverse reactions.

Piperine-rich herbal mixture (PMH) used in this study is a traditional Thai medicine called “Sahastara remedy”. It is used as an alternative medicine for muscle and bone pains and has been officially included in the Thai National List of Essential Medicine since A.D. 2011. The formulation of PHM contains the fruits of the black pepper (*Piper nigrum*) as a

major constituent and also the long pepper (*Piper retrofractum*) fruits as shown in Table 1. Therefore, the anti-inflammatory activities of PHM mostly come from the bioactivities of piperine, which consists of these pepper fruits [8]. It has been reported that piperine inhibited the production of nitric oxide (NO), prostaglandin E_2 (PGE_2) and tumor necrosis factor-α (TNF-α) in lipopolysaccharide (LPS)-activated RAW264.7 cells. As an inhibitor, it could thereby suppress inducible NO synthase (iNOS), COX-2 and TNF-α gene and protein expression. [9]. Pinsornsak et al. [10] investigated the efficacy of oral PHM for treatment of knee OA. The results showed that oral PHM reduced pain and improved ambulatory ability in patients who received orally 1,000 mg of PHM capsules 3 times per day for 28 days. Unfortunately, PHM sometimes caused heartburn and urticaria because of its high content of black pepper, as well as hepatic and renal toxicity from accumulation of camphor [10]. Consequently, alternative administration methods of PHM such as transdermal drug delivery could be considered as one of suitable administration methods to avoid the severe systemic side effects of PHM.

Film-forming solution (FFS) is a new product that is used for transdermal delivery of many drugs. Generally, FFS consists of drug(s), film-forming polymer(s) and necessary excipients, which are dissolved in a vehicle. FFS possesses fluidity characteristics, it thus can be sprayed or applied on skin easily. Upon evaporation of the vehicle, films will form on the skin and acts as a matrix for sustained release of drug to the skin [11-13]. FFS is currently accepted as one of attractive transdermal drug delivery systems [12]. It has favorable properties and advantages over the conventional transdermal drug delivery systems in many aspects, i.e., wearing off resistance, presence of an invisible film on the skin, convenience of use by either spraying or applying on the lesion area, and causing less fixing of the skin.

Nowadays, use of traditional medicines has been promoted in conserving folk wisdom for

healthcare. However, the actual efficacy and possible toxicity of some traditional medicines are still in doubt. Furthermore, they are usually inconvenient to be administered, for example, high doses with high frequencies of administration, unpleasant odors, unacceptable appearances and textures of the products themselves. Promoting the wide use of traditional medicines particularly among members of the younger generation will require consideration of the pharmacological effects of the remedies, along with the proper dosage form and the frequency of administration. Thus, the objectives of this study were to investigate anti-inflammatory activity of an alcoholic extract of PHM (PHM-E) and to evaluate physicochemical properties as well as anti-inflammatory activity of FFS containing PHM-E (PHM-E FFS).

2. Materials and methods

2.1. Materials

2.1.1. Chemicals

Dimethyl sulfoxide (DMSO), hydrochloric acid, sodium bicarbonate and sodium hydroxide were purchased from Univar, Australia. Ammonio methacrylate copolymer type A (Eudragit RL PO) and hydroxypropylcellulose (Klucel LF) were kindly provided by Darmstadt Ltd. (Germany) and Wilmington Ltd. (USA), respectively. All cell culture reagents were supplied by Gibco, USA. Cellulose dialysis tube with a molecular weight cutoff of 12,000, lipopolysaccharide (LPS) from *Escherichia coli*, 3-(4,5-dimethylthiazol-2-yl) -2,5-diphenyltetrazolium bromide (MTT), N-(1-Naphthyl) ethylenediamine dihydrochloride, polyethylene glycol 400 (PEG 400) and standard piperine were obtained from Sigma-Aldrich, USA**.** All other chemicals and solvents were analytical grade and were used as received.

2.1.2. Plant materials

All ingredients of PHM listed in Table 1 were purchased from local traditional medicine suppliers. They were identified and authenticated by Center of Excellence on Applied Thai Traditional Medicine Research, Faculty of Medicine, Thammasat University, Thailand. Their specimen voucher number was assigned by the Herbarium of Southern Center of Thai Traditional Medicine, Faculty of Pharmaceutical Sciences, Prince of Songkla University, Songkla, Thailand and also presented in Table 1.

2.2 Methods

2.2.1. Preparation of PHM-E

All ingredients in PHM formulation were weighed and mixed thoroughly. The mixture was macerated with 95% ethanol for three days to obtain PHM-E and then dried by use of an evaporator with a reduced pressure at 45 °C (Rotavapor R-205, Germany). The obtained PHM-E was chemically analyzed for piperine as a marker.

2.2.2. Determination of piperine content

Content of piperine in PHM-E and all samples was determined by using the high performance liquid chromatography (HPLC) technique. The analysis was performed by using the HPLC system (Agilent® 1200, USA) with a C18 column (Phenomenex® Luna, 4.6 x 250 mm, 5 micron). Ten µl of the samples were injected into the HPLC system and then eluted by gradient mobile phases composed of water/acetonitrile at various ratios as follows: 0 min, 60/40; 30 min, 50/50; and 60 min, 0/100 at a flow rate of 1.0 ml/min. The diode array detector was set at a wavelength of 340 nm.

2.2.3. Fourier-transform infrared (FT-IR) spectroscopy analysis

FT-IR spectroscopy analysis of standard piperine, PHM-E and obtained films from FFS with- and without PHM-E was carried out by using an FT-IR Spectrometer (PerkinElmer model Spectrum One, USA). Signal averages were obtained for 32 scans at a resolution of 4 cm^{-1} from 4,000 to 500 cm^{-1}.

2.2.4. Determination of in vitro anti-inflammatory activities

2.2.4.1. Effect of PHM-E on inhibition of nitric oxide (*NO) production by the RAW 264.7 cells*

The RAW 264.7 cells (ATCC, USA) were seeded in 96-well plates with a density of 10^4 cells/well containing 100 µl of a complete RPMI medium and were incubated until reaching a confluence (5% CO_2, 37 °C). The medium was then removed and replaced with 100 µl of fresh medium containing 4 ng/ml of lipopolysaccharide (LPS). Subsequently, 100 µl of PHM-E at various concentrations were added to each well, producing final concentrations of 0.1, 1, 10, 30 and 50 µg/ml. The cells were incubated for 24 hours. Finally, the medium in each well was transferred to a new 96-well plate with the addition of the Griess reagent to detect nitrite (NO_2^-), which is a stable and non-volatile breakdown product of NO. The optical density (OD) of the medium was determined by using a microplate reader (Molecular Devices, USA) at a wavelength of 570 nm. Percentage of inhibition was calculated by using Equation (1) and IC_{50} values were determined.

$$\text{Inhibition } (\%) = \frac{OD_{control} - OD_{sample}}{OD_{control}} x100 \qquad \text{Equation (1)}$$

$OD_{control}$ and OD_{sample} were the OD of the following media: the media from the cells

incubated with only LPS and the media from the cells incubated with LPS and the samples, respectively.

2.2.4.2. Effect of PHM-E on inhibition of prostaglandin E_2 (PGE_2) production by the RAW 264.7 cells

This study was performed by using a PGE_2 ELISA Kit (Cayman Chemical, USA). Briefly, after the RAW 264.7 cells were stimulated by LPS and incubated with PHM-E, supernatant (50 µl) was transferred to a 96-well pre-coated with mouse anti-rabbit IgG. Then, PGE_2 acetylcholinesterase tracer (50 µl) and PGE_2 monoclonal antibody (50 µl) were added into each well. They were incubated for 18 hours at 4 ºC without light exposure. The wells were then emptied and rinsed with a washing buffer. Thereafter, 200 µl of the Ellman's reagent were added to each well, and the plate was covered with plastic film and incubated in the dark for 1.5 hours at 37 ºC. The OD was read at a wavelength 412 nm by the microplate reader. The inhibition of PGE_2 production was calculated by using Equation (2), and IC_{50} values were determined.

$$\text{Inhibition (\%)} = \frac{OD_{sample} - OD_{activated}}{OD_{control} - OD_{activated}} \qquad \text{Equation (2)}$$

OD_{sample}, $OD_{activated}$ and $OD_{control}$ were the OD of the following media: the media from the cells incubated with LPS and the samples, the media from the cells incubated with only LPS, and the media from the cells without incubation with both LPS and the samples, respectively.

2.2.4.3. Effect of PHM-E on polarization of the RAW 264.7 cells

The activities of PHM-E in alteration of macrophage phenotype were studied in the RAW

264.7 cells following the previous publication by Chen et al. [14] with some modifications. The RAW 264.7 cells (M0) were incubated with either a mixture of LPS (100 ng/ml) and IFNγ (2.5 ng/ml) (Abcam, UK) or IL-4 (10 ng/ml) (Abcam, UK) for 12 hours to induce M1 and M2 phenotype, respectively. The content of M1 and M2 phenotype markers in the cell culture medium, i.e. IL-1β, and IL-10, respectively, were determined by ELISA test kits for the rat cytokines (Abcam, UK). They were performed following the product protocols. Moreover, the content of the cytokines were also determined after these M1 and M2 cells were further incubated with PHM-E (14 µg/ml) for 12 hours.

The results of this study were reported as fold changes of cytokine content in the medium. It was a ratio of the cytokine content released from the stimulated RAW 264.7 cells to the cytokine content released from the control, which was the untreated RAW 264.7 cells.

2.2.5. Determination of solubility of PHM-E in 65 % ethanol

The solubility of PHM-E in 65% ethanol, which was a vehicle of FFS, was investigated as follows: one ml of 65% ethanol was added to 1 gram of PHM-E contained in an Eppendorf tube. The mixture was continuously shaken for 24 hours at 37 °C and was centrifuged at 40,000 rpm for 30 min. The supernatant was filtered through a nylon filter (0.45 µm) and was then analyzed for the piperine content by the HPLC technique.

2.2.6. Preparation of FFS

FFS with PHM-E (PHM-E FFS) and FFS without PHM-E (Base FFS) containing Klucel LF, Eudragit RL PO and PEG 400 at a weight ratio of 4:4:1, respectively, were prepared. Briefly, Eudragit RL PO and Klucel LF were dispersed in 65% w/w ethanol and stirred continuously until clear solutions were obtained. PEG 400 was then added and stirred

thoroughly. In the case of PHM-E FFS, PHM-E was added to Base FFS to make a final concentration of 3%w/w. The pH value of preparations was determined in triplicate by using a pH meter (Hanna instruments 8417, USA).

2.2.7. Rheological evaluation of Base FFS and PHM-E FFS

The rheological evaluation of Base FFS and PHM-E FFS was performed in triplicate at 25 ± 0.1 °C using a controlled stress rheometer (Bohlin Gemini HR nano, Malvern instrument, UK) with a cone and plate geometry (2° cone and 55 mm diameter). Shear stress and shear viscosity of the samples were determined by a steady shear sweep mode with initial and final shear rates set at 0.1 and 1,000 s^{-1}, respectively.

2.2.8. Determination of mechanical properties of the films obtained from Base FFS and PHM-E FFS

Dry films of Base FFS and PHM-E FFS, which were called briefly as “Base film” and “PHM-E film”, respectively, were prepared as follows: Base FFS and PHM-E FFS (24 g) were poured onto Teflon molds (6×8 cm) and then dried in a hot-air oven at temperature of 45 °C (Memmert, Germany) for 12 hours.

To determine their mechanical properties, the films were cut into rectangular shapes (15×80 mm) and measured the tensile strength and %elongation at break by using a Universal Testing Machine (Instron 8801, USA) equipped with a 10 N load. The films were placed between two vertical grips, which were set at an initial distance of 40 mm. The movable grip was then moved upward at a speed of 500 mm/min until the films were rupture [13].

Tackiness of Base film and PHM-E film (2×2 cm) were determined by a probe tack test using a controlled-strain rheometer (model ARES-G2, TA Instrument, USA). The instrument

had a normal force-measuring unit equipped with a probe tack fixture (5 mm diameter). An axial force compression at 10 Pa-constant stress with 1 s-soak time duration, 0.01 mm-maximum gap change and 1 point/s-sampling rate were set. The tacking probe was moving away from the samples' surface at a speed of 10 mm/s with 5 s-soak time duration.

2.2.9. In vitro release study of PHM-E film

Release of piperine from PHM-E films through a cellulose dialysis membrane was determined by using modified Franz diffusion cells following the previous publication [13]. Briefly, PHM-E films were cut into 2x2 cm for a proper covering of the diffusion area (1.78 cm^2) and were then placed onto the cellulose dialysis membrane. The membrane with PHM-E film faced to a donor unit was placed between the donor and receptor units, which were filled with ethanol (10% v/v) in phosphate buffered saline (PBS) (pH 7.4) under continuously stirring by a magnetic stirrer and maintenance at 37±1 °C. The receiving solutions were withdrawn at 12 time-points (5, 10, 15, 30, 60, 120, 180, 240, 300, 360, 420 and 480 min.) and timely replaced with same volume of fresh media. Finally, the withdrawn receiving solutions were analyzed for piperine content by the HPLC technique.

2.2.10. In vitro skin permeation study of PHM-E film

Skin permeation of piperine from PHM-E films was investigated in triplicate by using modified Franz diffusion cells and the skin from newborn pigs those died naturally after birth. The skin was supplied by a local pig farm. It was removed subcutaneous fat and then cut into 2x2 cm before storage at -18 °C. One hour prior to the experiment, the skin was equilibrated in PBS (pH 7.4) at 37 °C [15]. PHM-E films with the size of 2x2 cm, which covered the diffusion area (1.78 cm^2), were placed on the epidermis of the skin and faced to

the donor unit. Then, they were put on the receptor unit containing ethanol (10% v/v) in PBS (pH 7.4), which was a receiving solution and was under stirring by a magnetic stirrer with temperature control at 37±1 °C. The receiving solutions were withdrawn at 1, 2, 3, 4, 6, 8, 10, 12, 14, 16, 18, 20 and 24 hours. Thereafter, the fresh solutions were replaced to maintain the constant volume of the receiving solution. The piperine content in the receiving solutions was determined by the HPLC technique. The flux of piperine through the skin was calculated according to Fick's first law of diffusion [15].

2.2.11. Skin toxicity of PHM-E FFS

In this study, Base FFS, PHM-E FFS and their films were tested for determination of their toxicity to skin fibroblasts. Each sample was dispersed in a complete DMEM medium to make sample dispersions with various concentrations of 2, 20, 60 and 100 µg/ml.

Human Dermal Fibroblasts, neonatal (HDFn) cells (Thermo Fisher Scientific, USA) were cultured in a complete DMEM and seeded in 96-well plates with a density of 10^4 cells/well/100 µl and incubated for 24 hours in a CO_2 incubator at 37°C. Thereafter, 100 µl of sample solutions at various concentrations were added to the wells, giving final concentration of 1, 10, 30, and 50 µg/ml. The cells were incubated with the sample solutions for 24 hours and washed twice with PBS (pH 7.4) after the end of incubation period. Fifty µl of MTT (0.5 mg/ml) in the medium were added to each well and incubated for four hours. The medium was then removed, and DMSO was added to dissolve the formazan crystal (100 µl/well). The OD of each well was measured at a wavelength of 570 nm by the microplate reader. Percentage of cell viability was calculated using Equation (3). The test samples were considered to be cytotoxic if the cell viability was less than 70% [16].

$$\text{Cell viability } (\%) = \frac{OD_{sample}}{OD_{control}} x100 \qquad \text{Equation (3)}$$

OD_{sample} and $OD_{control}$ were the OD of the following media: the media from the HDFn cells incubated with the samples and MTT solution, and the media from the HDFn cells incubated with only MTT solution, respectively.

2.2.12. Eye irritation test of PHM-E FFS

Due to fluidity properties of PHM-E FFS, this product could be sprayed or applied on the skin for pain relief easily. Meanwhile, it might be accidentally spilled and splashed into the eye. Therefore, the eye irritation potential of PHM-E FFS had to be evaluated. In this study, the short time exposure (STE) test was performed following the OECD guideline [17]. Briefly, SIRC cells (the rabbit corneal cell line) (ATCC, USA) were cultured in complete MEM and seeded in 96-well plates with a density of 10^4 cells/well/100 µl and incubated in a CO_2 incubator at 37°C until reaching a confluence. Then, they were exposed to 200 µl of either 5% or 0.05% w/v PHM-E FFS dissolved in normal saline for 5 min. Thereafter, the cells were washed twice with PBS (pH 7.4). Two hundred microliters of MTT (0.5 mg/ml) in the medium were added to each well and incubated for two hours. The medium was then removed, and 0.04 N hydrochloric acid-isopropanol was added to dissolve the formazan crystal (200 µl/well) for an hour. The OD of each well was measured at a wavelength of 570 nm by the microplate reader. For this study, the 100% cell viability (CV) was calculated from the OD of the wells containing the SIRC cells without exposure to the test solutions. The result was shown as a mean of CV ± SD.

The eye irritation potential from the test was scored following the criteria of the STE test.

The summed scores were used to rank the eye irritation potential as follows: the total score of 1, 2 and 3 were defined as the minimal ocular irritant, the moderate ocular irritant and the severe ocular irritant, respectively.

2.2.13. In vivo anti-inflammatory test of PHM-E FFS

Eighteen male Wistar rats weighing 120±10 g were purchased from the National Laboratory Animal Center, Mahidol University, Thailand. The procedure for use and care of the animals for this study was approved by the Animal Care Committee at the Thailand Institute of Scientific and Technological Research (TISTR) (Project code #PS-59002). The animal experiment was conducted in full compliance with local, national, ethical, and regulatory principles and local licensing regulations, in accordance with the spirit of the Association for Assessment and Accreditation of Laboratory Animal Care (AAALAC) for international's expectations of animal care and use/ethics committees.

Before starting the test for 7 days, a preliminary experiment was performed to determine the potential of Base FFS, phenylbutazone, PHM-E FFS and 5% w/v ethyl 3-phenylpropiolate (EPP) (Sigma-Aldrich, USA) solution in acetone, for induction of skin irritation by applying these test samples on the rats' inner and outer left ear surface (10 µl each) (n = 3). The signs of skin irritation and inflammation, i.e. skin rash, erythema and edema of the rats' ears were observed at day 1, 2 and 3 after application.

The *in vivo* anti-inflammatory test was modified based on the previous report by Dunstan et al. [18]. The rats were equally divided into three groups (6 rats/group) as follows: 1) a negative control group, 2) a positive control group and 3) a test group. They received Base FFS, phenylbutazone and PHM-E FFS dissolved in acetone, respectively. The thickness of the rats' right ear was measured before starting the test by a pocket thickness

gauge (Mitutoyo, Japan) for use at the baseline of ear thickness. Each test samples diluted with acetone was applied onto the inner and outer right ear surface (10 µl each). Thirty minutes later, the right ear of each rat was treated with 5% w/v ethyl EPP in acetone by application on both surfaces of each ear. Thereafter, the thicknesses of the ears were measured at 30 min, 1 hour and 2 hours after the inductions. The percentage of edema inhibition was calculated at the indicated time intervals.

At the end of the study, the rats were immediately euthanized and the treated ears were collected. The rats' ears were immersed in formalin solution (10% v/v in PBS) (Sigma-Aldrich, USA), paraffin-embedded, sliced and hematoxylin and eosin (H&E) stained [1]. The stained rats' ear tissues were then observed under a light microscope (Nikon Eclipse E200, Japan) for comparison of thickness as well as cell infiltration in the rats' ear tissue.

2.2.14. Determination of IL-1β and TNF-α content in the rats' ear tissue

To determine the cytokine content in the treated rats' ear, content of IL-1β and TNF-α in the rats' ear tissue were measured [19]. Each tissue sample (0.05 g) from the rats' ear that received PHM-E FFS, Base FFS or phenylbutazone and exposed to EPP for 2 hours were homogenized in PBS (pH 7.4) containing sodium chloride (0.4 mol/l), Tween 20 (0.05% w/v), bovine serum albumin (0.5% v/v), benzethonium chloride (0.1 mmol/l), EDTA (10 mmol/l) and aprotinin (20 KIU/ml). The lysates were centrifuged at 10,000 rpm at 4 °C for 60 min. Thereafter, the supernatant was collected for analysis of IL-1β and TNF-α by using ELISA kits for the rat IL-1β and TNF-α, respectively (Abcam, UK). They were performed following the product protocols.

2.2.15. Statistical analysis

Experimental results were presented as a mean with either standard deviation (SD) or standard error of mean (SEM). Statistical analysis for comparing treatment effects were performed by either an independent T-test or a one-way analysis of variance (ANOVA) with Tukey's HSD Post Hoc Test at a significant level of 0.05.

3. Results and discussion

3.1. Preparation and characterization of PHM-E

The obtained PHM-E was a clear solution with a slightly dark green color and a characteristic odor. The calculated percentage yield of PHM-E was 38.4% w/w as based on total weight of dry PHM. The pH value of PHM-E was 5.41±0.00 suggesting that it was compatible with the pH value of a normal skin surface (which is approximately 5.00) [20, 21].

HPLC chromatograms of PHM-E and standard piperine are shown in Fig. 1 (a) and (b). The chromatogram peak of the extract appeared at the same retention time of standard piperine, which was around 20 min. The timing of this peak indicated that the major constituent of the extract was piperine as derived mainly from the fruits of black pepper (*Piper nigrum*) and long pepper (*Piper retrofractum*). A linear regression equation for the determination of piperine content is presented in Equation (4)

$$\text{Area under curve}_{\text{piperine}} = 72.38(\text{Concentration}_{\text{piperine}}) + 203.2;\ r^2 = 0.9998 \quad \text{Equation (4)}$$

The content of piperine in PHM-E as determined by the HPLC technique and calculated by use of Equation (4) was 85.08±1.03 mg/g. This finding suggested that the extraction procedure used in this study could efficiently extract piperine from the remedy to

obtain PHM-E containing 8.51% w/w of piperine.

Fig. 2 (a) exhibited major IR absorption bands of standard piperine at wavenumbers of 1582, 1633, 2940 and 3008 cm^{-1} corresponding to ketone, amine, CH_2-CH_2-CH_3, and alkene groups in the piperine molecule, respectively. They were in consistent with the FT-IR spectrum of piperine presented in previous reports [22, 23]. The FT-IR spectrum of PHM-E illustrated in Fig. 2 (b) also showed IR absorption bands of the amine- and CH_2-CH_2-CH_3 group of piperine with trivial shifts to wavenumbers of 1632 and 2938 cm^{-1}, respectively. However, the characteristic bands of ketone and alkene groups found in FT-IR spectrum of standard piperine could not be observed in this spectrum. This finding could be explained by interactions between piperine and other compounds in PHM-E.

3.2. Determination of in vitro anti-inflammatories activity of PHM-E

3.2.1. Effect of PHM-E on inhibition of NO and PGE_2 production by the RAW 264.7 cells

The results shown in Fig. 3 (a) revealed that the higher the concentration of PHM-E, the higher the percentage inhibition of both NO and PGE_2 production. These findings were in agreement with the previous report by Bang et al. [24]. They found that anti-inflammatory activity of piperine was dependent on the doses being administered. Consequently, anti-inflammatory activities of PHM-E increased in a dose-dependent manner. Furthermore, the IC_{50} values of PHM-E for inhibition of NO and PGE2 production were 7.92±0.23 and 13.23±0.23 μg/ml, respectively.

3.2.2. Effect of PHM-E on polarization of the RAW 264.7 cells

In this study, the effect of PHM-E on phenotype polarization of the RAW 264.7 cells was investigated. The obtained results are shown in Fig. 3(b). It presents the fold change of the

released cytokine content that was a ratio of the released cytokine content from the stimulated cells to that of the control. It was found that the RAW 264.7 cells treated with the mixture of LPS and IFNγ released higher IL-1β content than that of the control (*p*-value = 0.000), while, the released content of IL-10 were comparable to that of the control (*p*-value = 0.952). This result suggested that the RAW 264.7 cells phenotype was polarized from M0 to M1 by the mixture of LPS and IFNγ. The data presented in Fig. 3 (b) also pointed out that the phenotype of the RAW 267.4 cells was changed from M0 to M2 by stimulation of the cells with IL-4. It showed that the IL-4-treated RAW 264.7 cells released IL-1β at the similar content to that of the control (*p*-value = 0.999). However, they released higher content of IL-10 than that of the control (*p*-value = 0.000) [14].

Fig. 3(b) indicated that IL-10 content from the medium of the cells incubated with the mixture of LPS and IFNγ and further incubated with PHM-E (M1+PHM-E) was significantly higher than that of the control and the cells incubated with the mixture of LPS and IFNγ without PHM-E (M1) (*p*-value = 0.000 and 0.000, respectively). Meanwhile, the content of IL-1β were dramatically decreased to the similar content to that of the control (M0) (*p*-value = 1.000) and were lower than that of the cells incubated with the mixture of LPS and IFNγ without PHM-E (M1) (*p*-value = 0.000). This finding evidenced that the RAW 264.7 cells phenotype was polarized from M1 to M2 by PHM-E.

The IL-10 content in the medium of the RAW 264.7 cells those were treated with IL-4 and PHM-E (M2+PHM-E) were comparable to that of the cells treated with IL-4 (M2) only (*p*-value = 0.511) and were higher than that of the control (M0) (*p*-value = 0.000). The IL-1β content from these cells were not significantly different with that of the cells treated with IL-4 only (M2) and the control (M0) at *p*-values of 0.969 and 0.996, respectively. The results demonstrated that the M2 phenotype of the RAW 264.7 cells was not changed to M1 by

PHM-E. Therefore, PHM-E could be accepted as an anti-inflammatory agent acting via the inhibition of NO and PGE_2 production by macrophages and promotion of macrophage phenotype polarization from M1 to M2.

The obtained results were consistent with the previous study [25]. It reported that PHM-E could inhibit production of IL-1β, which regulates the activity of other pro-inflammatory mediators of inflammatory process in the primary human dermal fibroblasts. PHM-E thus had potential for using as an alternative substance in treatment of inflammatory diseases in various organs which include muscle pain, rheumatoid arthritis, osteoarthritis and ankylosing spondylitis [26-30]

3.3. Determination of solubility of PHM-E in 65% ethanol

Solubility of PHM-E in 65% ethanol, which was a vehicle of PHM-E FFS, was investigated to determine the maximum content of PHM-E that could be loaded into the formulation. It was found that solubility of PHM-E in 65% ethanol was 0.37±0.00 g/ml (mean±SD; n=3) equivalent to the piperine content of 31.6±0.1 mg/ml (mean±SD; n=3). It could be concluded that PHM-E was freely soluble in 65% ethanol.

3.4. Preparation and characterization of Base FFS and PHM-E FFS

Base FFS and PHM-E FFS prepared in this study were homogeneous solutions without precipitation of any ingredients. The obtained Base FFS was clear in appearance and colorless. After PHM-E was added to Base FFS, the clear, brown PHM-E FFS with the mild characteristic odor of PHM-E was obtained. PHM-E FFS had a pH value of 5.98±0.03 which differed from the pH 6.74±0.04 (*p*-value = 0.000) of Base FFS since the acidity of PHM-E remained as reported in the previous section. However, this pH value was still in the

range of pH values that are generally known to be safe for transdermal applications.

3.5. Rheological evaluation of Base FFS and PHM-E FFS

The study of rheological properties showed the linear relationship between shear stress and shear rate of Base FFS and PHM-E FFS, which are represented by the Equation (5) and (6), respectively.

$$\text{Shear stress}_{\text{Base FFS}} = 0.087 \times \text{Shear rate}_{\text{Base FFS}};\ r^2 = 0.9998 \qquad \text{Equation (5)}$$

$$\text{Shear stress}_{\text{PHM-E FFS}} = 0.056 \times \text{Shear rate}_{\text{PHM-E FFS}};\ r^2 = 0.9997 \qquad \text{Equation (6)}$$

The results indicated that Base FFS and PHM-E FFS had the Newtonian flow behavior with a low viscosity of 0.087±0.003 and 0.056±0.004 Pas, respectively. They implied that both Base FFS and PHM-E FFS could be administered easily by either spraying or applying on skin. However, the lower viscosity of PHM-E FFS compared to Base FFS was observed. This result indicated that PHM-E in PHM-E FFS decreased polymer chain-solvent interactions [31].

3.6. Characterization of Base film and PHM-E film

The Fig. 2 (c) showed important bands of Base film at wavenumbers 1732 and 2955 cm^{-1} that were assigned to the carbonyl ester vibration and the C-H stretching of Eudragit RL PO, respectively; and 3422 cm^{-1} corresponded to the hydroxyl group in Klucel LF. In PHM-E film, characteristic bands of piperine with minor shifts were found as shown in in Fig. 2 (d); these shifts were observed at wavenumbers of 1630 and 2939 cm^{-1} representing amine- and CH_2-CH_2-CH_3 group in the piperine molecule, respectively. Although some important bands of film base still appeared at nearly the same wavenumber as previously shown in Fig. 2 (c), the band of hydroxyl group in Klucel LF at wavenumber of 3422 cm^{-1} had disappeared. It is

possible that intermolecular interactions such as H-bonding between the hydroxyl groups of film base and the piperine molecule had occurred.

The study of mechanical properties indicated that PHM-E film possessed an obviously lower tensile strength (0.99±0.09 MPa) than that of Base film (4.04±0.04 MPa) at a *p*-value of 0.000. It is possible that PHM-E reduced intermolecular forces between polymer chains and numbers of polymer-polymer contact leading to a decrease in the rigidity of the three-dimensional network in PHM-E film [32-34]. On the contrary, PHM-E film had significantly a greater percentage elongation at break (5.33±0.12%) than that of Base film (3.13±0.06%) at a *p*-value of 0.000. Thus, PHM-E had a plasticizing effect on the films [35]. The results from this study also showed that PHM-E film had a higher tackiness (18.05±0.05 gf) than that of Base film (13.97±0.05 gf) at a *p*-value of 0.000. It was due to the fact that PHM-E reduced the interactions of the polymer chain-chain causing the polymer chains to move freely, and then, interacted firmly with the test probe surface [33]. However, it did not cause an obviously sticky feel on the skin. Therefore, PHM-E FSS had advantages for the topical application of PHM-E because it provided PHM-E film having flexibility, extensibility and anti-peel-off properties.

3.7. In vitro release study of PHM-E film

The release profile of PHM-E film is illustrated in Fig. 4 (a). During the first 15 min of the experiment, the piperine content could not be detected in the receiving solutions. It is possible that the films needed more time for properly moistening by the receiving solution [36]. Furthermore, the amount of piperine released from the films at the beginning of the study was less than the limit of detection of the analysis method.

The release profile of the PHM-E film in Fig. 4 (b) showed that following the first 60

min, the piperine was released continuously to the receiving solutions consistent with a zero-order kinetic model as shown in Equation (7) at a constant rate of 0.19 µg/min.

Piperine released content = 0.19(Time) – 11.07; r^2 = 0.9928 Equation (7)

This finding indicated that the release rate of piperine from PHM-E film was constant for the entire experiment and independent of any drug concentrations in the film. A steady release rate constant of the PHM-E film over time made possible the benefits of this PHM-E film. It could minimize the frequency of drug administration and lessen the side effects of PHM-E from reduction in its usage [37]. Therefore, FFS could be used as an effective carrier for topically controlled release of piperine from PHM-E.

3.8 *In vitro skin permeation study of PHM-E film*

The skin permeation profile of piperine from PHM-E film is presented in Fig. 5 (a). It shows the non-steady state of skin permeation of piperine at the first 3 hours of the experiment, and then the steady state of skin permeation of piperine as seen in the linear portion of the plot. The lag time of skin permeation of piperine, which was determined by extrapolating the linear portion of the steady state permeation profile to the time axis (Fig. 5 (b)), was 57.6±0.5 min (0.96±0.01 hour). It indicated that the concentration gradient of piperine in the skin reached equilibrium at around 1 hour after the beginning of the experiment.

The linear portion of the permeation profile shown in Fig. 5 (b) was described by Equation (8). It was used for determination of the flux of piperine according to Fick's first law of diffusion [15].

Piperine permeated content = 0.55(Time) – 0.52; r^2 = 0.9977 Equation (8)

It was found that the flux of piperine through the skin was 0.31±0.04 µg/cm^2·hour. This result implied that approximately 0.31 µg of piperine from PHM-E film could permeate through a unit cross section of the skin in an hour.

3.9. Skin toxicity test of PHM-E FFS

The results of *in vitro* skin toxicity test of Base FFS, PHM-E FFS, Base film and PHM-E film on the HDFn cells are shown in Table 2. It indicated that the HDFn cells could survive after exposure to all test samples with the cell viability of around 100% which was more than 70%. The test samples, thus, were not toxic to the skin cells at entire test concentrations [38] and could be accepted as safe for further *in vivo* study.

3.10 Eye irritation test of PHM-E FFS

As previously mentioned, PHM-E FFS had fluidity characteristics, it could be either sprayed or topically applied on the skin. However, this product might be unintentionally splashed into the eye, therefore, eye irritation potential of PHM-E FFS was determined following the suggestion by the United Nations Globally Harmonized System of Classification and Labeling of Chemicals (UN GHS) [17]. The CV of the SIRC cells after exposure to 5% and 0.05% w/v of PHM-E FFS for 5 min are shown in Table 3. The total score from summation of the obtained scores following the criteria of STE test was equal to 1. Therefore, PHM-E FFS was categorized as a minimal ocular irritant when it was accidentally spilled or splashed into the eye.

3.11. In vivo anti-inflammatory test of PHM-E FFS

The results of preliminary experiment indicated that Base FFS, phenylbutazone and PHM-E FFS dissolved in acetone did not cause symptoms of skin irritation and inflammation in all treated rats' ears during the 3-day experiment. Meanwhile, skin rash, erythema and edema were obviously observed in the rats' ears which exposed to EPP solution within 1 hour after application. These results suggested that Base FFS, phenylbutazone and PHM-E FFS were safe to the rats' skin. On the other hand, EPP solution was a strong skin irritant that could induce skin inflammation in the rats' ear.

Fig. 6 (A) shows that the rats receiving PHM-E FFS had a significantly lower ear thickness than that of the rats receiving Base FFS at *p*-values of 0.001, 0.000 and 0.006 after ear edema induction for 30 min, 1 hour and 2 hours, respectively. They also had an obviously lower ear thickness than that of the rats receiving phenylbutazone at *p*-values of 0.022, 0.01 and 0.002 at the same time intervals. Although the ear thickness of the rats' ear treated with phenylbutazone and Base FFS were different at *p*-values of 0.003 and 0.007 after ear edema induction for 30 min and 1 hour, respectively, they were statistically comparable at 2 hours after ear edema induction (*p*-value = 0.100). This result suggested that anti-inflammatory activity of phenylbutazone dramatically decreased within 2 hours.

It was found that PHM-E FFS could inhibit rat ear edema by about 67.9%, 64.6% and 39.4% after ear edema induction for 30 min, 1 and 2 hours, respectively. Meanwhile, phenylbutazone and Base FFS could inhibit rat ear edema at 30 min by about 43.6% and 18.6%; at 1 hour by about 37.1% and 18.4%; as well as at 2 hours by about 16.7% and 15.5%, respectively. Dunstan et al. [18] recommended that the anti-inflammatory activity of test samples could be categorized according to the following criteria: strong activity = more than

70% of rat ear edema inhibition; moderate activity = 40-69%; low activity = 20-39% and not active = less than 20%. Therefore, PHM-E FFS had a moderate-to-high anti-inflammatory activity, while, phenylbutazone, a standard substance used as a positive control for this study, had a moderate-to-low activity. However, Base FFS did not have anti-inflammatory activity. The results implied that anti-inflammatory of PHM-E FFS was mainly from PHM-E consisting of the formulation.

These findings were confirmed by the photographs of H&E- stained rats' ear tissues after treatment with the test samples and ear edema induction for 2 hours as illustrated in Fig. 6 (B). Fig. 6 (B)-(a) demonstrated that the rats' ear treated with PHM-E FFS had lower thickness and less cell filtration than those of the rats' ear treated with Base FFS and phenylbutazone as depicted in Fig. 6 (B)-(b) and (c), respectively. It indicated that PHM-E FFS could effectively reduce ear edema and cell filtration, which was neutrophil-rich associated with edema [1].

3.12. Determination of IL-1β and TNF-α content in the rats'ear tissue

The content of IL-1β and TNF-α in the rats' ear tissue after treatment with the test samples and ear edema induction for 2 hours are presented in Fig. 7. The results showed that IL-1β content in the rats' ear receiving Base FFS and phenylbutasone were significantly higher than that of the rats' ear receiving PHM-E FFS at a *p*-value of 0.013 and 0.032, respectively. They were in agreement with the TNF-α content in the rats' ear treated with Base FFS and phenylbutasone, which were higher than that of the rats' ear exposed to PHM-E FFS at *p*-values of 0.006 and 0.022, respectively. These findings pointed out that PHM-E FFS could decrease the content of pro-inflammatory cytokines in the inflamed tissue, in particular, IL-1β and TNF-α and also evidenced that PHM-E FFS had a stronger anti-inflammatory

activity than that of Base FFS and phenylbutazone. Therefore, it has become possible to use PHM-E FFS for delaying the progress of inflammatory diseases.

4. Conclusions

PHM-E obtained from this study showed anti-inflammatory activity via inhibition of NO and PGE_2 released from the RAW 264.7 cells and promotion of the cell phenotype polarization from M1 to M2. After incorporation of PHM-E into FFS, physicochemical properties of the obtained PHM-E FFS, i.e. its physical appearance, pH, and viscosity were different from those of Base FFS. It was found that PHM-E film had a lower tensile strength, a greater percentage elongation at break and a greater tackiness than those of the Base film. The release of PHM-E from PHM-E FFS films was in agreement with a zero-order kinetic model. The skin toxicity test indicated that Base FFS, PHM-E FFS, Base film and PHM-E film could be accepted as safe for topical use. The result of eye irritation test suggested that PHM-E FFS could be categorized as a minimal ocular irritant when it was accidentally spilled or splashed into the eye. From the *in vivo* anti-inflammatory activity test, PHM-E FFS could reduce the rats' ear edema with a higher percentage inhibitory activity than Base FFS and phenylbutazone. PHM-E FFS was thus classified as a moderate-to-high anti-inflammatory product and had potential for being used in a clinical study to investigate its efficacy and safety in patients.

References

[1] Pivetta TP, Simões S, Araújo MM, Carvalho T, Arruda C, Marcato PD. Development of nanoparticles from natural lipids for topical delivery of thymol: Investigation of its anti-inflammatory properties. Colloids Sur B Biointerfaces. 2018;164:281–90.

[2] Sosa S, Balick MJ, Arvigo R, Esposito RG, Pizza C, Altinier G, et al. Screening of the topical anti-inflammatory activity of some Central American plants. J Ethnopharmacol. 2002;81:211–5.

[3] Vogl S, Picker P, Mihaly-Bison J, Fakhrudin N, Atanasov AG, Heiss EH, et al. Ethnopharmacological in vitro studies on Austria's folk medicine-An unexplored lore in vitro anti-inflammatory activities of 71 Austrian traditional herbal drugs. J Ethnopharmacol. 2013;149750–71.

[4] GBD 2016 Disease and Injury Incidence and Prevalence Collaborators. Global, regional, and national incidence, prevalence, and years lived with disability for 328 diseases and injuries for 195 countries, 1990–2016: a systematic analysis for the Global Burden of Disease Study 2016. Lancet. 2017;390:1211-1259.

[5] Goulet JL, Buta E, Brennan M, Heapy A, Fraenkel L. Discontinuing a non-steroidal anti-inflammatory drug (NSAID) in patients with knee osteoarthritis: Design and protocol of a placebo-controlled, noninferiority, randomized withdrawal trial. Contemp Clinl Trials. 2018;65:1–7.

[6] Terzi M, Altun G, Şen S, Kocaman A, Kaplan AA, Yurt KK, et al. The use of non-steroidal anti-inflammatory drugs in neurological diseases. J Chem Neuroanat. 2018;87:12–24.

[7] Porcheret M, Jordan K, Jinks C, Croft P. in collaboration with the Primary Care Rheumatology Society. Primary care treatment of knee pain—a survey in older adults. Rheumatology. 2007; 46: 1694–700.

[8] Kakatum N, Jaiarree N, Makchucit S, Itharat A. Antioxidant and anti-inflammatory activities of Thai medicinal plants in Sahasthara remedy for muscle pain treatment. J Med Assoc Thai. 2012; 95 Suppl.1: S120-6.

[9] Ying X, Yu K, Chen X, Chen H, Hong J, Cheng S, Peng L. Piperine inhibits LPS induced expression of inflammatory mediators in RAW 264.7 cells. Cell Immunol. 2013; 285 : 49-54.

[10] Pinsornsak P, Kanokkangsadal P, Itharat A. The clinical efficacy and safety of the Sahastara remedy versus diclofenac in the treatment of osteoarthritis of the knee: A double-blind, randomized, and controlled trial. Evid Based Complement Alternat Med.2015; 2015:103046: 1-8.

[11] Kathe K, Kathpalia H. Film forming systems for topical and transdermal drug delivery. AJPS. 2017;12:487–97.

[12] Mori NM, Patel P, Sheth NR, Rathod LV, Ashara KC. Fabrication and characterization of film-forming voriconazole transdermal spray for the treatment of fungal infection. B-FOPCU. 2017;55:41–51.

[13] Asasutjarit R, Larpmahawong P, Fuongfuchat A, Sareedenchai V, Veeranondha S. Physicochemical properties and anti-*Propionibacterium acnes* activity of film-forming solutions containing alpha-mangostin-rich extract. AAPS PharmSciTech. 2014; 15:306-16.

[14] Chen F, Guo N, Cao G, Zhou J, Yuan Z. Molecular Analysis of Curcumin-induced Polarization of Murine RAW264.7 Macrophages. J Cardiovasc Pharmacol. 2014;63:544-52.

[15] Cilurzo F, Minghetti P, Sinico C. Newborn pig skin as model membrane in in vitro drug permeation studies: a technical note. AAPS PharmSciTech. 2007;8:E94. doi: 10.1208/pt0804094.

[16] Romagna G, Allifranchini E, Bocchietto E, Todeschi S, Esposito M, Farsalinos KE. Cytotoxicity evaluation of electronic cigarette vapor extract on cultured mammalian

fibroblasts (ClearStream-LIFE): comparison with tobacco cigarette smoke extract. Inhal Toxicol. 2013; 25:354-61.

[17] Organisation for Economic Cooperation and Development (OECD). OECD guideline for the testing of chemicals (No. 491): Short time exposure in vitro test method for identifying I) chemicals inducing serious eye damage and II) chemicals not requiring classification for eye irritation for eye irritation or serious eye damage. ENV Publications, OECD, Paris, France. 2018.

[18] Dunstan AC, Noreen Y, Serrano G, Cox PA, Perera P, Bohlin L. Evaluation of some Samoan and Peruvian medicinal plants by prostaglandin biosynthesis and rat ear oedema assays. J Ethnopharmacol. 1997; 57:35–56.

[19] Loram LC, Fuller A, Fick LG, Cartmell T, Poole S, Mitchell D. Cytokine Profiles During Carrageenan-Induced Inflammatory Hyperalgesia in Rat Muscle and Hind Paw. J Pain. 2007; 8:127-36.

[20] Lambers H, Piessens S, Bloem A, Pronk H, Finkel, P, Natural skin surface pH is on average below 5, which is beneficial for its resident flora. Int J Cosmet Sci. 2006; 28: 359-370.

[21] Wang S, Zhang G, Meng H, Li L. Effect of Exercise-induced sweating on facial sebum, stratum corneum hydration, and skin surface pH in normal population. Skin Res Technol. 2013; 19: e312-e317.

[22] Sedeky AS, Khalil IA, Hefnawy A, El-Sherbiny IM. Development of core-shell nanocarrier system for augmenting piperine cytotoxic activity against human brain cancer cell line. Eur J Pharm Sci. 2018; 118: 103-12.

[23] Wang R, Han J, Jiang A, Huang R, Fu T, Wang L, Zheng Q, Li W, Li J. Involvement of metabolism-permeability in enhancing the oral bioavailability of curcumin in

excipient-free solid dispersions co-formed with piperine. Int J Pharm. 2019; 561: 9-18.

[24] Bang JS, Oh DH, Choi HM, et al. Anti-inflammatory and antiarthritic effects of piperine in human interleukin 1β-stimulated fibroblast-like synoviocytes and in rat arthritis models. Arthritis Res Ther. 2009; 11:R49. doi:10.1186/ar2662.

[25] Thamsermsang O, Akarasereenont P, Laohapand T, Panich U. IL-1β-induced modulation of gene expression profile in human dermal fibroblasts: the effects of Thai herbal Sahatsatara formula, piperine and gallic acid possessing antioxidant properties. BMC Complement Altern Med. 2017; 17:32. DOI 10.1186/s12906-016-1515-0.

[26] Butt MS, Pasha I, Tauseef Sultan M, Atif Randhawa MA, Saeed F, Ahmed W. Black pepper and health claims: a comprehensive treatise. Crit Rev Food Sci Nutr. 2012; 53:9, 875-86.

[27] Umar S, Golam Sarwar AHM, Umar K, Ahmad N, Sajad M, Ahmad S., et al. Piperine ameliorates oxidative stress, inflammation and histological outcome in collagen induced arthritis. Cell Immunol. 2013; 284:51–9.

[28] Sharma JN, Al-Omran A, Parvathy SS. Role of nitric oxide in inflammatory diseases. Inflammopharmacology. 2007; 15:252-9.

[29] Stettner N, Rosen C, BernPHMein B, Gur-Cohen S, Frug J, Silberman A., et al. Induction of nitric-oxide metabolism in enterocytes alleviates colitis and inflammation-associated colon cancer. Cell Rep. 2018; 23:1962–76.

[30] Anissian D, Ghasemi-Kasman M, Khalili-Fomeshi M, Akbari A, Hashemian M, Kazemi S, Moghadamnia AA. Piperine-loaded chitosan-STPP nanoparticles reduce neuronal loss and astrocytes activation in chemical kindling model of epilepsy. Int J Biol Macromol. 2018; 107 (Pt A): 973-83.

[31] A-sasutjarit R, Sirivat A, Vayumhasuwan P. Viscoelastic properties of carbopol 940 gels

and their Relationships to piroxicam diffusion coefficients in gel bases. Pharm Res.2005; 22:2134-2140.

[32] Felton LA. Mechanisms of polymeric film formation. Int J Pharm. 2013;457:423–7.

[33] Guo R, Du X, Zhang R, Deng L, Dong A, Zhang J. Bioadhesive film formed from a novel organic–inorganic hybrid gel for transdermal drug delivery system. Eur J Pharm Biopharm. 2011; 79:574–83.

[34] Lin SY, Lee CJ, Lin YY. Drug-polymer interaction affecting the mechanical properties, adhesion strength and release kinetics of piroxicam-loaded Eudragit E films plasticized with different plasticizers. J Control Release.1995; 33:375–81.

[35] Zelkó R, Orbán Á, Süvegh K, Riedl Z, Rácz I. Effect of plasticizer on the dynamic surface tension and the free volume of Eudragit systems. Int J Pharm. 2002; 244:81–6.

[36] Zhang L, Alfano J, Race D, Davé RN. Zero-order release of poorly water-soluble drug from polymeric films made via aqueous slurry casting. Eur J Pharm Sci. 2018; 117:245–54.

[37] Miastkowska M, Sikora E, Ogonowski J, Zielina M, Łudzik A. The kinetic study of isotretinoin release from nanoemulsion. Colloids Surf A Physicochem Eng Asp. 2016; 510:63–8.

[38] Asasutjarit R, Managit C, Phanaksri T, Treesuppharat W, Fuongfuchat A. Formulation development and *in vitro* evaluation of transferrin-conjugated liposomes as a carrier of ganciclovir targeting the retina. Int J Pharm. 2020; doi: https//doi.org/10.1016/j.ijpharm. 2020.119084.

Abstract

Piperine-rich herbal mixture (PHM) used in this study is a traditional Thai medicine that contains 21 oriental herbs. It is called "Sahastara remedy" and is officially included in the Thai National List of Essential Medicine since A.D. 2011. PHM has been used orally to relieve muscle and bone pains. It contains *Piper nigrum* fruits as a major constituent and also *Piper retrofractum* fruits, PHM thus has anti-inflammatory activities that mostly come from the bioactivities of piperine consisting of these pepper fruits. Unfortunately, PHM usually causes gastrointestinal side effects. Consequently, a topical product containing an alcoholic extract of PHM (PHM-E), i.e., film-forming solution (FFS) was developed to overcome this drawback. The aims of this study were to investigate the anti-inflammatory activity of PHM-E, to evaluate physicochemical properties and the anti-inflammatory activity of FFS containing PHM-E (PHM-E FFS). Anti-inflammatory activities of PHM-E were investigated in the RAW 264.7 cells. Physicochemical properties, *in vitro* toxicities and anti-inflammatory activities of PHM-E FFS including its dry film (PHM-E film) were determined. PHM-E showed anti-inflammatory activities with dose dependent manners via inhibition of nitric oxide and prostaglandin E_2 production by the RAW 264.7 cells and promotion of the cell phenotype polarization from M1 to M2. PHM-E FFS had low viscosity and exhibited the Newtonian behavior. It provided elastic PHM-E film with low tensile strength. The release profile of piperine from PHM-E film followed a zero-kinetic model. PHM-E FFS demonstrated compatibility with the skin cells, minimal ocular irritant when accidentally splashing into the eye and moderate-to-high potency for inhibition of inflammatory symptoms in the rats. PHM-E FFS thus had potential for use in the further clinical study to investigate its efficacy and safety in patients.

Keywords: Film; Polymer solution; Transdermal drug delivery; Skin permeation; Piperine; Traditional medicine; Anti-inflammatory activity; Eye irritation; Skin toxicity

Suggested running head: Film-forming solution containing piperine-rich herbal mixture extract for anti-inflammation

Application of Film-forming solution as a transdermal delivery system of piperine-rich herbal mixture extract for anti-inflammation

Rathapon Asasutjarit[a,*], Papawee Sookdee[b], Sukitaya Veeranodha[c], Asira Fuongfuchat[d] and Arunporn Itharat[b]

[a] Thammasat University Research Unit in Drug, Health Product Development and Application (DHP-DA), Department of Pharmaceutical Sciences, Faculty of Pharmacy, Thammasat University, Pathum Thani, 12120, Thailand.

[b]Department of Applied Thai Traditional Medicine, and Center of Excellence on Applied Thai Traditional Medicine Research (CEATMR), Faculty of Medicine, Thammasat University, Pathum Thani, 12120, Thailand.

[c]National Center for Genetic Engineering and Biotechnology, National Science and Technology Development Agency (NSTDA), Thailand Science Park, Pathum Thani, 12120, Thailand.

[d]National Metal and Materials Technology Center, National Science and Technology Development Agency (NSTDA), Thailand Science Park, Pathum Thani, 12120, Thailand.

[*]**Corresponding author**. Tel.: +6625644440 ext. 4387; Fax: +6625643156

E-mail address: rathapona@hotmail.com; rathapon@tu.ac.th

List of Abbreviations

Base FFS	Film-forming solution base
Base film	Dry film obtained from the film-forming solution base
CV	Cell viability
DMSO	Dimethyl sulfoxide
EPP	Ethyl 3-phenylpropiolate
ELISA	Enzyme-linked immunosorbent assay
FFS	Film-forming solution
H&E	hematoxylin and eosin
HPLC	High performance liquid chromatography
IC_{50}	Median inhibitory concentration
IFN	Interferon
IL	Interleukin
LPS	Lipopolysaccharide
min	Minute
MTT	3-(4,5-dimethylthiazol-2-yl)-2,5-diphenyltetrazolium bromide
NO	Nitric oxide
OD	Optical density
PBS	Phosphate buffered saline
PGE_2	Prostaglandin E_2
Polyethylene glycol 400	PEG 400
s	Second
STE	Short time exposure
PHM-E	Alcoholic extract of a piperine-rich herbal mixture

PHM-E FFS	Film-forming solution containing an alcoholic extract of a piperine-rich herbal mixture
PHM-E film	Dry film obtained from the film-forming solution containing an alcoholic extract of a piperine-rich herbal mixture
PHM	Piperine-rich herbal mixture (Sahastara Remedy)
TNF-α	Tumor necrosis factor-α

Acknowledgements

The authors gratefully acknowledge Thammasat University Research Unit in Drug, Health Product Development and Application (Project ID. 6305001), Faculty of Pharmacy, Thammasat University. The National Research Council of Thailand and Center of Excellence on Applied Thai Traditional Medicine Research, Faculty of Medicine, Thammasat University, as well as The Thailand Research Fund (TRF) and Thammasat University for their financial support under the research Grant No.168596/2558A10601001 and the Research Career Development Grant: grant No. RSA6080034, respectively.

Figure

Fig. 1

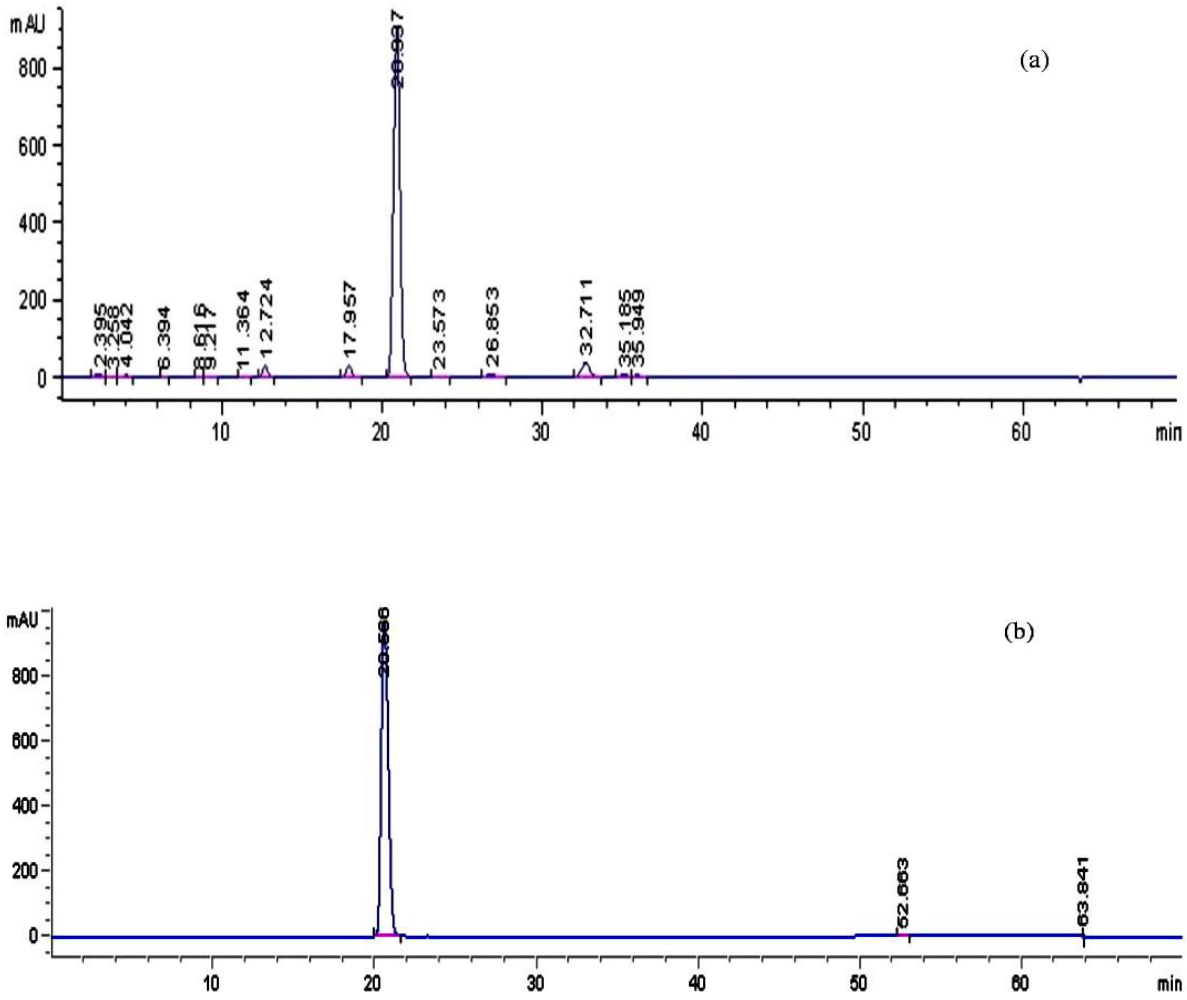
mAU
800
600
400
200
0
2.395
3.258
4.042
6.394
8.617
9.217
11.364
12.724
17.957
20.937
23.573
26.853
32.711
35.185
35.949
10
20
30
40
50
60
min
(a)
mAU
800
600
400
200
0
20.566
52.663
63.841
10
20
30
40
50
60
min
(b)

Fig. 2

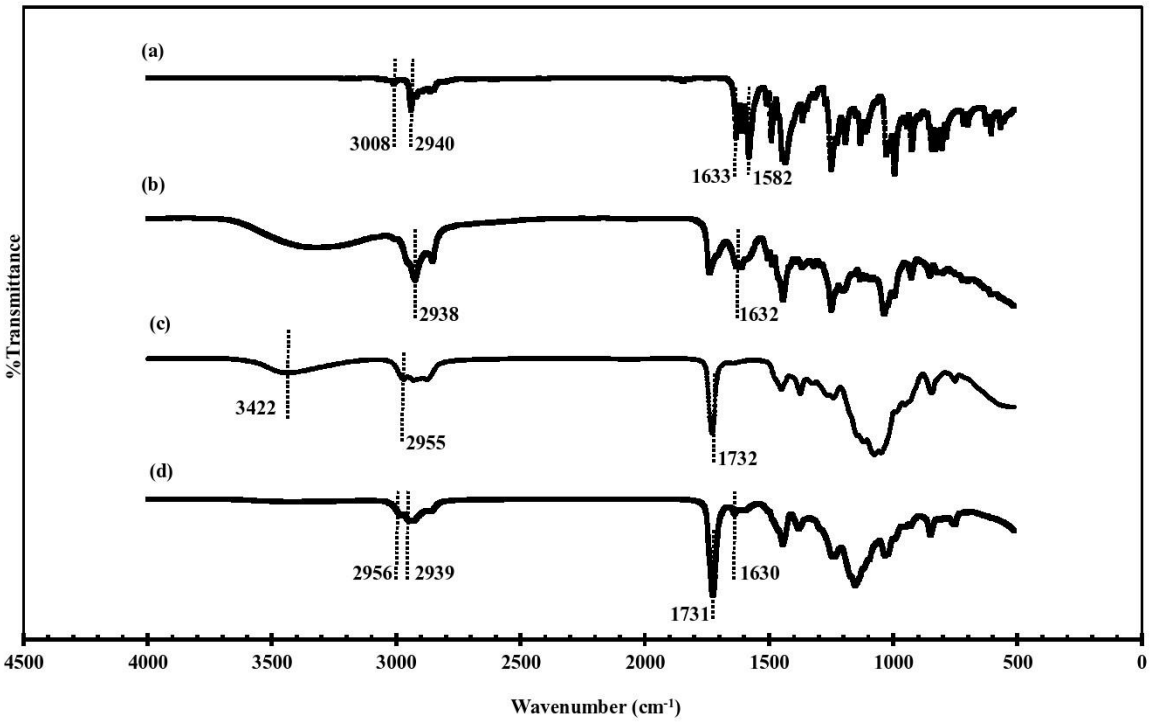
(a)
3008
2940
1633
1582
(b)
2938
1632
(c)
3422
2955
1732
(d)
2956
2939
1731
1630
%Transmittance
4500
4000
3500
3000
2500
2000
1500
1000
500
0
Wavenumber (cm-1)

Fig. 3

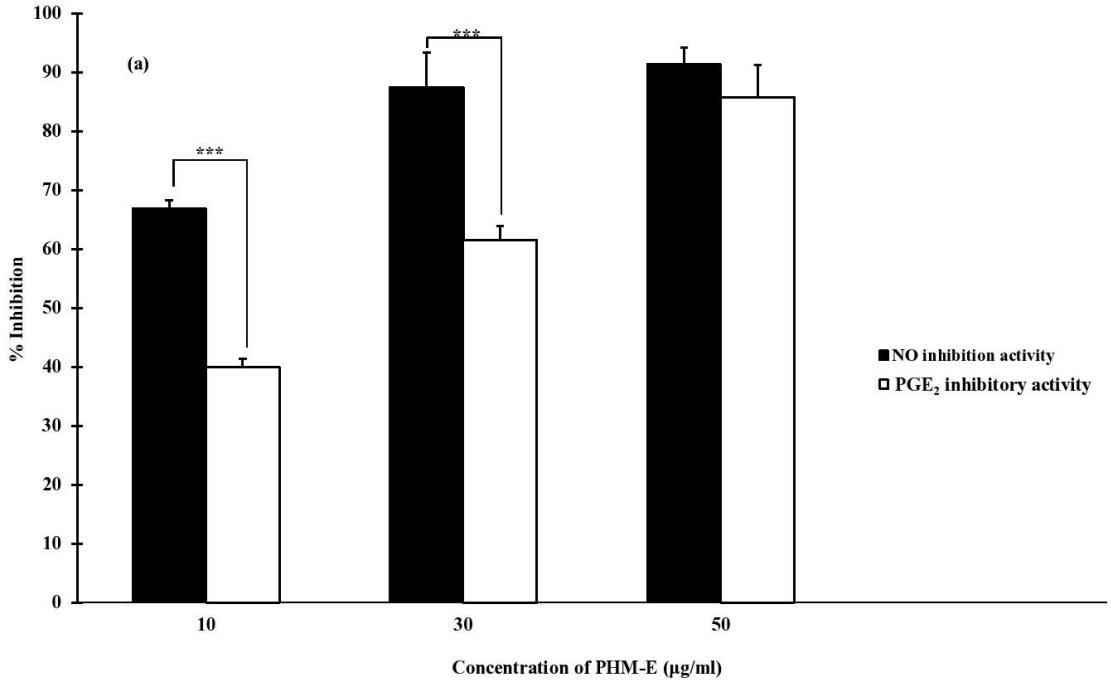
(a)
% Inhibition
100
90
80
70
60
50
40
30
20
10
0
***
***
NO inhibition activity
PGE2 inhibitory activity
10
30
50
Concentration of PHM-E (μg/ml)

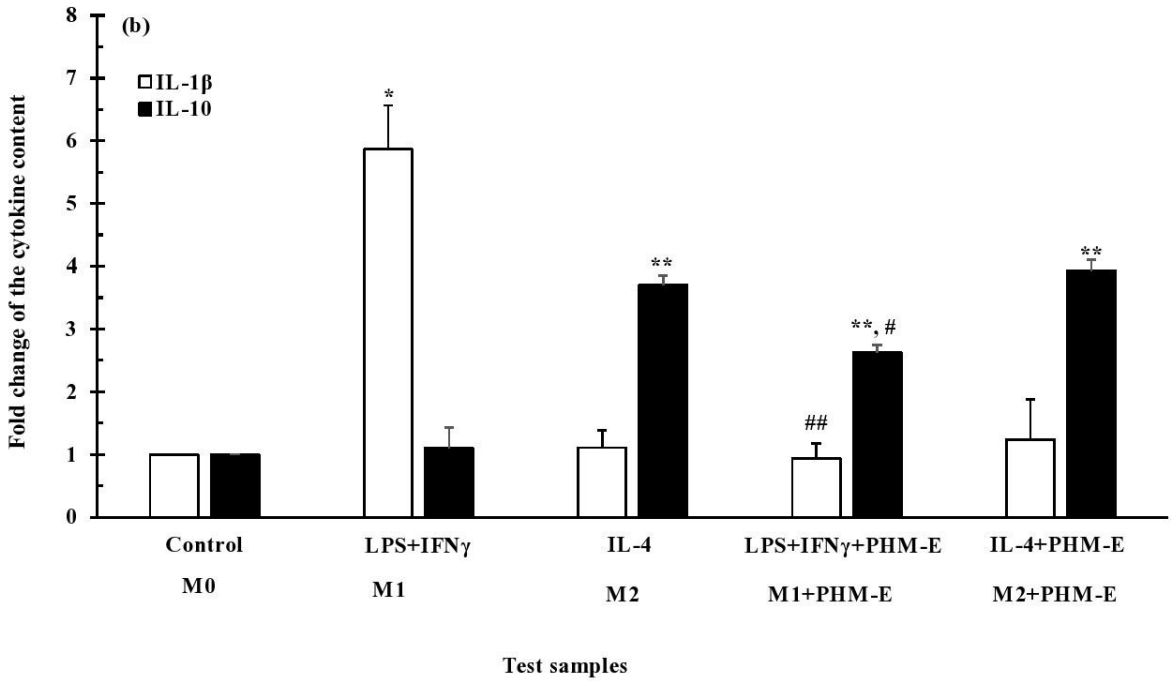
(b)
IL-1β
IL-10
Fold change of the cytokine content
8
7
6
5
4
3
2
1
0
*
**
**, #
##
**
Control
M0
LPS+IFNγ
M1
IL-4
M2
LPS+IFNγ+PHM-E
M1+PHM-E
IL-4+PHM-E
M2+PHM-E
Test samples

Fig. 4

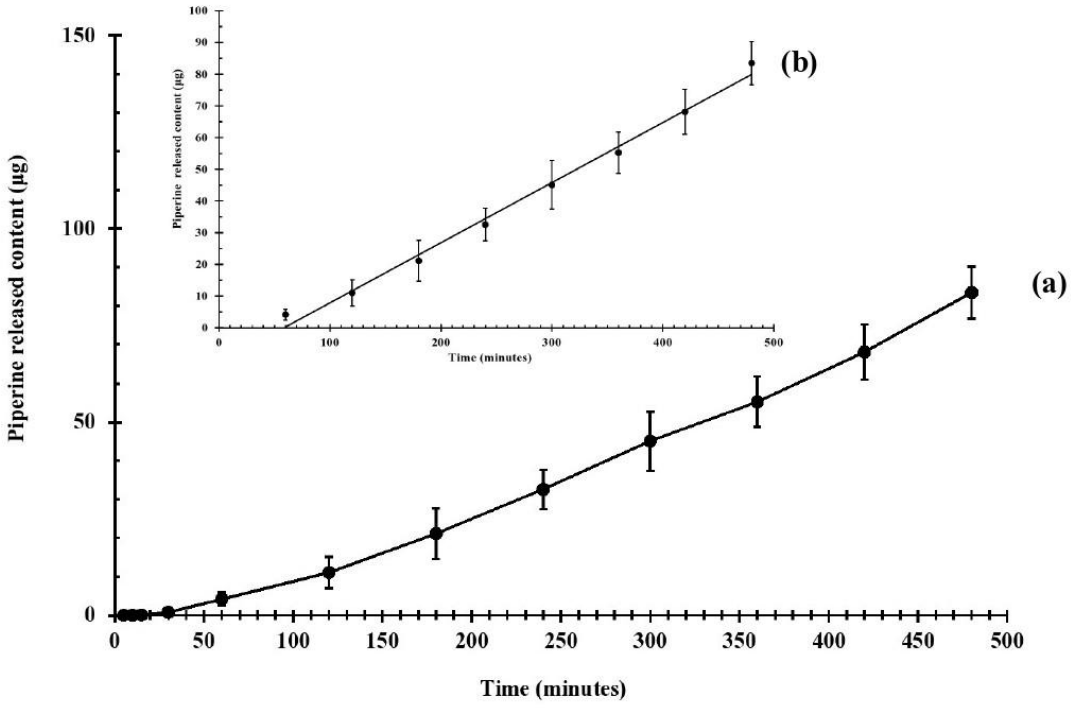
Piperine released content (µg)
Time (minutes)
(a)
(b)
Piperine released content (µg)
Time (minutes)

Fig. 5

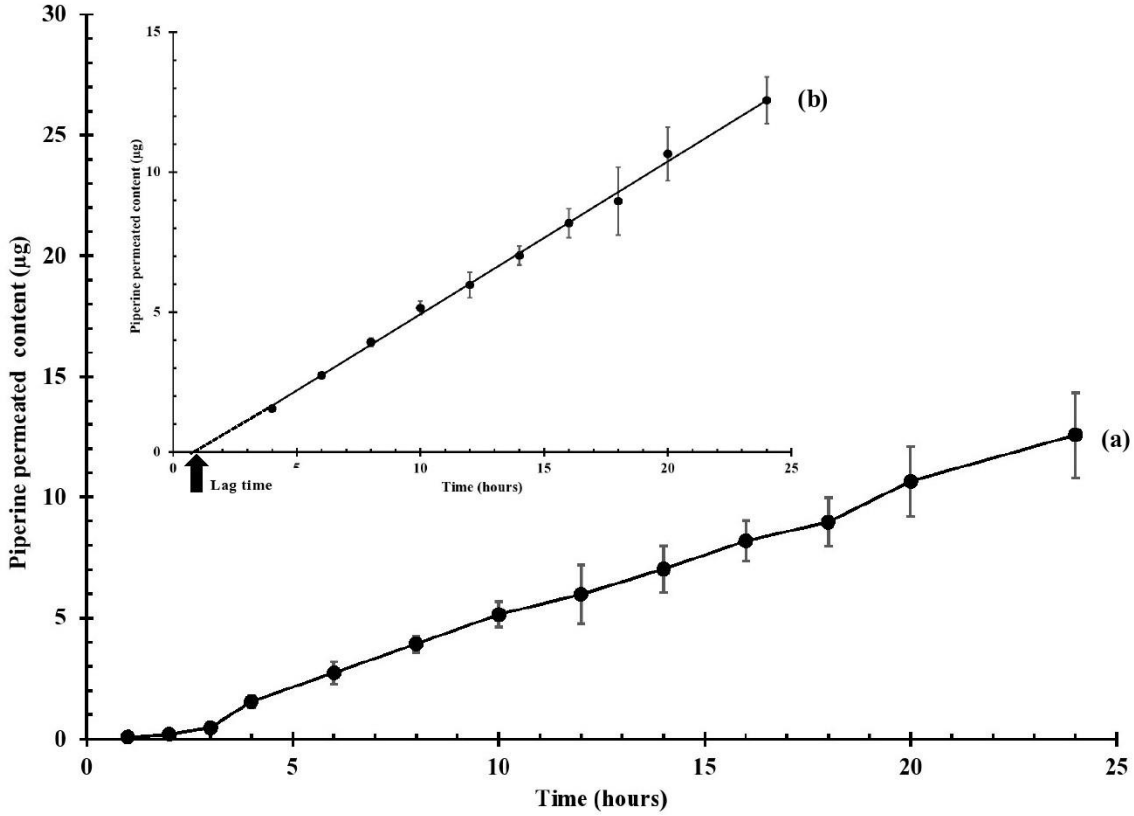
Piperine permeated content (µg)
Time (hours)
(a)
(b)
Lag time
Piperine permeated content (µg)
Time (hours)

Fig. 6

(A)

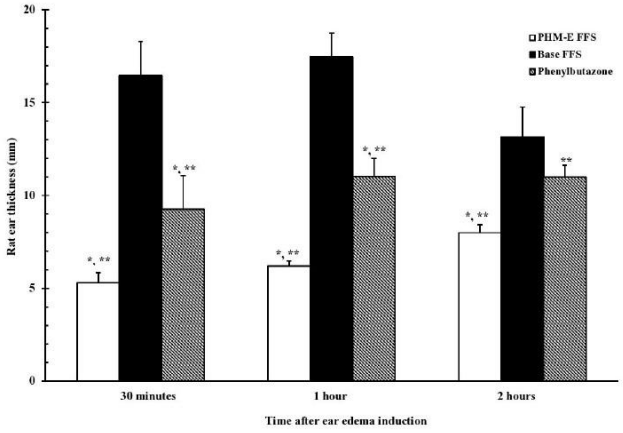
20
15
10
5
0
Rat ear thickness (mm)
PHM-E FFS
Base FFS
Phenylbutazone
*, **
*, **
*, **
*, **
*, **
**
30 minutes
1 hour
2 hours
Time after ear edema induction

(B)

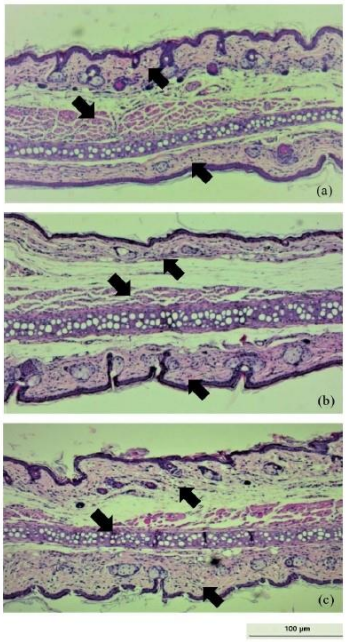
(a)
(b)
(c)
100 μm

Fig. 7

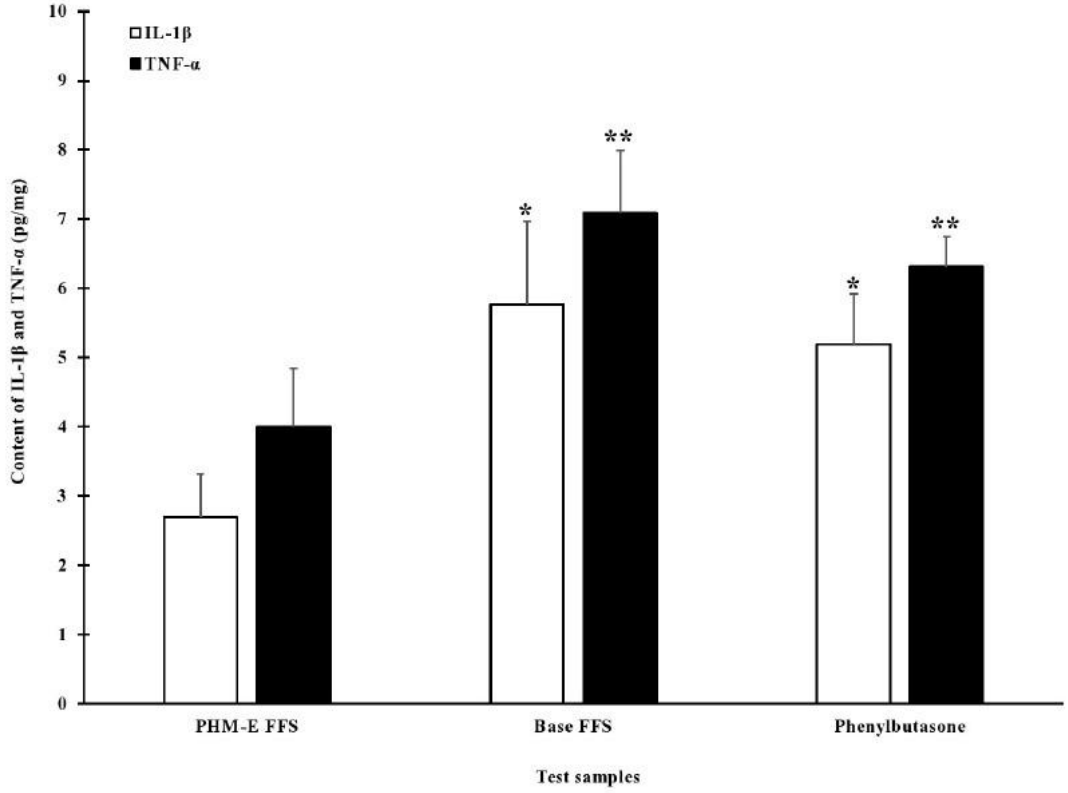
10
9
8
7
6
5
4
3
2
1
0
□IL-1β
■TNF-α
Content of IL-1β and TNF-α (pg/mg)
*
**
*
**
PHM-E FFS
Base FFS
Phenylbutasone
Test samples

Figures –caption list

Fig. 1 Chromatograms: (a) piperine in PHM-E and (b) standard piperine.

Fig. 2 FT-IR spectra: (a) standard piperine; (b) PHM-E; (c) base film; (d) PHM-E film.

Fig. 3 Anti-inflammatory activities of PHM-E (mean±SEM; n = 3): (a) percentage of inhibitory effect of PHM-E on NO and PGE_2 production (*** significantly different at *p*-value < 0.05); (b) Fold change of IL-1β and IL-10 after incubation of the RAW 264.7 cells with the test samples (*, ** significantly different from each cytokine content of the control (M0) at *p*-value < 0.05; #, ## significantly different from each cytokine content of the cells treated with a mixture of LPS and IFNγ without PHM-E (M1) at *p*- value < 0.05).

Fig. 4 Release profile of piperine from PHM-E film (mean±SD; n=3): (a) piperine released content against time; (b) linear relationship between piperine released content and time during 60-480 min.

Fig. 5 Skin permeation profile of piperine from PHM-E film (mean±SD; n=3): (a) piperine permeated content against time; (b) linear relationship between piperine permeated content and time during 4-24 hours.

Fig. 6 *In vivo* anti-inflammatory activity test: (A) Thickness of the rats' ear after treatment with the test samples and ear edema induction (mean±SD; n = 6) (*significantly different from Base FFS, **significantly different of each other between PHM-E FFS and phenylbutazone, at *p*-value < 0.05).

(B) Photographs of longitudinal section of the rats' ear with H&E staining after treatment with the test samples and ear edema induction for 2 hours: (a) PHM-E FFS; (b) base FFS and (c) phenylbutazone.

Fig. 7 Content of IL-1β and TNF-α in the rats' ear tissue after treatment with the test samples and ear edema induction for 2 hours (mean±SD; n = 3) (*, **significantly different from each cytokine content of the rats' ear receiving PHM-E FFS at *p*-value < 0.05).

Table list

Table

Table 1. Formulation of PHM [10]

Ingredients-Scientific name of the plants	Part of the used plants	Content (g)	Voucher specimen
1. *Acorus calamus*	Rhizome	8.8	SKP015010301
2. *Atractylodes lancea*	Rhizome	0.5	SKP051011201
3. *Anacyclus pyrethrum*	Root	0.6	SKP051011601
4. *Baliospermum montanum*	Root	8.0	SKP121021301
5. *Kleinhovia hospita*	Root	4.8	SKP183110801
6. *Merremia vitifolia*	Root	0.8	SKP054132201
7. *Picrorhiza kurroa*	Root	0.4	SKP177161101
8. *Plumbago indica*	Root	22.4	SKP148160901
9. *Anethum graveolens*	Fruit	1.0	SKP199010701
10. *Cuminum cyminum*	Fruit	0.8	SKP199030301
11. *Piper nigrum*	Fruit	24.0	SKP146161401
12. *Piper retrofractum*	Fruit	9.6	SKP146160301
13. *Terminalia chebula*	Fruit	10.4	SKP049200301
14. *Lepidium sativum*	Seed	1.1	SKP057121901
15. *Myristica fragrans*	Seed	1.2	SKP121130601
16. *Nigella sativa*	Seed	0.7	SKP160141901
17. *Pimpinella anisum*	Seed	0.9	SKP199160101
18. *Terminalia chebula*	Gall	0.3	SKP019200301
19. *Ferula assafoetida*	Oleo gum resin	0.1	SKP199060101
20. *Myristica fragrans*	Seed aril	1.3	SKP121130601
21. Camphor (powder)	-	1.4	SKP096030301

Table 2. Cell viability of the HDFn cells exposed to test samples (mean±SD, n=3)

Test Sample	Cell viability (%) of the cells at various concentrations of test samples			
	1 μg/ml	10 μg/ml	30 μg/ml	50 μg/ml
FFS base	102.3±2.2	103.2±5.0	102.5±2.2	102.6±4.6
PHM-E FFS	100.6±3.6	101.4±3.8	99.7±4.7	100.8±5.0
Base film	100.3±5.8	101.5±3.8	101.7±5.0	101.1±6.0
PHM-E film	102.9±5.1	101.3±2.0	100.3±5.0	100.2±4.2

Table 3. Scores obtained from the short time exposure (STE) test of PHM-E FFS

Concentration (w/v)	CV of SIRC cells (%)*	Criteria for scoring	Obtained scores
5%	98.4±1.8	If CV > 70% : scored 0 If CV ≤ 70% : scored 1	0
0.05%	101.0±0.2	If CV > 70% : scored 1 If CV ≤ 70% : scored 2	1
		Total score	1

*(mean± SD, n=6)

COI declaration

Graphical abstract

In vitro Evaluation of Liposomal Ganciclovir Targeting the Retinal Cells

Rathapon Asasutjarit[1], Kriyapa Lairungruang[1], Papawee Sookdee[2], Chittima Managit[3], Teva Phanaksri[4], Worapapar Treesuppharat[5]

[1]*Novel Drug Delivery Systems Development Center, Department of Pharmaceutical Sciences, Faculty of Pharmacy, Thammasat University, Pathum thani, 12120, Thailand.*
[2]*Department of Applied Thai Traditional Medicine, College of Allied Health Sciences, Suan Sunandha Rajabhat University, Samut songkhram, 75000, Thailand.*
[3]*Department of Pharmaceutical Technology, Faculty of Pharmacy, Srinakharinwirot University, Nakhon Nayok, 26120, Thailand.*
[4]*Chulabhorn International College of Medicine, Thammasat University, Pathum Thani, 12120, Thailand.*
[5]*Drug Discovery and Development Center, Thammasat University, Pathum Thani, 12120, Thailand*

Abstract

Ganciclovir (GCV) is an antiviral drug currently approved for treatment of ophthalmic viral infections, for example, acute herpetic keratitis and cytomegalovirus retinitis. Nowadays, topical products of GCV for ophthalmic use are available as ophthalmic gels and eye drop solutions. Unfortunately, they are limited for the treatment of the anterior eye segment infection. For the treatment of the posterior eye segment diseases, novel formulations of GCV eye drop have to be developed. Liposomes (LPs) are phospholipid vesicles. Their surface can be modified to achieve specific receptors on the retinal cells surface such as transferrin (Tf) receptors. The previous study showed that submicron-sized (100 nm) LPs were potential drug carriers for targeting the posterior eye segment, in particular, the retina by instillation to the eye. The objectives of this study were to develop GCV-loaded LPs (GCV-LPs) for ophthalmic use targeting the retinal cells and to evaluate their physicochemical properties. GCV-LPs were prepared by reverse phase evaporation technique. Particle size, zeta potential and entrapment efficiency (%) of GCV-LPs were measured. Thereafter, GCV-LPs were conjugated with Tf to obtain Tf-GCV-LPs. The release of GCV from Tf-GCV-LPs with various degrees of conjugation were investigated. Cytoxicity and cellular uptake of GCV-LPs and Tf-GCV-LPs in the retinal cells (ARPE-19 cells) were determined. The particle size and zeta potential of the obtained LPs were in a range of 88-113 nm and -28.4 to -34.4 mV, respectively. The entrapment efficiency (EE) was 26.0%-35.3%. The release profile of GCV from all LPs were consistent with the Higuchi's equation and affected by the degree of conjugation of Tf-GCV-LPs. The cellular uptake of GCV-LPs and Tf-GCV-LPs containing coumarin-6 in the retinal cells indicated that Tf conjugated to LPs increased cellular uptake of GCV-LPs without cytotoxicity. Therefore, Tf-GCV-LPs had a potential for the further studies in an animal model.

Keywords— Drug targeting; Ganciclovir; Liposomes; Ophthalmic drug delivery

Professional Biography

Rathapon Asasutjarit has completed his Ph.D. from Chulalongkorn University, Thailand. He is an Associate Professor in Pharmaceutics at Department of Pharmaceutical Sciences, Faculty of Pharmacy, Thammasat University, Thailand. His research interests are ophthalmic and transdermal drug delivery by using polymers, surfactants and nanotechnology.

Email Id: rathapona@hotmail.com; rathapon@tu.ac.th

Any Comments:

-

International Conference 2019

EuroSciCon

40 Bloomsbury Way Lower Ground Floor London, United Kingdom WC1A 2SE

Certificate

of Recognition

Special Recognition to

Rathapon Asasutjarit

in appreciation of his esteemed support as
Organizing Committee Member for
the "Euroscicon Conference on Nanoscience and Graphene Nanotechnology"
held during November 25-27, 2019, Tokyo, Japan

Zhongfan Liu
Peking University, China

Nanoscience and Graphene 2019

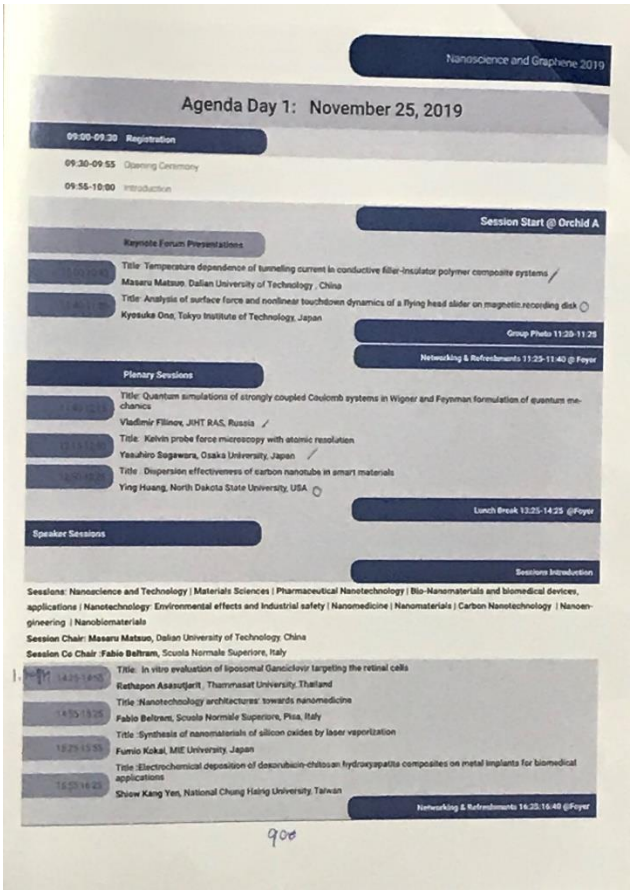

Nanoscience and Graphene 2019

Agenda Day 1: November 25, 2019

09:00-09:30 Registration

09:30-09:55 Opening Ceremony

09:55-10:00 Introduction

Session Start @ Orchid A

Keynote Forum Presentations

Title: Temperature dependence of tunneling current in conductive filler-insulator polymer composite systems
Masaru Matsuo, Dalian University of Technology, China

Title: Analysis of surface force and nonlinear touchdown dynamics of a flying head slider on magnetic recording disk
Kyosuke Ono, Tokyo Institute of Technology, Japan

Group Photo 11:20-11:25

Networking & Refreshments 11:25-11:40 @ Foyer

Plenary Sessions

Title: Quantum simulations of strongly coupled Coulomb systems in Wigner and Feynman formulation of quantum mechanics
Vladimir Filinov, JIHT RAS, Russia

Title: Kelvin probe force microscopy with atomic resolution
Yasuhiro Sugawara, Osaka University, Japan

Title: Dispersion effectiveness of carbon nanotube in smart materials
Ying Huang, North Dakota State University, USA

Lunch Break 12:25-14:25 @Foyer

Speaker Sessions

Sessions Introduction

Sessions: Nanoscience and Technology | Materials Sciences | Pharmaceutical Nanotechnology | Bio-Nanomaterials and biomedical devices, applications | Nanotechnology: Environmental effects and industrial safety | Nanomedicine | Nanomaterials | Carbon Nanotechnology | Nanoengineering | Nanobiomaterials

Session Chair: Masaru Matsuo, Dalian University of Technology, China

Session Co Chair :Fabio Beltram, Scuola Normale Superiore, Italy

Title: In vitro evaluation of liposomal Ganciclovir targeting the retinal cells
Rathapon Asasutjarit, Thammasat University, Thailand

Title :Nanotechnology architectures: towards nanomedicine
Fabio Beltram, Scuola Normale Superiore, Pisa, Italy

Title :Synthesis of nanomaterials of silicon oxides by laser vaporization
Fumio Kokai, MIE University, Japan

Title :Electrochemical deposition of doxorubicin-chitosan hydroxyapatite composites on metal implants for biomedical applications
Shiow Kang Yen, National Chung Hsing University, Taiwan

Networking & Refreshments 16:25-16:40 @Foyer

90